Time-Resolved Spectroscopy of Energy Transfers in Optoelectronic Media

Izeddin Aguirre, I.

Publication date
2008
Document Version
Final published version

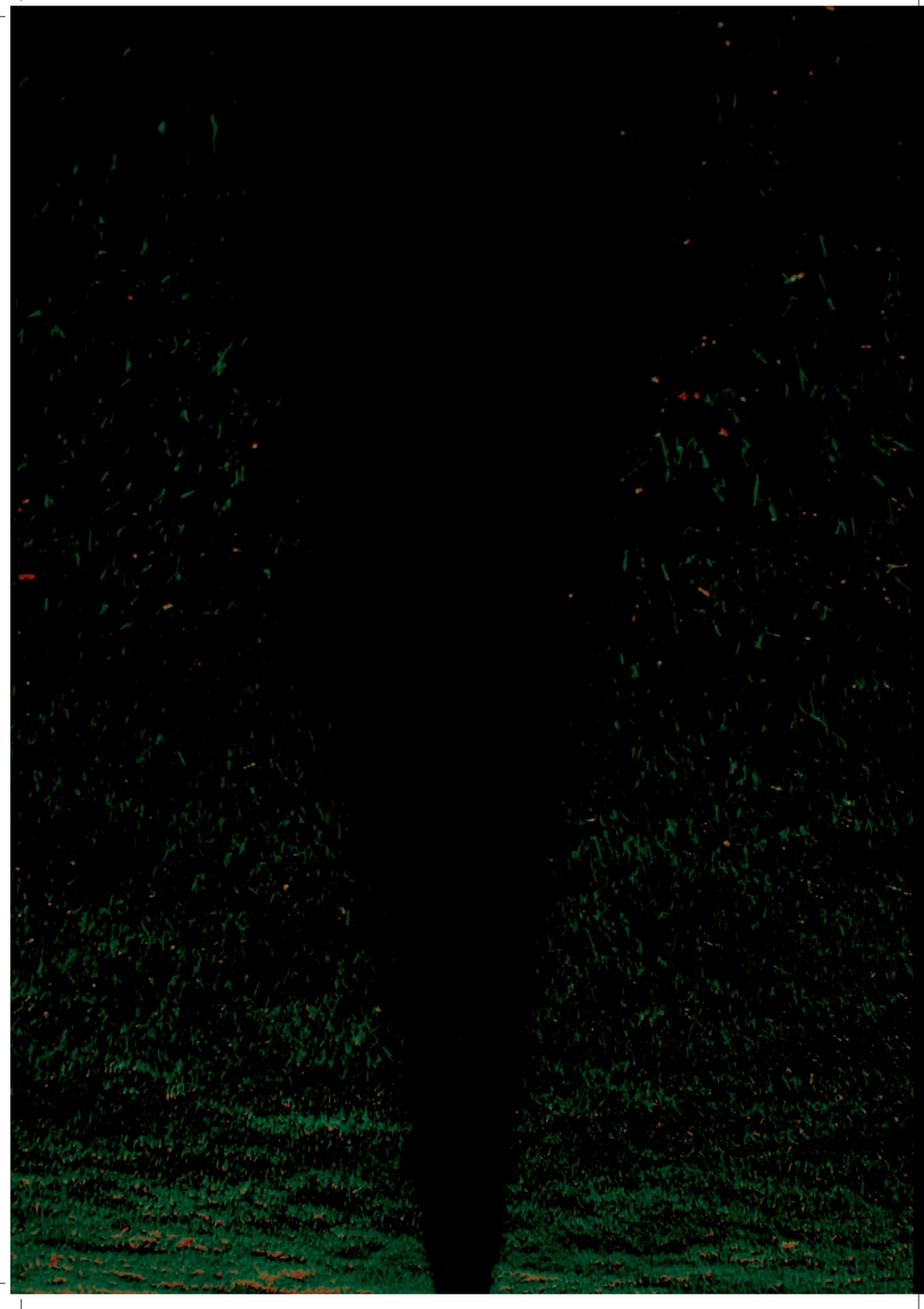

Time-Resolved Spectroscopy of Energy Transfers in Optoelectronic Media

Ignacio Izeddin Aguirre

Time-Resolved Spectroscopy of Energy Transfers in Optoelectronic Media

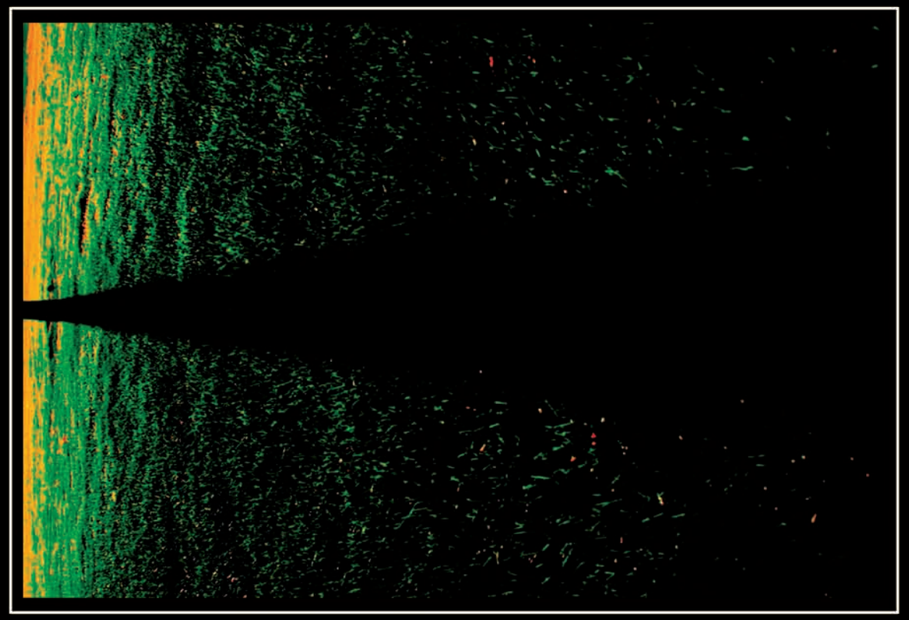

Ignacio Izeddin Aguirre

Uitnodiging

voor het bijwonen van de openbare verdediging van mijn proefschrift getiteld:

Time-Resolved Spectroscopy of Energy Transfers in Optoelectronic Media

op donderdag 17 april 2008 om 12:00 uur in de Agnietenkapel van de Universiteit van Amsterdam, Oudezijds Voorburgwal 231 te Amsterdam.

Na afloop van de promotie zal hier tevens de receptie plaatsvinden.

Invitation

to attend the public defense of my PhD thesis, titled:

Time-Resolved Spectroscopy of Energy Transfers in Optoelectronic Media

on Thursday, April 17 2008, at 12:00 hours in the Agnietenkapel of the University of Amsterdam, Oudezijds Voorburgwal 231, Amsterdam.

After the promotion a reception will take place.

Paranimfen:

Diego Altamirano
(diego@science.uva.nl)

Salvo Minissale
(sminissa@science.uva.nl)

Ignacio Izeddin Aguirre
Valckenierstraat 65
1018XE Amsterdam
izeddin@science.uva.nl

Time-Resolved Spectroscopy of Energy Transfers in Optoelectronic Media

This document, in full color, is available at
www.science.uva.nl/∼izeddin/thesis

The author can be reached at
izeddin@science.uva.nl

Cover photo: *Tree shadow*, by Gabriele Merolli (www.gabrielemerolli.com)

Ignacio Yasser Izeddin Aguirre

Time-Resolved Spectroscopy of Energy Transfers in Optoelectronic Media

ACADEMISCH PROEFSCHRIFT

ter verkrijging van de graad van doctor
aan de Universiteit van Amsterdam
op gezag van de Rector Magnificus
prof. dr. D. C. van den Boom
ten overstaan van een door het college voor promoties
ingestelde commissie,
in het openbaar te verdedigen in de Agnietenkapel
op donderdag 17 april 2008, te 12.00 uur.

door

Ignacio Yasser Izeddin Aguirre

geboren te Zaragoza, Spanje

Promotiecommissie:

Promotor:	Prof. dr. T. Gregorkiewicz
Overige leden:	Prof. dr. M. Bonn
	Prof. dr. Y. Fujiwara
	Prof. dr. M. S. Golden
	Prof. dr. W. Sinke
	Prof. dr. J. J. M. Walraven
	Dr. ir. F. W. Widdershoven

Faculteit der Natuurwetenschappen, Wiskunde en Informatica

The research reported in this thesis was carried out at the Van der Waals-Zeeman Institute for Experimental Physics, University of Amsterdam. Some of the experimental work was performed at the Dutch Free Electron Laser facility for Infrared eXperiments (FELIX) at the FOM Institute for Plasma Physics 'Rijnhuizen' in Nieuwegein.

A mi familia, por mantenerme con los pies en el suelo.

Licht! Mehr licht!

Attributed to J. W. von Goethe on his deathbed

OK, so flower-power didn't work... So what? We'll just start again.

John Lennon

Parce que moi je rêve, moi je ne le suis pas.
[...]

Léolo Lauzonne

Papers by the author related to this thesis:

Chapter 1

Donor state enabling Er-related luminescence in silicon: Direct identification and resonant excitation
I. Izeddin, M. A. J. Klik, N. Q. Vinh, M. S. Bresler, and T. Gregorkiewicz
Physical Review Letters **99**, 077401 (2007)

Er-doped electro-optical memory element for 1.5 μm silicon photonics
T. Gregorkiewicz, B. A. Andreev, M. Forcales, I. Izeddin, W. Jantsch, Z. F. Krasil'nik, D. I. Kryzhkov, and J. M. Zavada
IEEE Journal of Selected Topics in Quantum Electronics **12**, 1539 (2006)

Chapter 2

Nanosecond Dynamics of the Near-Infrared Photoluminescence of Er-Doped SiO_2 Sensitized with Si Nanocrystals
I. Izeddin, A. S. Moskalenko, I. N. Yassievich, M. Fujii, and T. Gregorkiewicz
Physical Review Letters **97**, 207401 (2006)

Non-radiative sub-microsecond recombination of excited Er^{3+} ions in SiO_2 sensitized with Si nanocrystals
I. Izeddin, M. Fujii, and T. Gregorkiewicz
Physica E: Low-dimensional Systems and Nanostrucures **38**, 144 (2007)

Energy Transfer Processes in Er-doped SiO_2 Sensitized with Si Nanocrystals
I. Izeddin, A. A. Prokofiev, A. S. Moskalenko, I. N. Yassievich, D. Timmerman, M. Fujii, and T. Gregorkiewicz
Submitted to Physical Review B

Space-separated quantum cutting with Si nanocrystals for photovoltaic applications
D. Timmerman, I. Izeddin, P. Stallinga, I. N. Yassievich, and T. Gregorkiewicz
Nature Photonics **2**, 105 (2008)

Chapter 3

Photoluminescence and excitation spectroscopy of the 1.5 μm Er-related band in MBE-grown GaN layers
I. Izeddin, D. S. Lee, A. J. Steckl, and T. Gregorkiewicz
Superlattices and Microstructures **36**, 701 (2004)

On 2.7 μm emission from Er-doped large band gap hosts
H. Vrielinck, I. Izeddin, V. Yu Ivanov, T. Gregorkiewicz, F. Callens, D. S. Lee, A. J. Steckl, and N. M. Khaidukov
MRS Symposia Proceedings Vol. **866**, 13 (2005)

Other papers by the author:

Isotope dependence of the lifetime of the 1136 cm^{-1} vibration of oxygen in silicon
K. K. Kholi, N. Q. Vinh, D. West, S. K. Estreicher, T. Gregorkiewicz, I. Izeddin, K. M. Itoh, and G. Davies
Physical Review Letters **96**, 225503 (2006)

Isotope effects and temperature-dependence studies on vibrational lifetimes of interstitial oxygen in silicon
K. K. Kohli, G. Davies, N. Q. Vinh, D. West, S. K. Estreicher, T. Gregorkiewicz, I. Izeddin, and K. M. Itoh
Nuclear Instruments and Methods in Physics Research, Section B: Beam Interactions with Materials and Atoms **253**, 200 (2006)

Mid-infrared spectroscopy of the Er-related donor state in Si/Si:Er^{3+} nanolayers
I. Izeddin, M. A. J. Klik, N. Q. Vinh, M. S. Bresler, and T. Gregorkiewicz
Materials Science and Engineering B **146**, 131 (2008)

Contents

Symbols and Abbreviations

Greek symbols

α	absorption coefficient
ε	dielectric constant
δ	Dirac delta function
η	quantum efficiency
λ	wavelength
μ	micro-
ν	frequency
ξ	envelope function
π	number pi
σ	excitation cross section
τ	lifetime
ϕ	flux
ψ	wave function
ω	angular frequency

Abbreviations

BE	Bound Exciton
CB	Conduction Band
CMOS	Complementary Metal Oxide Semiconductor
c-Si	crystalline Si
DLTS	Deep-Level Transient Spectroscpy
EL	ElectroLuminescence
FE	Free Exciton
FEL	Free Electron Laser
FWHM	Full Width at Half Maximum
LO	Longitudinal Optical
(M)IR	(Mid-)InfraRed

PL(E)	PhotoLuminescence (Excitation)
RE	Rare Earth
(SS)MBE	(Solid Source) Molecular Beam Epitaxy
TO	Transversal Optical
TR	Time-Resolved
VB	Valence Band

Introduction

On s'engage et puis on voit

Napoleon

The transistor is considered by many as one of the greatest inventions of the twentieth century. It is not the aim of this introduction to validate nor to refute this consideration, but to hint at the massive influence that the transistor—the fundamental building block of electronic devices and computers—, and therefore semiconductors, have on society and the recent History of mankind. Although the material with which the first practical transistor (built by William Shockley, John Bardeen and Walter Brattain in 1947) was germanium, it was thanks to the implementation of the silicon transistor—the basis of the integrated circuit—that miniaturization, cost reduction, and higher degrees of complexity could be achieved, giving rise to the so-called "silicon age". It is not exaggerated to affirm that silicon is present in almost every aspect of our daily life.

However, the same dramatic pace of miniaturization that has translated into cheap production, popularization of electronic components and computers, and a seemingly unstoppable increasing computing speed, is bringing silicon technology towards its fundamental physical limits, and novel approaches need to be found, studied, and developed. The use of photons as information carriers—photonics—is an attractive way to overcome the forthcoming limitations and to open a whole new world of possibilities in a well known, cheap, environmentally friendly, and versatile technology. Doping of semiconductors with rare earth ions, and the use of nanostructured silicon are two prominent examples. In the last decade, semiconductor photonics and in particular silicon photonics have progressed significantly, but great effort remains yet to be done in the whole spectrum ranging from basic understanding of physical processes to design of devices for applications. From a purely experimental approach, based on optical time-resolved techniques—let us not forget that almost everything known in physics has been discovered or confirmed by look-

ing at light (although almost everything in the Universe is utterly invisible)—, the work presented in this thesis deals with various aspects of energy transfer processes in optoelectronic media, studied from a fundamental point of view, but always considering the consequences of the drawn conclusions in view of the prospective practical applications. Theoretical modelling was developed within this framework, in order to support the proposed models.

0.1 Semiconductors. Silicon

A broad classification of materials can be established regarding the dependence of their resistivity with temperature: those materials whose resistivity increases linearly with temperature are classified as metals; those whose resistivity decreases exponentially with temperature are classified as semiconductors and insulators. The interpretation for the different behavior is the following: in metals, free carriers exist in the material, independently of the temperature; in semiconductors and insulators, it is necessary to provide a supplementarily energy in order to create charge carriers. The *band gap* of a semiconductor or an insulator is the energy necessary to generate carriers which enable conductivity in the material. A semiconductor is commonly defined as a material whose energy gap for electronic excitation lies between zero and about 4 eV—there is no fundamental difference between a semiconductor and an insulator. Semiconductors occur in many different chemical compositions, as well as a large variety of crystal structures. Some semiconductors exhibit magnetic or ferroelectric behavior, others become superconductors when appropriately doped...

The best known semiconductor is element silicon (Si). Together with germanium (Ge), it is representative for a large group of semiconductors with similar crystal structures: the diamond structure. In this configuration, each atom is surrounded by other four nearest neighbors, forming a tetrahedron. Si and Ge are *elemental semiconductors*, other forms are *binary compounds*, *oxides*, *organic semiconductors*, etc. Together with the chemical composition, the crystal symmetry of the semiconductor will determine its band structure, *i.e.* the allowed energy range for an electron in the matrix, due to the overlap of the electronic wave functions, conveniently expressed in terms of the reciprocal space. The band structure of a semiconductor will ultimately determine the electronic and optical properties of the material. The valence band (VB) is the highest range of electron energies where electrons are present at the temperature of the absolute zero; the conduction band (CB) is the range of energies where an electron can move freely in the lattice structure, thus being susceptible to create electric current. The energy distance between the top of

the VB and the bottom of the CB determines the energy band gap E_g of a semiconductor. When the top of the VB and the bottom of the CB coincide in the reciprocal space, the semiconductor is called of direct band gap.

In an ideal semiconductor, where no defects or impurities are present (intrinsic semiconductor), light can not be absorbed when the incoming photon energy is smaller than the band gap E_g of the semiconductor. When the photons have sufficient energy, they can be absorbed by the semiconductor, promoting an electron from the VB to the CB, *i.e.* creating a free electron in the conduction band and a free hole in the valence band. In order to re-establish equilibrium, the electron-hole pair will recombine: radiatively by emission of a photon, or non-radiatively dissipating the energy in the form of phonons (collective lattice vibrations). When the semiconductor has an indirect band gap, electrons in the bottom of the CB and holes in the top of the VB have different $\overrightarrow{\boldsymbol{k}}$-vectors, and the recombination can not take place without involving a third particle, in order to comply with the momentum conservation law; usually phonons are the third particle involved. In an indirect band gap semiconductor—as it is the case of Si—the probability of radiative recombination of an electron-hole pair is small compared to that of non-radiative recombination, and radiative recombinations of electron-hole pairs are only observed at low temperatures, where creation of phonons in the lattice is less probable.

When an electron-hole pair is created, due to the charge difference, Couloumb interaction appears between the two carriers; if the thermal energy k_BT is smaller than the attractive potential between the carriers (binding energy) a free exciton is formed. A free exciton can be considered as a pseudo-particle that can move in the crystal, and eventually recombine radiatively. The photoluminescence properties of intrinsic crystalline Si are basically limited to radiative recombination of excitons, and their replicas involving different types of phonons. As mentioned before, due to the indirect nature of the band gap of Si, the probability of this processes is negligible when compared to the non-radiative processes at room temperature, and only at cryogenic temperatures excitonic photoluminescence from Si can be observed.

0.2 Optical doping

The electrical properties of a semiconductor can be altered by adding impurity atoms to the crystal lattice; this is known as doping. Let us consider the case of Si, an element of the group IV of the table of elements, *i.e.* with four valence electrons. If one atom of Si is substituted in the lattice by an atom from the group V (N, As, P, Sb, Bi), with five valence electrons, the "fifth"

electron will remain unbound, and the doped impurity "donates" an extra electron; these type of dopants are called "donors". Substitutional Dopants from the group III (B, Al, Ga, In, Tl), with one less valence electron than Si, will "accept" an extra electron from the valence band, creating a hole; these dopants are therefore called "acceptors". In general, all impurities added to a semiconductor can create energy levels within the band gap of the material. The appropriate choice of doping impurities and their concentration allows manipulation and tailoring of the properties of the semiconductor. In particular for Si, the ability to induce conductivity in the bands formed the basis for the development of active elements in semiconductors technology.

Impurities can also act as recombination centers, influencing the photoluminescence properties of the semiconductor. The alteration of the optical properties by addition of impurities is called optical doping. Optical doping is capable of influencing both, emission and absorption of the material, and plays a major role in optoelectronics; semiconductor lasers, optical discs, image sensors and optical fibers are key elements for the information industry.

0.2.1 Rare earth ions

Rare earth (RE) ions are used in a wide number of applications: from solid state lasers and full color displays, to magnetic refrigeration, paints, or catalysts... The RE atoms belong to the lanthanide series of the periodic table, comprising the elements from cerium (Ce, atomic number 58) to ytterbium (Yb, atomic number 70). Their electronic configuration can be expressed as $[\mathrm{Xe}]4f^{n+1}6s^2$, with n ranging from 1 (Ce) to 13 (Yb); when a RE atom is incorporated into a solid, its configuration changes to $[\mathrm{Xe}]4f^n5s^25p^6$. The "color" and paramagnetism of a RE are determined by the configuration in the $4f$ shell, and due to the screening by the completely filled outer $5s$ and $5p$ shells, the environment have little influence on these properties. Therefore, optical transitions within this level are characterized by sharp spectral lines, with emission wavelength independent of the host material. This is a major advantage for practical applications, since a required wavelength can be selected by choosing the appropriate RE atom which can be incorporated in a variety of host materials—the most well-known example being perhaps the Nd:YAG lasers—; a careful selection of different RE ions can in fact cover the whole visible to near-infrared range.

Si is not a good optical emitter *per se*, due to the indirect nature of its band gap. RE doping of Si, and Er doped Si (Si:Er) in particular, is a possible way to achieve the silicon-based optical emitter. In Er^{3+}, the transition from the first excited state to the ground state of the $4f$ shell ($^4\mathrm{I}_{13/2} \rightarrow {}^4\mathrm{I}_{15/2}$)—allowed after the inversion symmetry breaking by the crystal field—corresponds to an

energy of 0.8 eV, or emission of a 1.5 μm photon when realized by a radiative transition. This is the preferred wavelength in telecommunications, since it coincides with the minimum losses of optical fibers. When Er^{3+} is incorporated in Si, only the first excited state $^4I_{13/2}$ (0.8 eV) lies within the Si band gap (1.12 eV), and an Er-related donor level is created in the band gap of Si, as a consequence of the incorporation of Er ions in the lattice.

In order to emit light, Er^{3+} ions must be excited. Direct excitation into the $^4I_{13/2}$ state is possible, but the effective excitation cross section is orders of magnitude smaller than the excitation via the host. The latter proceeds via creation of electron-hole pairs in the Si host, formation of a bound exciton connected to the Er-related donor level, and energy transfer to the Er^{3+} ion. In the first chapter of this thesis, the carrier mediated Er^{3+} excitation will be discussed in detail.

0.2.2 Silicon nanocrystals

Using the Si host as the excitation mediator for Er^{3+} offers the advantage of the high photoluminescence excitation cross section. However, light emission in this system is not thermally stable, due to energy back-transfer processes, activated by the thermal energy k_BT, and enabled due to the small band gap of Si. This is not the case in large band gap semiconductors—where many RE-based room temperature applications already exist— or insulators, like silicon dioxide (SiO_2), with a band gap energy of 8.9 eV. One approach to combine the features of both systems is the use of Si nanocrystals (Si NCs) as sensitizers of Er^{3+} in SiO_2. Due to the confinement of the electron wave function in a nanocrystal of the order of the Bohr radius, the band gap energy of the Si NCs increases in respect to that of bulk Si, and the valence and conduction bands become represented by a series of discrete levels. Room temperature luminescence, and high excitation cross section are achieved in this system. The physical mechanisms underlying the energy transfer processes between Si NCs and Er^{3+} is investigated in detail in this thesis.

References used for this introduction: [1], [2], [3], [4], and [5].

1 Si/Si:Er multinanolayers

Nihil volitum quin praecognitum.
Nihil cognitum quin praevolitum.

In this chapter an in-depth study of the optical properties of silicon doped with erbium ions is presented. The first section 1.1 deals with fundamental aspects of the energy transfer processes between the host and the optically active material, *i.e.* the excitation mechanisms that result in the optical excitation of Er^{3+}; experimental evidence is provided to prove the role of the Er-related donor in its excitation via the Si host, and a new excitation mechanism is proposed and demonstrated. The sample chosen for this study consists on a Si/Si:Er^{3+} multinanolayer structure—details are given further in the chapter. Previous work has shown that a single type of Er center is predominantly formed in such a system [6], simplifying thus the realization of experiments that will provide a comprehensive understanding of the energy transfer process: a single Er center would presumably form a single Er-related donor level.

Whereas the first section 1.1 of this chapter focuses on the basic mechanisms underlying optical excitation of Er-doped crystalline silicon (c-Si:Er^{3+}) and involves cryogenic temperatures and experiments at a free electron laser (FEL) users facility, the second section 1.2 proves the potential of the Si/Si:Er^{3+} multinanolayer system for *real-life* applications. Here, a fully CMOS compatible electro-optical converter with a memory function is presented and its functionality demonstrated. Following previous work on the observed memory effect of c-Si:Er^{3+} in photoluminescence [7,8], we demonstrate full *write-read-erase* electrically driven functionality realized outside of cryogenic temperatures. Finally, an erbium-doped silicon based cross point memory array is proposed as a possible future memory photonic device.

1.1 Donor-state enabling Er-related luminescence in silicon

A direct link between formation of an Er-related donor gap state and the 1.5 μm emission of Er in Si will be conclusively established in this section. The experiment was performed on Si/Si:Er nanolayers where a single type of Er optical center dominates. We show that the Er emission can be resonantly induced by direct pumping into the bound exciton state of the identified donor. Using two-color spectroscopy with a free-electron laser, the ionization energy of the donor state enabling Er excitation was determined as $E_D \approx 218$ meV. Quenching of the Er-related emission upon ionization of the donor is also demonstrated.

1.1.1 Introduction

Doping with Er is possibly the most investigated way for improving photonic properties of crystalline silicon. Nevertheless, the low level of optical activity of Er^{3+} and thermal quenching of emission intensity—two major obstacles precluding application of Si:Er for practical devices—have not been resolved. Moreover, the physical basis of these limitations is not fully understood. This justifies further research in fundamental aspects of energy transfer mechanisms governing excitation and de-excitation processes of Er^{3+} ions embedded in a c-Si matrix. Among different issues related to this problem, the proposed formation of a gap state mediating energy flow between extended effective-mass-like shallow levels of the host and localized 4f-electron states of Er^{3+} is of profound importance. Thus far only indirect evidence in support of the Er-related donor level has been derived from thermal quenching of Er luminescence [9] and deep-level transient spectroscopy (DLTS) measurements [10,11], where ionization energy E_D values between 150 and 250 meV have been reported. These measurements, however, are not able to discriminate between optically active—*i.e.*, taking part in the photoluminescence process—and non-active fractions of Er dopants. Consequently, the often postulated link between formation of a donor level and optical activity of Er^{3+} is not supported by these experiments, that naturally reflect properties of the majority of Er dopants, which do not take part in light emission. In addition, the formation of an Er-related donor level in Si has never been justified by theoretical modelling; this in contrast to Yb^{3+} in InP [12]. Therefore it is possible that the donor level observed in c-Si:Er is induced by Er doping but bears no microscopic relation to optical activity of Er^{3+}. One possibility could be formation of the so called *thermal donor* [13], since Er is known to promote oxygen aggregation which leads to generation of thermal donors.

As can be concluded from the above, the identification of a gap state mediating the energy transfer to (and from) the Er^{3+} ion, and in this way controlling its optical activity in c-Si, remains open. At the same time, this issue is of paramount importance, both fundamental (for understanding of energy transfer processes) and practical (for excitation engineering towards improvement of thermal stability of emission). In the present study we resolve this long-standing problem: using complementary information obtained by excitation and two-color spectroscopies, we identify a specific donor state and establish its unambiguous link with the 1.5 μm emission in c-Si:Er.

1.1.2 Experiment

Photoluminescence (PL) excitation spectroscopy (PLE) was performed at T = 10 K under pulsed excitation with an optical parametric oscillator (OPO), tunable in the near-infrared range, close to the band gap of c-Si. The two-color measurements were performed at the free-electron laser users facility FELIX in Nieuwegein, the Netherlands. The third harmonic of the FEL was used to enable a probe wavelength in the spectral range between 2.55 and 8.27 μm (150 to 485 meV). For primary excitation, the second harmonic of a Nd:YAG laser (532 nm) was applied. The duration of the Nd:YAG pulse was shorter than 100 ps, while the full width at half maximum (FWHM) of the total FEL macro-pulse was about 5 μs. The delay time Δt between the primary (Nd:YAG) and secondary (FEL) pulse could be tuned at will. The measurements were taken at T = 4.2 K using a gas-flow cryostat. PL spectra were resolved with a TRIAX 320 spectrometer and detected with an InGaAs photomultiplier tube.

Sample

The study was conducted on a Si/Si:Er multinanolayer structure grown by sublimation MBE technique, comprising 400 alternating Si and Si:Er layers on a Cz-Si substrate. As discussed before [6], the Er^{3+} ions in this sample form predominantly only a single type of center, whose PL is characterized by homogeneous and ultra-small linewidth of $\Delta E < 10$ μeV. The low temperature PL spectrum of the investigated sample—see *e.g.* [6]—features a series of very sharp lines related to the $^4I_{13/2} \rightarrow ^4I_{15/2}$ transition of the Er^{3+} ion, with the main emission at 1538 nm. This system is particularly suitable for the investigation of the Er-related level in the excitation process. It can be expected that a single type of optical center will create a single level in the Si band gap, thus considerably simplifying the experiment.

1.1.3 Results and Discussion

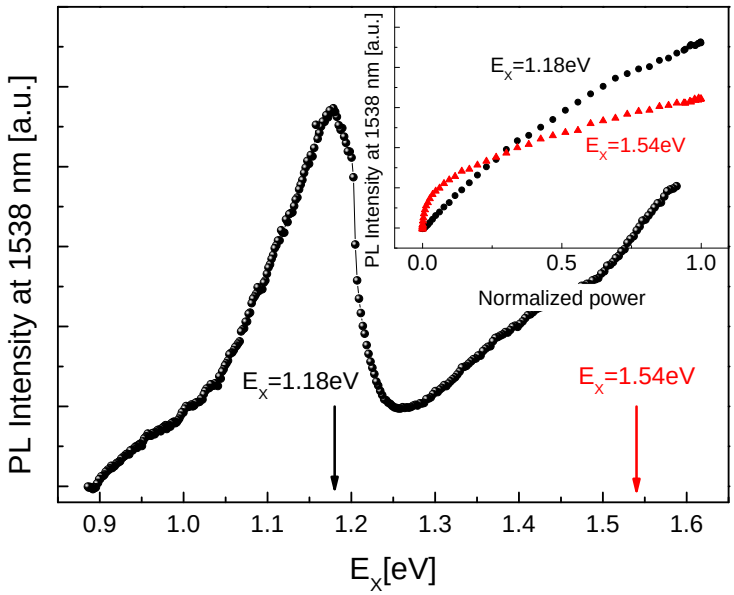

Figure 1.1: *PLE spectrum of the 1.5 μm Er-related emission. For two excitation wavelengths indicated with arrows, normalized power dependence of the PL intensity is given in the inset.*

In Fig. 1.1, the PLE spectrum of the Er-related emission measured in the investigated structure for excitation energy E_X close to the band gap of c-Si is presented. As can be seen, in addition to the usually observed contribution produced by (the onset of) the band-to-band excitation, also a resonant feature, peaking at the energy around $E_X = E_R \approx 1.18$ eV is clearly visible. We propose to identify this with a different excitation channel appearing in this energy range. Such a hypothesis is directly supported by PL intensity power dependence, shown in the inset, for the two photon energies indicated with arrows. While the data obtained for the higher energy value of $E_X = 1.54$ eV exhibit the saturating behavior characteristic of the band-to-band excitation mode [14], the dependence for $E_X = E_R \approx 1.18$ eV has a strong linear component superimposed on this saturating background. Such a linear dependence is expected for "direct" pumping. For Er in c-Si a resonant excitation could indeed take place via a bound exciton state induced by the long-sought Er-related donor discussed earlier. In that case, the energy E_R

required for this resonant pumping would be given by:

$$E_R \approx E_G - E_{FEX} + E_{LO} - E_{BE}, \tag{1.1}$$

where E_G is the c-Si band gap energy $E_G = 1.17$ eV, $E_{FEX} = 15$ meV is the exciton formation energy, E_{LO} is the energy of the lattice phonon whose participation in the excitation process is necessary in view of the indirect band gap of c-Si, and E_{BE} is the exciton-donor binding energy. Using the $E_R \approx 1.18$ eV value derived from the PLE spectrum given in Fig. 1.1, we can estimate the exciton binding energy as $E_{BE} \approx 30$ meV. Since exciton binding and donor ionization energies of a donor are mutually related—for effective-mass donors $E_{BE} \approx 10\% E_D$ is commonly found—, this implies that the relevant donor state involved in the postulated resonant excitation of Er is relatively deep, with the ionization energy in the range of 200-300 meV.

PL quenching

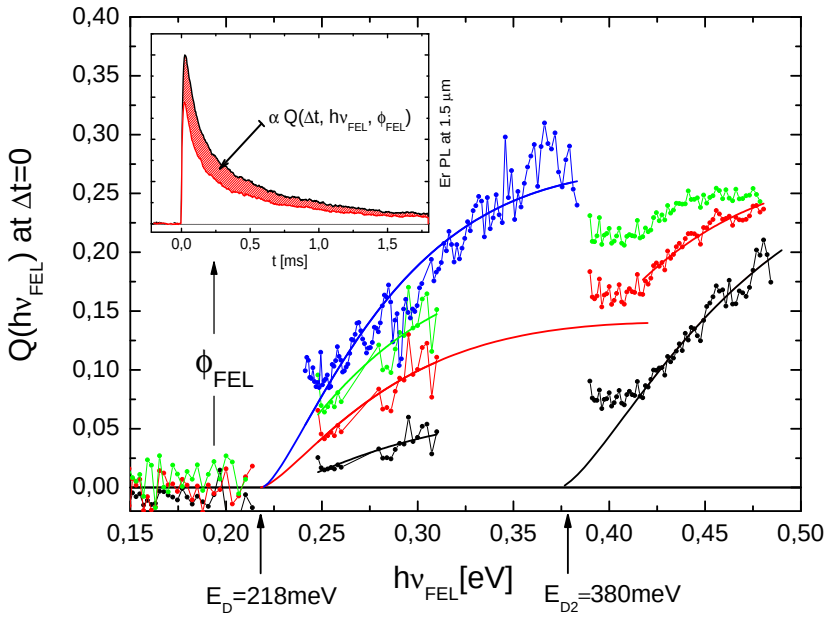

Figure 1.2: *FEL wavelength dependence of the induced quenching ratio of Er-related PL at 1.5 µm, for several flux settings of the FEL. Solid lines correspond to simulations with Eq. 1.3. In the inset: illustration of the FEL-induced quenching of Er-related PL.*

Direct identification of this donor state governing the optical activity of Er in c-Si and enabling its excitation has been obtained by two-color spectroscopy

in the visible and the mid-infrared (MIR) regions. In the past, this powerful experimental technique [8] has been successfully applied for investigation of excitation mechanisms in rare-earth-doped matrices [15–17], spin relaxation in semiconductors [18], and excited states of atomic clusters [19]. In these experiments one monitors the PL of the system emitted after band-to-band excitation with the primary pulse, which is then altered by the secondary MIR beam (FEL). In the current case, we have observed that the Er-related PL is quenched upon application of a FEL pulse with a sufficiently large photon quantum energy. This is illustrated in the inset to Fig. 1.2, which shows the change of the PL transient induced by the MIR pulse. Amplitude of the relative quench remains independent of temperature, up to at least 70 K, thus indicating a deeper character of the levels involved in the process [8, 20, 21]. Detailed investigations revealed that the magnitude of quenching depends on the timing of the FEL with respect to the band-to-band excitation Δt, and on the quantum energy $h\nu_{FEL}$ and the flux ϕ_{FEL} of the MIR photons. In order to quantify these effects, we define the quench ratio as

$$Q(\Delta t, h\nu_{FEL}, \phi_{FEL}) = \frac{\Delta I}{I} = 1 - \frac{\int_{\Delta t}^{\infty} E^*_{FEL}(t)dt}{\int_{\Delta t}^{\infty} E^*_{noFEL}(t)dt}, \tag{1.2}$$

where I stands for the time-integrated PL intensity, from the moment when the MIR pulse is fired, and E^*_{FEL} and E^*_{noFEL} are the PL signals observed with and without the FEL pulse, respectively. $Q = 1$ corresponds to the total quench of the PL signal. Fig. 1.2 shows the wavelength dependence of PL quench for several flux values. As can be seen, PL quenching is observed for the MIR photon energy $h\nu_{FEL} \geq 250$ meV, but not in the region $h\nu_{FEL} \leq 210$ meV. We conclude that the quenching effect appears once the photon quantum energy exceeds a certain threshold value located between 210 and 250 meV, and saturates at a higher photon flux—see Fig. 1.3—with the maximum signal reduction of $Q \approx 0.35$. Fig. 1.4 shows the quench ratio as a function of the time delay Δt. As can be seen, the quenching does not take place when the FEL is fired before the pump, gradually increases as the two pulses overlap (-8 μs $\leq \Delta$t ≤ 0 μs), attains maximum for Δt ≈ 0 μs—see the detailed kinetics in the inset—and then slowly, on the time scale of $\tau_d \approx 300$ μs, reduces towards an equilibrium value of $Q_{eq} \approx 10\%$. This observation excludes heating as a possible explanation for the reduction of PL, since this has a relaxation time of an order of milliseconds and therefore PL quenching should take place also for FEL pulses applied before the Nd:YAG. We conclude that application of FEL induces an additional, non-radiative de-excitation of Er^{3+} ions. One possible candidate for such a process could be cooperative up-conversion, well-known from Er-doped glasses. In this case energy is transferred between two excited

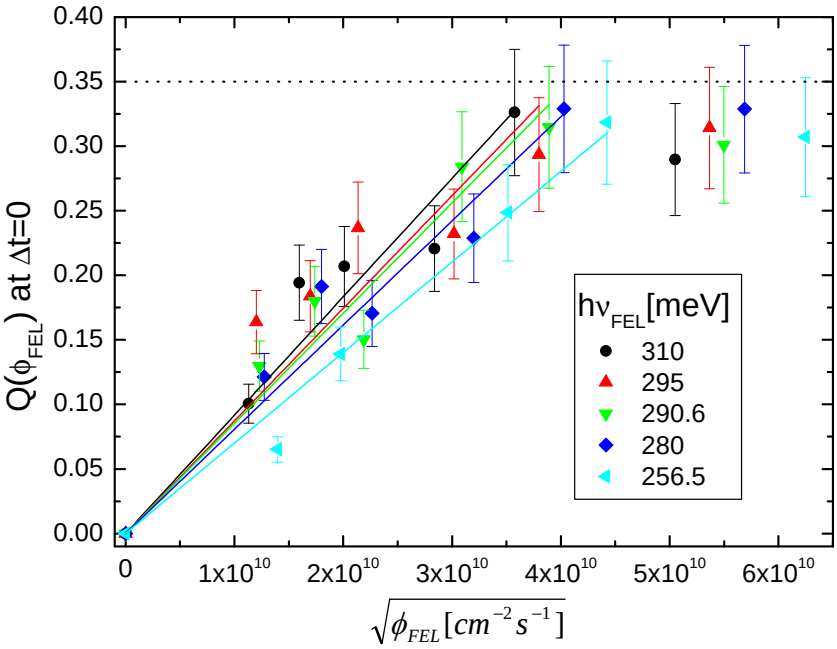

Figure 1.3: *Quenching ratio as a function of the square root of the FEL photon flux for $h\nu_{FEL}$ = 310, 295, 290.6, 280, and 256.5 meV, T = 4.2 K, Δt = 0. Linear dependence is shown for low flux values; the saturation level is indicated with the dotted line at* Q = 0.35.

Er^{3+} ions. Effectively, this means that one excitation is lost. However the up-conversion process depends only on the average distance between ions and on the medium, and can not be influenced by photons from the FEL. This rules out up-conversion as a possible mechanism of the FEL-induced PL quenching.

A prominent non-radiative recombination processes pertinent to Er-doped c-Si is the excitation reversal ("back-transfer"). It has been identified as the main reason for reduction of Er^{3+} luminescence at elevated temperatures and involves creation of an electron-hole pair at the Er-related level at the expense of Er^{3+} de-excitation. At higher temperatures, the additional energy required for this process is provided by multi-phonon absorption. For InP:Yb, it was shown that the "back-transfer" can also be induced by intense FEL illumination. In that case a step-like dependence on photon energy and a linear dependence on photon flux, leading to complete quenching of the emission, have been observed [17]. This is clearly different in the present case, where a pronounced wavelength dependence and also saturation of the quench

ratio are measured. We note further that when we assume that the resonant feature of Fig. 1.1 represents the Er-related BE state, then the minimum activation energy necessary for the back-transfer can be estimated as $E_{bt} \geq E_R - E_{PL} \approx 1180 - 800$ meV $= 380$ meV. In contrast to that, data in Fig. 1.2 show PL quench already at much smaller energies. Taken together, the evidence at hand argues against identification of the observed PL quenching with the "back-transfer". Also the afore mentioned thermal stability of the observed quenching points against the "back-transfer", as this process should enhance upon temperature increase—to this end we point out that complete PL quench is indeed observed at higher temperatures.

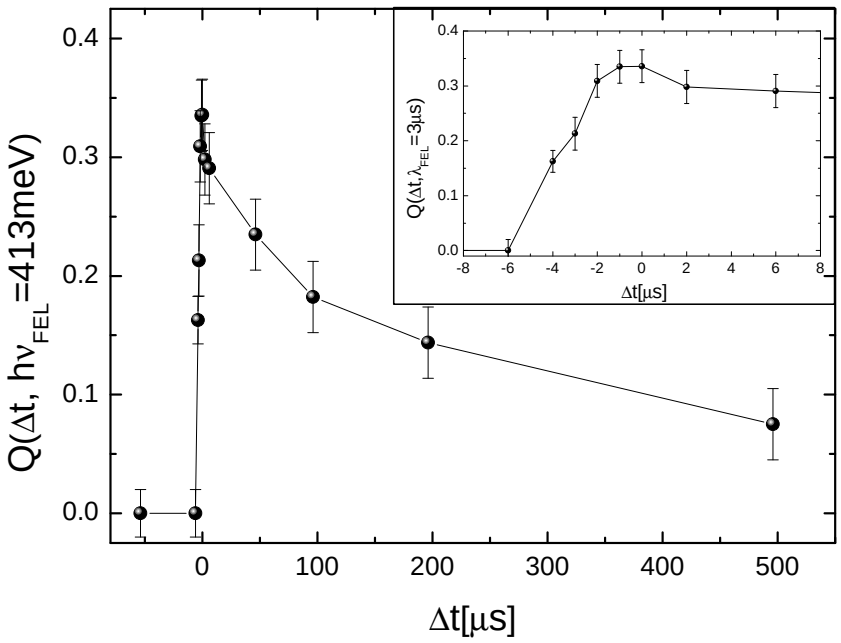

Figure 1.4: *Quenching ratio as a function of mutual delay of pump and probe pulses Δt, for $h\nu_{FEL} = 413$ meV. In the inset: detailed behavior for the region of overlap between the pump and the FEL pulses.*

In the past, also Auger process has been found to hamper PL process of Er in c-Si: a carrier in the conduction or valence band can absorb the energy of an excited Er^{3+} ion, leading to PL quenching [22]. Auger quenching can be induced with the FEL by optical ionization of trap states [21]. In that case, the quench rate is proportional to the concentration of carriers liberated by the FEL pulse. Assuming that an equilibrium carrier concentration is

maintained during FEL illumination, the PL quenching should increase with the square root of photon flux [14] towards saturation determined by full ionization of relevant traps. As evidenced by Fig. 1.3, this characteristic square root dependence is indeed observed in the experiment for small photon fluxes. On the other hand, the quench should increase (practically linearly) with the exposure time of excited Er population to free carrier concentration, *i.e.* with the "effective" duration of the FEL pulse, again in agreement with the experiment—see Fig. 1.4. (In view of the relatively slow character of processes considered in this study, the "macropulseï¿½ of FEL, featuring a 1 GHz train of picosecond pulses, can be seen as being practically "rectangularï¿½, with picosecond rise and decay slopes.) We also note that following the full overlap of the two pulses, a small decrease of the quench takes place upon further increase of the delay time. It is plausible to attribute this gradual reduction to decay of (non-equilibrium) population of traps involved in the Auger process. This effect additionally supports the proposed microscopic identification of the PL quenching being an Auger process rather than the "back-transfer", which should be time-independent. Finally, it is only fair to point out that the energy (back-)transfer process in Si:Er is significantly more complex than in direct band gap materials; therefore we cannot rule out that it indeed contributes to the observed quenching.

Since for the fixed duration of the FEL pulse, the Auger effect should saturate at a level determined by trap concentration, then the quenching saturation level can be used to estimate this concentration. Taking the maximum quench to be 35% of the original signal—Fig. 1.3—and the FEL pulse FWHM as 5 μs, and using the frequently quoted value of the Auger coefficient for free electrons of $C_A \approx 10^{-13} - 10^{-12}$ cm^{3}s^{-1} [22], we arrive at a trap concentration of $10^{17} - 10^{18}$ cm^{-3}. This concentration is much higher than the donor/acceptor doping level of the matrix and can only be compared to the concentration of Er-related donors found in an oxygen-rich material [23].

Following our microscopic interpretation of the quenching mechanism, its wavelength dependence should reflect photoionization spectrum of traps releasing carriers taking part in the Auger energy transfer. It has been shown [24] that the ionization cross section for traps can be described by:

$$\sigma(h\upsilon) \propto \frac{(h\upsilon - E_D)^{3/2}}{h\upsilon^{3+2\gamma}}, \tag{1.3}$$

with $h\upsilon$ and E_D corresponding to the quantum energy of the ionizing radiation and the ionization energy of the trap, respectively. The parameter γ depends on the specific form of the binding potential, being $\gamma = 0$ for δ-like potentials and $\gamma = 1$ for Coulomb potentials. Since $Q \propto \sigma(h\upsilon)$ then we can fit the data in Fig. 1.2 with Eq. 1.3. In this way we find the thermal ionization energy

of the involved level as $E_D = 218 \pm 15$ meV. Note that only the low FEL flux data are used for fitting, in order to minimize saturation effects. The best fit has been obtained for a localized potential, with $\gamma \approx 0$. We recall that $E_D \approx 218$ meV is similar to the trap level found in Si:Er by DLTS [11]. Therefore, it appears plausible that the FEL ionizes electrons from the donor level associated with Er^{3+}, the same as identified earlier from the PLE data. Further, it appears that in the high photon energy range, another deeper trap, with ionization energy in 350 - 450 meV range, contributes to the free carrier density.

1.1.4 Conclusions

We conclude that the results obtained in two-color and excitation spectroscopy explicitly demonstrate that optical activity of Er in c-Si is related with a gap state. Taking advantage of the preferential formation of a single optically-active Er-related center in sublimation MBE-grown Si/Si:Er multinanolayer structures, we determine the ionization energy of this state as $E_D \approx 218$ meV. We prove that this level provides indeed the gateway for Er^{3+} excitation by demonstrating 1.5 μm emission upon resonant pumping into the bound exciton state of the identified donor. We point out that the relatively large width of the resonant excitation band, exceeding that for bound exciton recombination bands in Si [25], follows directly from the involved physical mechanism. In the current case, the absorption of a photon by a bound exciton is accompanied by a simultaneous excitation of Er^{3+} ion and a transfer of a donor electron into the conduction band. Therefore, the minimum energy E_{Xmin} required for this process is given by the sum of Er excitation (800 meV) and donor ionization (218 meV): $E_{Xmin} \approx 1.020$ eV. This corresponds precisely to the onset of the resonant excitation band, as evidenced by Fig. 1.1, thus supporting the proposed identification.

At the same time, we show that carriers located at the Er-related donor state introduce a channel of effective non-radiative relaxation of excited Er^{3+} ions via Auger process of energy transfer. In this way, new light is shed on the long standing puzzle concerning the physical origin of the low emission intensity from Er-doped c-Si: while formation of the donor state enables Er core excitation, the same donor level opens also an efficient path of non-radiative relaxation. Future research will tell whether these two processes can be separated by careful material engineering. We would also like to point out that the direct "resonant" pumping into the bound exciton state identified here allows for excitation of Er^{3+} while avoiding Auger quenching by free carriers.

1.2 Electro-optical memory effect for 1.5 μm photonics

Silicon photonics is rapidly growing and a number of Si-based active and passive components have recently been shown. Here we demonstrate new functionality of Er-doped silicon: a memory effect in electroluminescence. This finding opens a prospect of necessary and thus far not available component for Si optoelectronics—a fully CMOS compatible electro-optical converter with a memory function—operating in the technologically important 1.5 μm band. When developed and optimized, prospect applications could include optical intra- and inter-chip connectors and volatile flash memory elements.

1.2.1 Introduction

In spite of its natural constraint of a small and indirect band gap, crystalline silicon continues to attract interest as a photonic material. Research is clearly fuelled by prospects of a photonic technology fully compatible with CMOS microelectronics. Photonics would constitute silicon's natural extension toward generating smaller, cheaper and ever faster devices. Somewhat surprisingly, c-Si features some properties of an excellent optical material [26, 27]. In particular, the exceedingly high level of impurity control and surface/interface passivation leads to very long minority carrier lifetimes, as non-radiative recombination can be largely suppressed. As a result of continued effort, efficient room-temperature emission has been demonstrated for a number of structures [28–32]. In a parallel development, the optical properties of Si nanocrystals have been exploited leading to the observation of optical gain [33], optical memory [34], and fabrication of LED's [35]. In a different approach, doping with erbium (Er) has been intensively studied as a convenient way to enhance the photonic properties of Si. For c-Si:Er, some promising optical behavior, such as afterglow effects—typical features of standard optical materials such as phosphors—has been revealed using two-color spectroscopy with a free-electron laser [7, 8]. Here we show that c-Si:Er has come of age by demonstrating full *write-read-erase* optical memory functionality for Si:Er structures grown using sublimation molecular beam epitaxy (SMBE) [36]. The breakthrough here is that this embryonic technology does not rely on the use of free-electron lasers or other exotic optical tools, but is facilitated purely via electroluminescence (EL). These findings open new routes for the development of an optoelectronic converter with memory functions for Si-based photonic circuits operating in the 1.5 μm telecommunication wavelength, and thus ushers in an era of optical memory fully integrable with the CMOS platform.

As c-Si-based microelectronics continues its impressive development, breaking speed and definition limits predicted only a few years ago, there appears a

growing awareness that silicon may also be a basis of future optoelectronic and photonic technology. While several other materials, and most notably III-V compounds, have clearly better optical properties, their processing technologies are less advanced, more expensive and unlikely to ever compete or become compatible with the Si platform. For the practical realization of Si photonics, all the components necessary for light manipulation, *i.e.* generation, modulation, mixing and splitting, storage and detection need to be developed. Moreover, these photonic circuits should preferably operate around a wavelength of $\lambda \approx 1.5$ μm, which coincides with the absorption minimum of glass fibers used for transmission of optical signals. Here, impressive progress has been made in the last few years. In addition to the afore mentioned room temperature Si-based emitters [29–34], an optically pumped Si Raman laser has recently been developed [37–39] and a fast optical modulator with operational frequency of 1 GHz has also been demonstrated [40]. While these achievements bring the development of all-Si photonic circuits [41] closer, a crucial part of the puzzle is still missing: a CMOS compatible electro-optical memory element.

1.2.2 Preliminaries

In the past decade, considerable research effort has been aimed at designing storage devices for use in optoelectronics and photonics. A particularly vigorous activity has concentrated on the development of non-magnetic, all-optical storage media. Most of these investigations have been focused on electron trapping at deep centers and/or structural transformations of centers upon carrier trapping, which promise very high *read/write* data transfer rates [42, 43]. In such an approach, information is written by photoionization of deep traps; this effectively sensitizes the material by generating metastable states that modulate locally its electric and/or optical properties. Information can be retrieved optically by exposing the sensitized areas to a *reading* laser beam. Three-dimensional holographic storage in photorefractive materials is another approach towards optical memory devices making use of the interference pattern in non-linear crystals [44].

Up to now, the storage potential of c-Si:Er has only been shown in fundamental laboratory experiments involving optical pumping at very low temperatures [7]. In this case—see Fig. 1.5—it was demonstrated that Er emission could be excited by a pulse of a free-electron laser operating in the mid-infrared range with $h\nu \ll E_G$, but only if it was applied shortly ($\Delta t \lesssim 100$ ms) after band-to-band excitation of the Si matrix ($h\nu > E_G$). The 1.5 μm emission did not appear if the mid-infrared pulse was not preceded by a band-to-band excitation. This memory effect has been explained in terms of temporary stor-

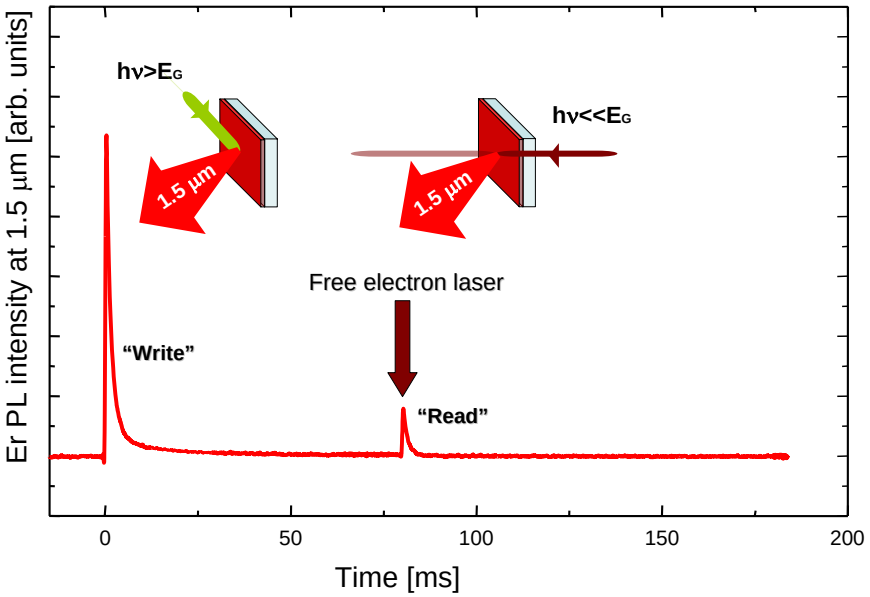

Figure 1.5: *The memory effect in photoluminescence observed for c-Si:Er at low-temperatures (<50 K) in a two color experiment. At time t = 0, a short pulse from a laser (depicted in green) provides band-to-band excitation. This results in filling of the trapping centers (*writing *operation) and an Er-related luminescence signal (at λ = 1.54 µm) with a characteristic decay time of 1 ms. After a delay time, a pulse of mid-infrared radiation from a free-electron laser releases the trapped carriers and thus recovers the stored information (*reading *operation), inducing an Er-related PL signal.*

age of photo-excited carriers at deep traps. Releasing them optically by the mid-infrared laser irradiation—*reading*—, results then in Er^{3+} excitation, but only upon prior exposure of the material to the *writing* laser pulse.

1.2.3 Results

Since this phenomenon of optical memory in Si:Er had been observed only at cryogenic temperatures T $\lesssim$ 50 K and with a free-electron laser as the mid-infrared *reading* beam, it was certainly not relevant for applications. Nevertheless, it indicated that c-Si:Er can be coaxed into having the right kind of optical properties for a Si-based optical storage element for 1.5 μm photonics. Now we are able to take a real step towards commercial exploitation of

these advantageous optical properties, as we present an electrically controlled memory element with optical output. We have succeeded in accomplishing a complete sequence of *writing*, *reading*, and *erasing* operations using electrical pulses of small amplitude, while the optical signal is being emitted in the technologically relevant 1.5 μm band. In comparison to the original concept [7], the operational parameters have been significantly improved. The temperature range has been increased by a factor of 3, to 120 K, and retention times between the *writing* and the *reading* pulses are of the order of seconds. Moreover, there appear to be no fundamental reasons which would prohibit room-temperature operation, as EL of Si:Er under the reverse bias regime is well-known to be thermally stable. Also, a further increase of the retention time should be possible, as a more detailed understanding of the relevant physical processes develops. Fig. 1.6 shows the layer sequence of

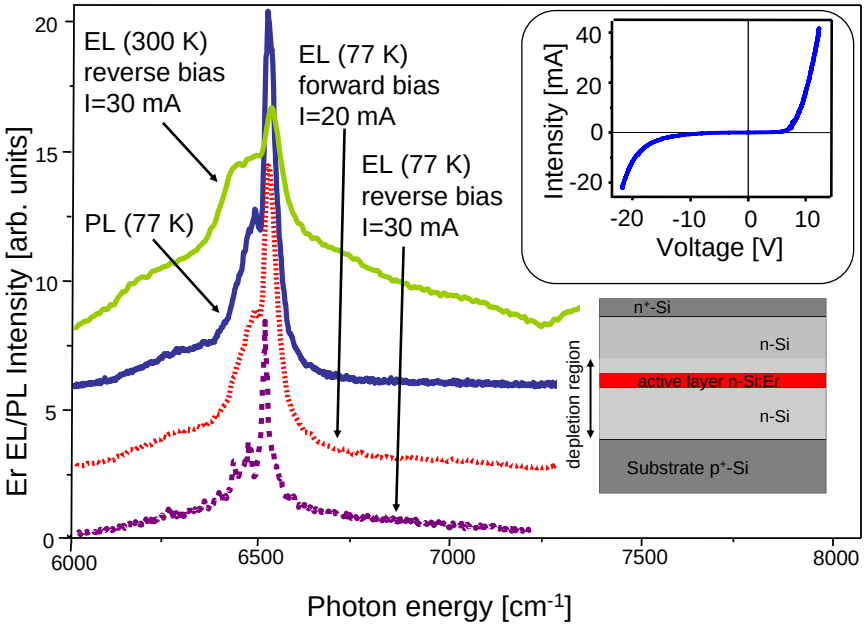

Figure 1.6: *Photo- and electroluminescence spectra of the structure used in the study: the* $\sim$ *1.5 μm band is characteristic of the* $^4I_{13/2} \rightarrow {}^4I_{15/2}$ *transition of* Er^{3+} *ions in oxygen-rich Si. The layer sequence of the diode is given in the right-lower corner. As can be seen, the Er-doped active layer is contained within the depletion region (shaded). The upper inset shows current-voltage characteristics of the structure.*

the n^+-Si/n-Si/n-Si:Er/n-Si/p^+-Si electroluminescent memory element. The

structure was grown by the SMBE technique on a p-type (100)-oriented Si substrate with a carrier concentration of p $\approx 10^{17}$ cm^{-3}. It comprises a 1 μm layer of n-type Si with a free carrier concentration of n $\approx 2\times10^{15}$ cm^{-3}, followed by a thin Er-doped active layer of 70 nm thickness, another layer of n-type Si, of 10 μm, and finally an n$^+$ layer with n $\approx 6\times10^{18}$ cm^{-3}. The Er concentration in the active layer is estimated as [Er] $\approx 10^{18}$ cm^{-3}. The diode structure geometry was chosen in such a way that the Er-doped active layer was located within the space charge region. As can be seen from Fig. 1.6, the structure shows intense Er-related $\lambda \approx 1.5$ μm PL and EL under forward bias at low temperatures. Under reverse bias, strong EL was observed up to room temperature. The emission spectra are typical for Er^{3+} ions in a matrix of oxygen-rich Si [45]. The current-voltage characteristic of the structure (at T = 77 K) is also shown as an inset. It exhibits an avalanche-type breakdown for a reverse bias of $U_B \approx$ -(18-20) V. Investigations of the structure

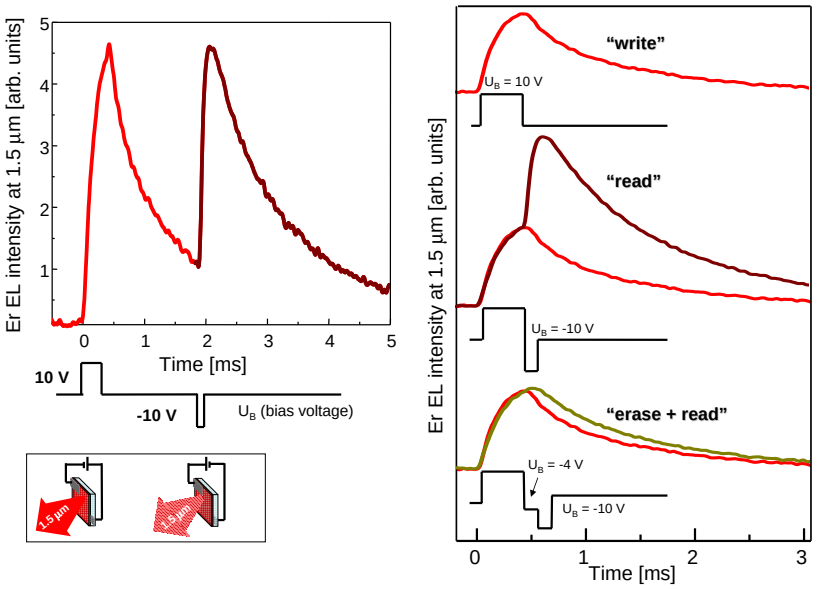

Figure 1.7: *Memory effect in electroluminescence observed at T = 77 K for the p-i-n structure investigated in the present study: information is written by a positive bias pulse, and subsequently read by a negative bias pulse of sufficiently large amplitude. (A negative bias pulse of sub threshold amplitude erases the information written with a positive bias.) The* write-read *and* write/erase-read *pulse sequences are shown. Note that the reverse bias of U_B = -10 V used for the* read *operation is considerably lower than the breakdown voltage.*

revealed that a long-term memory effect in EL under forward bias. Following a forward-bias pulse, additional emission—"stored" EL—from Er^{3+} ions could be induced by the application of a subsequent reverse bias pulse. This is illustrated in the left-hand panel of Fig. 1.7, where the EL response ($\lambda \approx 1.5$ μm) of the investigated structure is shown for a sequence of forward and reverse bias pulses, of $U_B = 10$ V, separated by a delay. It is important to note that the magnitude of the reverse bias pulse giving rise to this emission is well below the breakdown voltage, meaning that it cannot be due to EL resulting from avalanche breakdown of the reverse-biased p-n junction. Indeed, observation of the "stored" EL is possible only if the structure has been previously exposed to a forward bias pulse, thus representing a true memory function. Furthermore, a threshold dependence of the "stored" EL on the amplitude of the reverse-bias (*reading*) pulse has been found. A reverse-bias pulse of subthreshold magnitude, which did not induce emission, had an *erasing* effect, removing the *writing* effect of the initial pulse. This *write-erase-read* pulse sequence is also depicted on the right side in Fig. 1.7.

1.2.4 Discussion

Based on the available information, we propose the following microscopic mechanism for the observed EL memory effect: During the forward bias pulse, trapping centers available in the material are filled with carriers. This corresponds to the *write* operation, and can be accompanied by Er emission induced in a parallel process of electron-hole recombination. Under negative bias, the carriers localized in the traps are liberated into the band. If the electric field is higher than the threshold value (*e.g.* U_B = -10 V for the investigated structure), the carriers gain sufficient energy to excite Er^{3+} ions by impact. This is the *reading* process. A lower reverse bias (U_B = -4 V) removes the trapped carriers but does not provide enough energy for impact excitation; such a situation corresponds to *erasing*. This mechanism is schematically illustrated in Fig. 1.8, where it has been assumed that electrons are the carriers active in the process, since impact excitation of an Er^{3+} ion by electrons is known to be three orders of magnitude more efficient than by holes [46]. For the particular structure investigated here, the amplitude of the "stored" EL pulse was only slightly diminished when the delay time between the *write* and *read* pulses was set to 100 ms. This indicates a retention time of at least 0.5 s. As for thermal stability of the signal, very little signal deterioration was observed up to 120 K with the retention time being practically independent of temperature. This suggests that trapping centers responsible for the memory effect in the device are of deep rather than shallow character. Moreover, this moderate thermal quenching of signal intensity seems to be due to a less efficient filling of traps

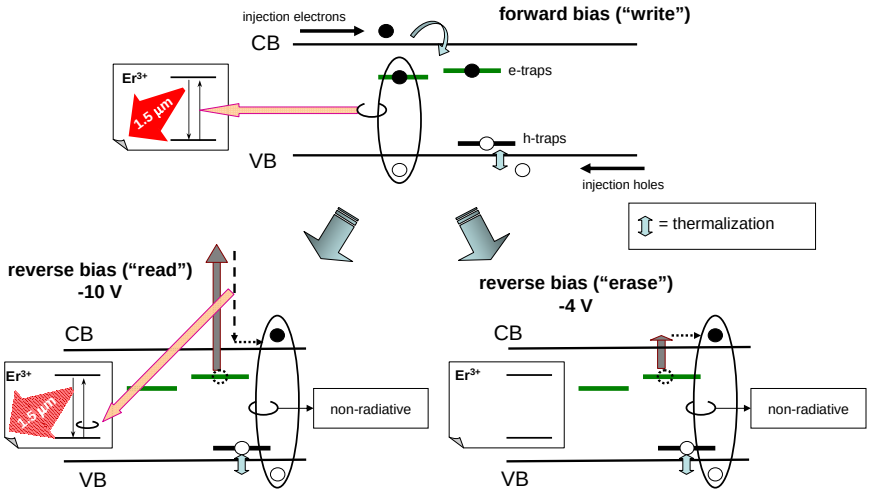

Figure 1.8: *Illustration of the proposed microscopic mechanism for the memory effect in electroluminescence. The positive bias pulse injects electrons and holes into the active layer in the depletion region. These fill traps available in the material. Parallel to that process, at higher injection rates, electron-hole recombination at specific Er-related centers may lead to excitation of* Er^{3+} *ions (initial emission pulse). The negative bias pulse liberates the (non-equilibrium) trapped carriers into the band; if its amplitude is sufficiently high, the carriers attain sufficient energy for impact excitation of Er.*

or to a less efficient excitation of Er at a higher temperature, rather than trap ionization. As mentioned before, these operational parameters of the future structures are very likely to be improved by the forthcoming investigations.

In current electronic technology, the storage hierarchy is governed by a compromise between density, access rate, and total data capacity as well as the cost of the individual memory element. For optical storage media, such as CD and DVD, the laser spot—currently of an order of 0.5 μm—limits the bit density. Furthermore, the access rate is determined by movement of mechanical parts that are required for precise beam positioning and, as such, represents a rather slow process. On the other hand, magnetic storage is currently reaching the physical limits of domain spacing as regards information density, and the spinning speed, with its access rate being, again, determined by mechanical movement of the *read/write* head. Semiconductor memories (DRAM, SRAM, ROM) are currently at the top of the storage hierarchy pyramid. These are basically transistors, which can be electrically programmed. While the development of transistors still follows Moore’s law [47], the cost of nanotooling increases exponentially with integration level, and thus it is generally acknowl-

edged that a further reduction of element size while maintaining a low-cost per element is likely to meet fundamental limitations already within the next few years.

The findings presented here indicate a possibility of using erbium-doped silicon for the development of future photonic memory devices. The investigated structure is the very first electrically operated Si:Er memory device to be fabricated and, as such, represents a "proof-of-principle". While its operational temperature and retention time are clearly not yet optimal, we believe that detailed understanding of the underlying physical mechanisms and consequent modification of material properties and device design can further improve these parameters. As the operating temperature range is enhanced, also the access rate will increase, as Er lifetime shortens and MHz signal modulation becomes possible [48]. Even higher rates should be feasible due to the fact that the device could be "reset" at a chosen clock frequency by an *erasing* pulse of reverse bias or by a flash of infrared laser light penetrating through the structure. In addition, massively parallel architectures might be used. A cartoon of a future Si:Er-based cross point memory array is shown in Fig. 1.9. The information is stored in active regions at the intersections of the "word" and "bit" lines. Similar to current flash memories, this array does not require any moving mechanical parts and individual elements are addressed by an appropriate choice of word and bit lines. By using vertical stacking and a 100 nm separation between lines, a hypothetical data density of up to 100 GB/cm^3 could be reached. This is comparable to values reached in prototypes of holographic memories [42], but in contrast to those, it does not require expensive laser systems. Nevertheless, it is only fair to point out, that intensity of individual light pulses emitted in the depicted structure during *read* operation would be very small, in view of a small number of Er ions contained in each memory element and non-radiative recombination increasing with temperature. Moreover, while the proposed concept is all-Si, the voltages of electrical pulses for *read* and *write* operations exceed those currently used in CMOS technology.

In addition to the storage applications, the memory function reported here might find an even more direct use in low-rate optical interconnects. Being, in fact, an all-silicon electro-optical converter operating at the 1.5 μm glass-fiber wavelength, it can provide an optical link between *e.g.* galvanically isolated parts of the system. The memory function could then be used for consecutive *writing* and parallel (packet) *reading* of information. Yet another highly speculative but exciting prospect, which could be explored, are spintronics applications, as the proposed device could, in principle, translate spin-polarization of electrons (in the electric pulses) into the polarization of emitted light—an effect which could be utilized in quantum computing schemes for spin read-out.

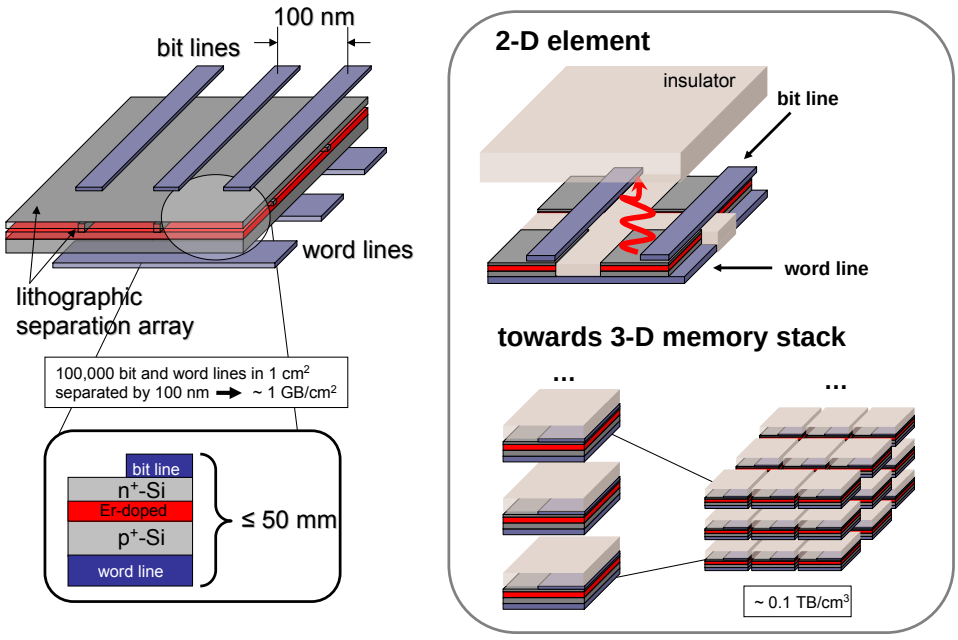

Figure 1.9: *A cartoon of an all-silicon photonic cross-memory array device based on the observed effect. The active layer is contained between crossed grids of bit and word lines; in that way an array of memory elements can be created. Similar to the current flash memories, each element can be individually addressed without any moving elements. Assuming a 100 nm repetition of line pattern, a density of* $\sim$ *1 GB/cm*^{2} *can be realized. Such "memory sheets" could be stacked vertically, resulting in a hypothetical volume density around 0.1 TB/cm*^{3}*.*

1.2.5 Conclusions

In summary, the presented here new functionality of c-Si:Er opens a route toward the ultimate goal of room-temperature photonic applications and on-chip-integrated optoelectronics. Coupled with advanced Si processing technology, this Si-based optoelectronic converter possessing true optical memory capability could be directly incorporated into nano-scale photonic circuits, enabling a new class of optoelectronic Si-based devices.

2 Sensitization of Er^{3+} with silicon nanocrystals in a SiO_2 matrix

Einmal ist keinmal

German saying

SiO_2 matrix doped with Er^{3+} ions and Si nanocrystals (Si NCs) is intensively investigated as an interesting system where room temperature 1.5 μm Er-related emission can efficiently be induced by non-resonant excitation; some time ago it has been noted that photo- and electroluminescence of Er^{3+} ions in SiO_2 can be effectively sensitized with Si quantum dots [49–51]. In photoluminescence, upon illumination, incoming photons are predominantly absorbed by band-to-band transitions in Si NCs. Since the indirect band structure of Si is preserved also in the nanocrystalline form [52], electron-hole pairs generated in this way are characterized by a relatively long lifetime. This allows energy transfer to Er^{3+} ions located in vicinity of Si NCs. In that way an indirect channel of excitation of Er dispersed in SiO_2 is created and the 1.5 μm Er-related emission appears. Its temporal characteristics is given by a microsecond rise time, corresponding to Si NC-to-Er energy transfer, followed by predominantly radiative and temperature independent decay in the millisecond range, characteristic for Er^{3+} ions in SiO_2. In particular, it has been concluded that dispersion of Si nanocrystals in Er-doped SiO_2 matrix SiO_2:(Er, Si NCs) combines to a certain extent positive features of Er-doped crystalline Si with those of Er-doped SiO_2:

- In contrast to the situation for SiO_2:Er, introduction of Si NCs enables indirect excitation of Er^{3+} ions. This process is non-resonant

and relatively efficient, with an (effective) excitation cross-section of $\sigma \approx 10^{-17} - 10^{-16}$ cm^{-2}, which represents an increase by a factor 10^3 [50] in comparison to SiO_2:Er.

- In contrast to the situation in crystalline Si:Er, emission from Er^{3+} ions does not suffer from thermal quenching and is readily observed at room temperature, similar to SiO_2:Er^{3+} [50, 51].

These promising characteristics raised considerable hopes on possible applications of the SiO_2:(Er, Si NCs) for Si photonics and specific devices have been proposed [35,53,54]. Particularly attractive is the potential application of SiO_2:(Er, Si NCs) for development of flash-lamp pumped optical amplifier—a much welcome replacement for the currently used fiber amplifier which requires resonant and high power laser pumps for its operation. In order to achieve that, the Si NC-induced sensitization process of Er emission in SiO_2 has to be thoroughly understood.

In the past, Förster (dipole-dipole) mechanism has been proposed in order to explain the energy transfer from Si NCs to Er^{3+} [55, 56] and different locations of Er in respect to Si NC have been considered [57, 58]. However, in spite of a considerable progress by both modelling and experiment [50, 59], many issues still lack sufficient explanation. In this field, while preliminary reports on optical gain have been published [60], detailed investigations revealed important drawbacks of the SiO_2:(Er, Si NCs) system: it has been realized that (i) only a relatively small part of all the Er^{3+} ions is susceptible to the indirect excitation via Si NCs [61, 62], and (ii) upon introduction of Si NCs, a considerable portion of Er dopants do not contribute photons regardless of the excitation mode (via Si NCs or direct by resonant pumping) [61]. Therefore it has become clear that dispersion of Si NCs in SiO_2:Er is a challenging and complex physical system, which has to be understood, and possibly engineered at a microscopic level, before device applications can be considered.

Following from the above, it is the objective of this chapter to advance the understanding of the sensitization of Er^{3+} PL by Si NCs. In Section 2.1, we report on an observation of a fast, sub-microsecond, Er-related 1.5 μm PL; since the radiative decay of Er^{3+} in SiO_2 takes place on a milliseconds time scale, this "fast" contribution is easily overlooked when the appropriate experimental techniques are not applied. Taking into account the relative intensity of the reported "fast" component, we show that about 50% of the total Er content in the studied sample is excited by the Si NCs—two orders of magnitude increase with respect to previous reports—, but does not contribute significantly to the radiative emission. In order to account for this "fast" PL, we propose a new excitation channel, comprising Auger-like excitation of the

Er^{3+} ions via intra-band transitions of (hot) carriers in the Si NCs.

The following section of the chapter, Sec. 2.2, works out further details of the suggested excitation mechanism, featuring a series of detailed high-resolution PL and PL kinetics experiments. Based on these measurements, we develop a model for energy transfer between Si NCs and Er^{3+} ions, yielding microscopic information on the sensitization by Si NCs and on its limitations. Following our investigations, the existence of two different mechanisms of excitation taking place between Si NCs and Er dispersed in SiO_2 is confirmed: due to band-to-band recombination of carriers in the NC, and to intra-band transitions of carriers in the NC, giving rise to the "slow" and "fast" Er-related PL, respectively. In order to verify our model, experiments concerning the effective excitation cross section of Er- and NC-related PL, and the optical absorption of Si NCs are also presented in Sec. 2.2.

Not only the model is confirmed by the excitation cross section measurements, showing the proposed mechanism for Er^{3+} excitation, but also energy transfer involving a similar mechanism taking place between Si NCs is demonstrated. This is the core of the last section of this chapter, Sec. 2.3, where the occurrence of double excitation by a single incoming photon absorbed by a Si NC is demonstrated. There, following the experiments involving excitation cross section and absorption measurements, the relative quantum efficiency of the systems under consideration was studied. This effect—termed space-separated quantum cutting—is shown to take place not only for Er^{3+} excitation, but also to increase the excitation efficiency of Si NCs, in an Er-free sample. The implications of this effect in photovoltaic applications is discussed, opening the door to overcome the Shockley-Queisser limit [63] of the solar cell efficiency.

Samples

A series of Si NC- and Er-doped SiO_2 2 μm layers were prepared by radio frequency (RF) co-sputtering on a SiO_2 substrate, and kindly provided by Dr. M. Fujii, from Kobe University. The samples were characterized by different concentration of Er dopants and size and concentration of Si NCs. Details of sample preparation procedure can be found in Ref. [64]. Following preliminary selection, the detailed investigation of recombination dynamics have been conducted on a particular sample with the most intense 1.5 μm Er-related emission. It was characterized by atomic concentrations of 0.11% of Er, 41.8% of Si, and 12.6% of excess Si. After the sputtering procedure, the sample underwent annealing at 1100 °C which resulted in formation of Si NCs with the average diameter of 3.1 nm with a size dispersion of $\sim$ 14%, and a density of $[NC] \approx 4.1\times10^{18}$ cm^{-3}.

For the evaluation of the concentration of optically active Er^{3+} reported in Sec. 2.1, the PL intensity has been compared with that of a SiO_2:Er sample prepared by multiple Er^{3+} implantations and carefully annealed for full Er^{3+} activation.

In Sections 2.2 and 2.3, a twin sample without Er dopant and the same concentration and size of Si NCs was chosen for the absorption measurements.

Experiments

The photoluminescence experiments were performed under pulsed excitation in the visible provided by a tuneable optical parametric oscillator pumped by the third harmonic of a Nd:YAG laser, with pulse duration of 5 ns and repetition rate of 10 Hz. In the UV range experiments in Sections 2.2 and 2.3, the excitation was provided by the third harmonic of a Nd:YAG or a dye laser pumped by a XeCl (308 nm) excimer laser. The samples were placed on a cold finger of closed-cycle cryostat and the measurements were taken at 10 K and room temperature (RT). PL spectra were resolved with a TRIAX 320 spectrometer and detected with an InGaAs photomultiplier tube (PMT) with flat response in the visible to near-infrared range or a Ge photodiode (Edinburgh Instruments EI-A) connected to a digital oscilloscope where signal integration was done. For time-resolved measurements of PL dynamics, the PMT was working in time-correlated photon counting mode with temporal resolution up to 2 ns.

The absorption measurements were performed in two experimental configurations: Direct transmission measurements under OPO pulsed illumination, and in a UV flash lamp absorption photo-spectrometer.

2.1 Nanoseconds dynamics of the 1.5 μm Er-related photoluminescence

We report on an observation of a fast 1.5 μm photoluminescence band from Er^{3+} ions embedded in SiO_2 matrix doped with Si nanocrystals, which appears and decays within the first microsecond after the laser excitation pulse. We argue that the fast excitation and quenching are facilitated by Auger processes related to transitions of confined electrons or holes between the space-quantized levels of Si nanocrystals dispersed in SiO_2. We show that a great part—about 50%—of all Er dopants is involved in these fast processes and contribute to the sub-microsecond emission.

2.1.1 Introduction

In this section we address and clarify important issues concerning the optical activity of Er^{3+} susceptible to sensitization by Si NCs. In contrast to earlier findings, we show that the majority of Er^{3+} ions in the Si NC-sensitized SiO_2 matrix is excited by a fast Auger process involving hot carriers generated in Si NCs by a laser pulse. This process, which proceeds directly into the first $^4I_{13/2}$ excited state, occurs on nanosecond scale and is paralleled by a reverse non-radiative de-excitation, in which energy from an excited Er^{3+} ion is transferred to a carrier inside a Si NC. As a result, intense Er-related emission appears and quenches within the first microsecond after the laser pulse. This feature has been easily overlooked in experiments, leading to the underestimation of the optical activity of Er^{3+} ions.

2.1.2 Results

Fig. 2.1 shows a RT PL spectrum of the investigated sample measured with the excitation wavelength set to $\lambda_{exc} = 450$ nm, *i.e.* not in resonance with internal transitions of Er^{3+}. Both Er- and Si NC-related bands can be observed. The amplitude ratio of these bands is well-known to be determined by Er^{3+} concentration [50]. In the inset to Fig. 2.1, we show intensity of the 1.5 μm Er^{3+} PL band as function of photon flux for two excitation wavelengths of 512 and 522 nm, corresponding to non-resonant and resonant ($^4I_{15/2} \rightarrow {}^4S_{3/2}$) excitation modes, respectively. On the upper horizontal axis, the estimated average number of excitons generated per Si NC is indicated. Also the intensity of the 1.5 μm PL band observed under resonant excitation (522 nm) in the SiO_2:Er standard sample is depicted. Using calibration procedure described in detail elsewhere [61], the implanted SiO_2:Er sample serves to ascribe a particular concentration of Er^{3+} emitters contributing to the PL intensity measured

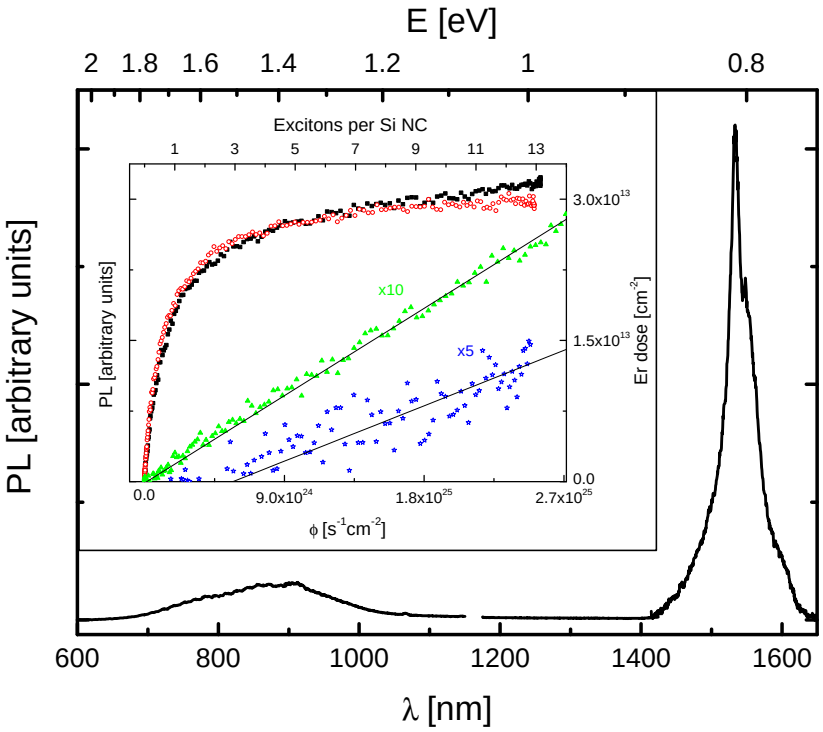

Figure 2.1: *RT PL spectrum of the investigated sample, λ_{exc} = 450 nm. In the inset: flux dependence of the PL intensity at λ = 1.5 μm for non-resonant (λ_{exc} = 512 nm, open circles) and resonant (λ_{exc} = 522 nm, solid squares) excitation. Open stars represent the difference between the two curves. Right hand scale has been calibrated using the data obtained for the SiO_2:Er reference sample (solid triangles).*

in the investigated sputtered layer. The appropriately corrected Er^{3+} density is given by the right hand scale of the inset. Using these data, we conclude that the Si NCs sensitized 1.5 μm PL saturates for Er^{3+} areal density of $[Er^{3+}] \approx 3.1 \times 10^{13}$ cm^{-2}, *i.e.*, at $\sim 0.55\%$ of the total Er^{3+} content. While it is possible that the saturation level can slightly increase by excitation diffusion under continuous pumping [61], this represents a marginal part of the total Er^{3+} doping. At the same time, the difference between the two experimental curves (for resonant and non-resonant excitation, also shown) indicates that only $\sim$ 25% of Er^{3+} dopants can contribute to photon emission upon resonant pumping. This result illustrates the main problem of Si NC induced sensitization of SiO_2:Er: the apparent loss of optical activity of Er^{3+} dopants.

Since the signal intensity depicted in Fig. 2.1 represents the time-integrated PL response of the sample, therefore in order to address this problem, we have examined in detail PL decay dynamics. The result is shown in a double-logarithmic representation in Fig. 2.2. Three different temporal regimes can be distinguished:

I ($t \lesssim 1$ μs): An intense emission appears shortly after the laser pulse and rapidly decays toward a (temporary) minimum. This indicates an almost instantaneous ($\sim$ ns) excitation directly into the first $^4I_{13/2}$ excited state of Er^{3+}, followed by fast relaxation.

II (1 μs$\lesssim t \lesssim 10$ μs): The PL intensity rises again, at a slower rate, and attains a maximum. This regime corresponds to the Si NC - to - Er energy transfer, as revealed in the inset to Fig. 2.2, where dynamics of Er emission band is compared with that of Si NCs at $\lambda_{SiNC} = 860$ nm, for the first 10 μs after the laser pulse. As can be seen, the decay of Si NCs, characterized by a (stretched) exponential behavior with a time constant of $\tau_{SiNC} \approx 1.2$ μs, is paralleled by an increase of the Er-related emission on a similar time scale, $\tau_{Er}^{rise} \approx 3.5$ μs.

III ($t \gtrsim 10$ μs): The final decay. The time constant of this process, $\tau_{Er}^{D} \approx 2.4$ ms, is characteristic for the (predominantly) radiative recombination of $^4I_{13/2}$ excited state of Er^{3+} ion in SiO_2.

From inspection of Fig. 2.2, it is clear that the time-integral of the Er-related PL signal is determined by the "slow" emission in regimes II and III. Therefore, it is this "slow" Er^{3+} PL, with the $\sim$ μs rise time and $\sim$ ms decay, that has been represented in the inset to Fig. 2.1, and which, as discussed before, represents a contribution of $\sim 0.5\%$ of the total Er^{3+} content. We remark that while sub-μs PL related to Si NCs has been reported [65], all previous studies of Er-related PL dynamics in SiO_2:(Er+Si NCs) concentrated on the "slow" emission, overlooking the initial fast component (regime I) whose amplitude is much higher, but whose contribution to the integrated PL signal is negligible.

2.1.3 Discussion

We will now discuss the microscopic origin of the different kinetics identified in Fig. 2.2. Electronic structure of Si NCs has been investigated before [66, 67]. We have considered a theoretical model of carriers confined in spherical Si quantum dots inside SiO_2 with finite energy barriers for electrons (3.2 eV) and holes (4.3 eV) in the framework of the multiband effective mass approximation [68]. Outside the NC, electrons are considered to have an isotropic mass equal

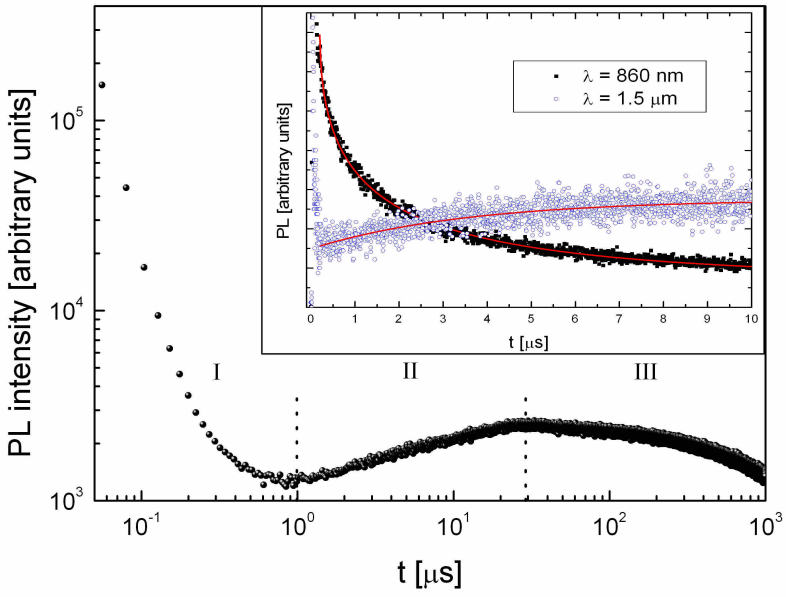

Figure 2.2: *Double logarithmic representation of the Er-related 1.5 μm PL decay, showing three different temporal regimes (RT, λ_{exc} = 450 nm). In the inset: RT PL temporal evolution for the first 10 μs after the excitation pulse, measured at λ = 1.5 μm for Er^{3+} (open circles) and at λ = 860 nm for Si NCs (solid squares). Stretched exponential decay formula has been used to fit the Si NCs decay (τ = 1.2 μs, β = 0.5) and single exponential rise for Er^{3+} (τ = 3.5 μs).*

to the free electron mass m_0 and for holes we assume the same Hamiltonian as inside the NC but with parameters corresponding to a single isotropic mass equal to $5m_0$, which is in accordance to band structure calculations of SiO_2. In contrast to Ref. [68], we do not use the approach of infinitely high barriers but calculate the carrier states exactly. The carrier quantization energies up to 1.5 eV have been calculated for electron levels C1 to C7 as 0.33, 0.52, 0.76, 0.79, 1.05, 1.06, and 1.36 eV above the conduction band of bulk-Si, and for hole levels V1 to V9 as 0.19, 0.33, 0.43, 0.59, 0.71, 0.75, 0.92, 1.01, and 1.17 eV below the valence band of bulk-Si—see Fig. 2.3—for Si NCs with diameter D = 3.1 nm.

Under optical pumping with photon energy of 2.75 or 2.42 eV, as used in the experiment, "hot" electron-hole pairs (electrons in up to the fifth excited state and holes up to the seventh) can be generated. In view of the large level separation, especially pronounced for electrons, these hot carriers can

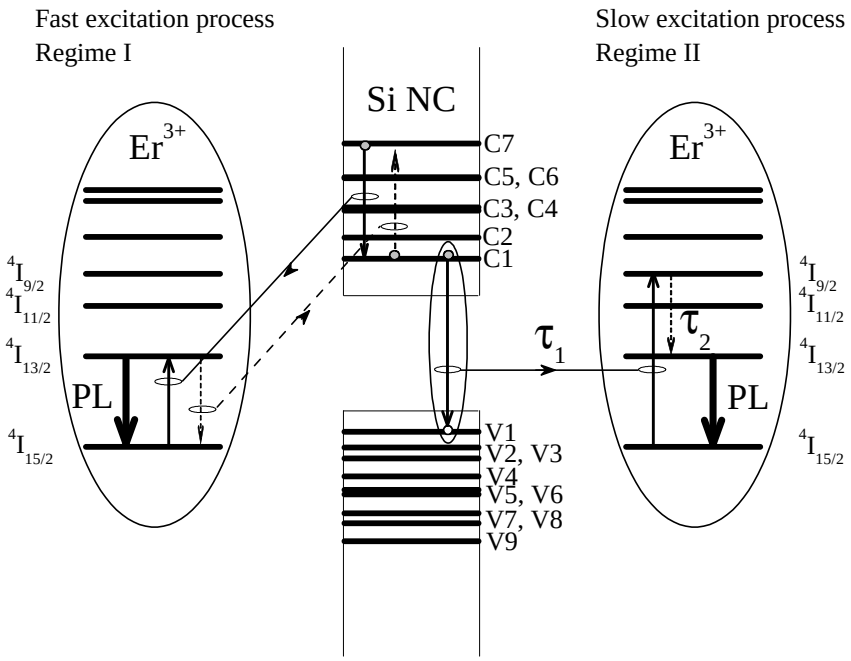

Figure 2.3: *Schematic illustration of different excitation mechanisms proposed to be responsible for the "fast"—regime I—, and the "slow"—regimes II and III—Er PL.*

relax to the ground exciton state only by multiphonon processes, which are considerably slower than those assisted by a single phonon. A faster cooling of hot excitons can be facilitated by an Auger process of energy transfer to Er^{3+} ions, which are then excited directly to the first $^4I_{13/2}$ excited state—see Fig. 2.3. Such a process is similar to impact excitation by hot carriers in bulk Si, but should also be multiphonon assisted. The probability of the phonon-assisted Auger process has been calculated by the generalized Fermi rule. We use the Born-Oppenheimer approximation decomposing the probability amplitude for the transition into the matrix element of Coulomb interaction between confined carriers states and Er electron states and the Franck-Condon phonon part. The phonon part is calculated in the model of two equivalent shifted parabolic potentials. The result is averaged over the nanocrystal size distribution. Our estimations show that this process is effective for Er^{3+} dopants located within a distance comparable with the radius of a Si NC, *i.e.* in our case $\sim$ 1.55 nm.

Depending on the actual distance, the effective transfer time is found to change within the 1 - 100 ns range. This Auger process is then responsible

for appearance of the ultrafast Er^{3+} PL within nanoseconds after the laser pulse. We note that under strong pumping, when several electron-hole (e-h) pairs per Si NC are created, more than one Er^{3+} can be excited by a single Si NC. However, parallel to the excitation process, fast Er luminescence quenching should take place by a reverse process, in which a carrier confined in a Si NC acquires energy bringing the excited Er^{3+} ion back to its ground state. This process (similar to Auger de-excitation by free carriers in bulk Si) induces fast decay of the initial Er PL. Therefore it is the Auger process of energy exchange between Er^{3+} ions and carriers confined in Si NCs which gives rise to the ultrafast Er^{3+} excitation and Er-related PL band depicted in Fig. 2.2. A small part of the rapidly excited ions will escape Auger quenching giving rise to the long-living component overlapping with the "slow" PL band and responsible for its initial amplitude—see the inset to Fig. 2.2. It is necessary to remark that in Si NCs, the Auger recombination rate controlling the lifetime of confined e-h pairs at high pumping levels is influenced by the discrete character of the energy structure. Previous investigations, both theoretical [69] and experimental [70] have found these to be in the 1-100 ns range, which is comparable with the time constant of "impact" Auger excitation and quenching considered above.

Both fast processes of Auger excitation and quenching will continue as long as hot carriers are available in Si NCs. At a final stage, with only one e-h pair in a Si NC, another possible Er^{3+} excitation process will appear due to a multiphonon assisted Auger recombination of the last e-h pair—see Fig. 2.3. We note that previous studies almost exclusively concentrated on this type of energy transfer. In accordance with our calculations and confirmed by the existing experimental data [66], the ground state energy of an exciton in our sample is in the 1.4 - 1.7 eV range. Recombination of such excitons (as well as "hot" excitons) can excite Er^{3+} ions exclusively into higher excited states: the second $^4I_{11/2}$, transition energy 1.24 eV, or the third $^4I_{9/2}$, transition energy 1.55 eV. In contrast to the excitation by hot carriers, this process requires transfer of a large momentum from the recombining carriers to the Er ion and, therefore, the interaction is dominated by the short range contributions [68]. Our calculation has shown that the excitation of Er^{3+} to the second or third excited states is very effective for Er^{3+} inside Si NCs or very close to their surface (at a distance of 0.2 - 0.4 nm). In this case, excitation time (τ_1) is smaller than 100 ns, and increases exponentially with distance. Following an energy transfer from Si NC, relaxation of Er^{3+} ions to the first excited state takes place, resulting in 1.5 μm emission. We have experimentally determined this relaxation time as $\tau_2 \lesssim 2.6$ μs, by measuring the rise of the 1.5 μm PL in SiO_2:Er under resonant pumping to the $^4S_{3/2}$ level. Thus, excitation of

the $^4I_{13/2}$ level is in this case a two-step process with a characteristic time $\tau_{eff} = \tau_1 + \tau_2$. It will manifest itself as a (relatively) slow rise of the 1.5 μm PL correlated with the simultaneous intensity decrease of the excitonic band, in agreement with the measurement depicted in the inset to Fig. 2.2. Er^{3+} ions excited in this way will then decay predominantly radiatively with a long time constant in the ms range—regime III in Fig. 2.2. As evidenced by the experimental data in the inset to Fig. 2.1, only a small part of Er^{3+} ions (of the order of 0.5%) can participate in this "slow" PL. Since exclusively this type of Er PL was considered in previous studies, this explains why only contribution from a minor part of all the dopants has been accounted for.

Finally, we address a specific case of a number of Er^{3+} ions which might be located inside Si NCs. Here one may expect that an Er-related donor state is formed, in analogy with the situation of crystalline Si:Er, with ionization energy of ~ 0.2 eV [71], as discussed in the first section of the previous chapter 1.1. Therefore, in equilibrium conditions, an electron will be localized at a level in the band gap of a Si NC. Upon exciton recombination, this electron can compensate the energy difference and enable fast Auger excitation of Er^{3+} into the first excited state. However, the same electron will also induce fast Auger recombination of Er^{3+} (10 - 100 ns time scale). Therefore Er^{3+} ions inside Si NCs will contribute to the ultrafast Er PL band discussed before.

In conclusion, this section shows that there appears an efficient Auger process of energy exchange between carriers inside Si NCs and Er^{3+} ions. This process is responsible for both rapid generation of the $^4I_{13/2}$ excited state of Er^{3+} and its non-radiative quenching. In result, an ultrafast 1.5 μm PL band appears and quenches within the first microsecond after the laser pulse. The proposed energy transfer model has been confirmed by additional experiments which have shown that the relative intensity of this ultrafast band decreases upon lowering of hot carrier concentration as realized under (i) excitation at a longer wavelength, when "hot" excitons are not created, and (ii) lower excitation flux, when generation of hot carriers due to two-photon absorption and/or Auger processes (of energy relaxation or recombination) involving multiple excitons confined in the same Si NC is suppressed. As can be judged from Fig. 2.2, the amplitude of the non-radiatively decaying fast Er PL band is about two orders of magnitude higher than that of the "slow" one. Since we have established that the "slow" PL represents a contribution of $\sim 0.5\%$ of the total Er content, this result implies that about 100 times more dopants can also be excited but decay non-radiatively, contributing to the "ultrafast" PL band identified in this study. Our estimations show that about 50% of all Er is involved in this fast energy exchange process. It is therefore clear that investigations of optical gain in SiO_2 sensitized with Si NCs should concen-

trate on the time domain of the first microsecond after the laser pulse, when population inversion can be possibly realized.

As a side remark, we note that the efficient non-radiative quenching, induced by Si NCs, rendering PL decay up to 2 orders of magnitude faster than ever reported for Si:Er [72], enables GHz modulation of Er-related 1.5 μm emission and therefore opens new application horizons for light emitting devices based on Si:Er.

2.2 Energy transfer processes between Si NCs and Er^{3+}

We present a high-resolution photoluminescence study of Er-doped SiO_2 sensitized with Si nanocrystals (Si NCs). Emission bands originating from recombination of excitons confined in Si NCs, internal transitions within the 4f-electron core of Er^{3+} ions and a band centered at $\lambda \approx 1200$ nm have been identified. Their kinetics have been investigated in detail. Based on these measurements, we present a comprehensive model for energy transfer mechanisms responsible for light generation in this system. The key problem of this section is energy transfer between silicon nanocrystals and Er^{3+} ions in a SiO_2 matrix. A unique picture of energy flow between these two subsystems is developed, yielding a truly microscopic information on the sensitization effect and its limitations. In particular, we show that most of the Er^{3+} ions available in the system are participating in the energy exchange. The long standing problem of apparent loss of optical activity of majority of Er dopants upon sensitization with Si NCs is clarified and assigned to appearance of a very efficient energy exchange mechanism between Si NCs and Er^{3+} ions. Application potential of SiO_2:Er sensitized by Si NCs is discussed in view of the newly acquired comprehensive description.

2.2.1 Introduction

In section 2.1 and [73], sub-μs Er-related luminescence in the SiO_2:(Er, Si NCs) system was reported, and an Auger-facilitated energy transfer process between carriers within the quantized levels of the NCs and Er^{3+} was proposed as the excitation and de-excitation mechanism. It was also shown that up to $\sim 50\%$ of the total Er content is involved in this process and contributes to the sub-μs emission. In this section, we study in depth temporal details of emission bands from SiO_2:(Er, Si NCs). Using optical excitation with nanosecond pulses and time-correlated photon counting detection mode, we resolve true kinetics of emissions related to Si NCs and Er^{3+} ions present in the investigated material. Based on this information, we propose a complete microscopic scenario of energy transfer processes in the SiO_2:(Er, Si NCs) system. The chosen approach allows us to identify emissions from most of the Er dopants available in the material. Using a theoretical model, we discuss microscopic aspects of energy transfer processes between Si NCs and Er^{3+} ions and comment on their (mutual) location in the SiO_2 matrix.

2.2.2 Results

Photoluminescence spectra

Figure 2.4 shows the PL spectra of the investigated sample at RT and at 10 K. The measurements have been performed under pulsed excitation, with the pump laser at $\lambda = 450$ nm (2.75 eV), *i.e.* not in resonance with any internal transition of Er. The total time-integrated PL response of the sample is given, which reflects the number of photons emitted. Both, Er- and Si NC-related PL bands are observed simultaneously, with their mutual intensity ratio determined by the Er concentration, in agreement with earlier studies [64]. In addition, at low temperature, a weaker band centered at $\lambda \approx 1200$ nm can be seen; it has a short decay time constant and therefore its time-integrated intensity is small compared to the other two bands.

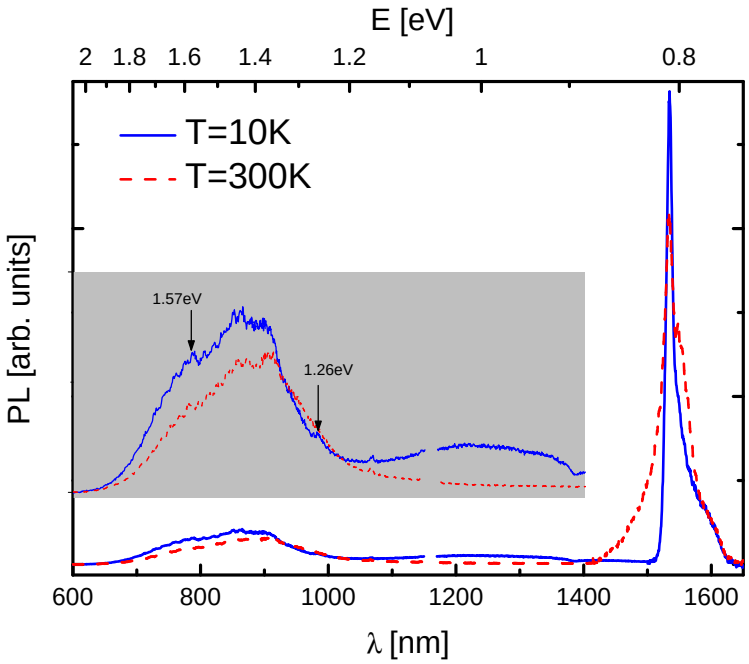

Figure 2.4: *Time-integrated PL spectra at $T = 10$ and 300 K, and excitation wavelength $\lambda_{exc} = 450$ nm. Si NCs, Er-related, and a third (at low T) PL bands can be observed. The Si NC-related band is blown up for clarity. The arrows show PL peaks related to emission from higher excited states of the Er^{3+} ion, superimposed to the NCs excitonic PL.*

We note that the Er-related emission band broadens at RT, keeping its wavelength integrated intensity practically constant, also in concordance with previous reports. The broadening at RT is produced mainly in the higher

energy side of the spectrum, and the full width at half maximum (FWHM) increases from $\sim$ 6.7 meV to $\sim$ 20 meV at 10 K and RT, respectively. This could be due to thermal population of upper states of the multiplet $^4I_{13/2}$ at RTc.

The Si NCs show a broad excitonic-related PL band. If we take into account the NCs size (R_{NC} = 1.55 nm) and dispersion ($\sim$ 14%), the position and width of the excitonic-related PL band can be estimated on the basis of the calculated band gap of the NCs as a function of their size [74]. The emission energy is given by $E = E_g^{Si}$ + E1e + E1h - E_{excit} - $\hbar\omega \approx$ 1.46 eV (with E_g^{Si}, E1e, E1h, E_{excit}, and $\hbar\omega$ corresponding to the energy band gap of crystalline silicon, the electron and hole levels quantization corrections, the excitonic correction, and the phonon value, respectively—the value for E_{excit} is taken from reference [74]—, and $\hbar\omega$ = 60 meV), *i.e.* a band centered at 850 nm, ranging from $\sim$ 820 nm to $\sim$ 870 nm taking into account their size dispersion. Comparison with experiment shows that the center of the band is in very good agreement with the expected value but the experimentally recorded band is broader than expected from the calculations, with the higher energy side of the band suffering from strong temperature quenching. Optical excitation was provided by short wavelength photons of 450 nm (2.75 eV), thus creating hot carriers in the higher energy states of the Si NCs, then it is reasonable to consider the origin of the higher energy side of the NC-related PL band as arising from "hot" carriers in the upper electron (and/or hole) levels of the Si NCs.

Superimposed on the Si NCs PL band recorded at 10 K, peaks with positions at 1.26 eV and 1.57 eV are observed. These correspond to emissions from the second and the third excited states of Er and disappear at room temperature. We note that in view of the exclusively non-resonant excitation mode, the observation of these peaks indicates that the Er^{3+} excitation proceeds, at least partly, via higher excited states.

The effective lifetime of the excited state of Er in SiO_2 with Si NCs lies within 2-3 ms. Decay of excitons in Si NCs is governed by a stretched exponential function, with a long final tail, with decay time constant of 20 μs to 50 μs as will be shown later. The decay of the band centered at $\lambda \approx$ 1200 nm is clearly faster, being predominantly non-radiative; the lifetime shortens further at a higher temperature, leading to a strong reduction of the time-integrated PL intensity of this band at RT.

High-resolution photoluminescence kinetics

Using the time-correlated photon-counting technique to resolve the time evolution of the PL transient revealed new insight into excitation and de-excitation

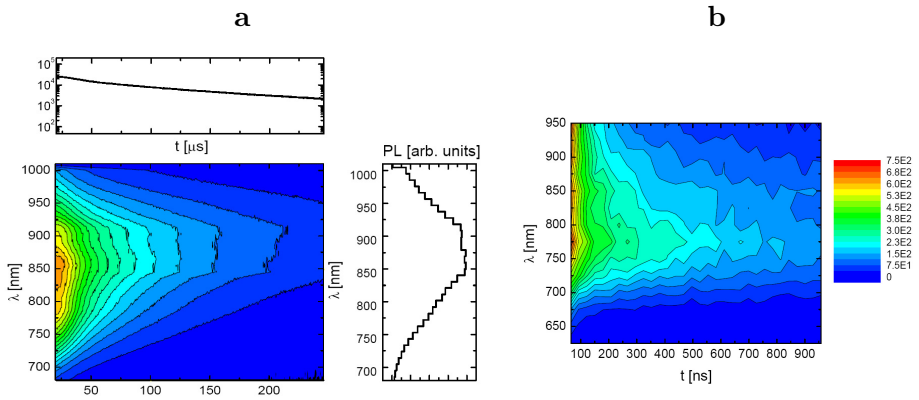

Figure 2.5: *Time-resolved contour plot of the PL spectrum of the Si NCs excitonic-related band, in the microseconds (***a***) and in the sub-microsecond (***b***) time ranges. The PL intensity (color contour plots) is represented as a function of time (X axis) and detection wavelength (Y axis). Panel* **a** *also shows the spectrum recorded at* $t = 100\ \mu s$*, and the PL decay at* $\lambda = 850$ *nm (sections from the contour plot). Drift of the band maximum toward longer wavelength is observed for longer time delay in panel* **a**. *Note the difference between the center of the bands in both figures (*≈ 200 *meV).*

dynamics in the SiO_2:(Er, Si NCs) system [73]. This experimental technique allows for simultaneous recording of very different dynamical ranges without suffering from signal distortion.

Panel **a** in Fig. 2.5 presents a time-resolved PL spectrum of the excitonic PL band from Si NCs. The contour plot shows how the peak of maximum intensity of luminescence drifts to longer wavelengths—*i.e.* lower energy—at longer delays. Consequently, the PL decay constant of the luminescence increases for longer wavelengths. This is understandable when we consider the NCs size distribution: excitonic PL dynamics in smaller NCs is faster than in larger quantum dots, as a result of the enhanced electron/hole wavefunctions overlap due to stronger confinement. In the panel **b** of the figure, the time-resolved PL spectrum of Si NCs is shown in the sub-microseconds time range; we can observe the center of the band at $\lambda = 775$ nm (1.6 eV), in contrast to the previous figure. If we compare the spectra measured at 100 ns and at 100 μs after the excitation pulse, a difference of ≈ 200 meV separates the centers of the two bands. We can assign the sub-microsecond PL to recombination of carriers from the higher Si NC states.

Figure 2.6 shows measurements related to the broad PL band appearing in the spectral range between the NC- and Er-related emissions. In the inset, the spectrum recorded at 200 ns (with a time window of 2 ns) after the excitation

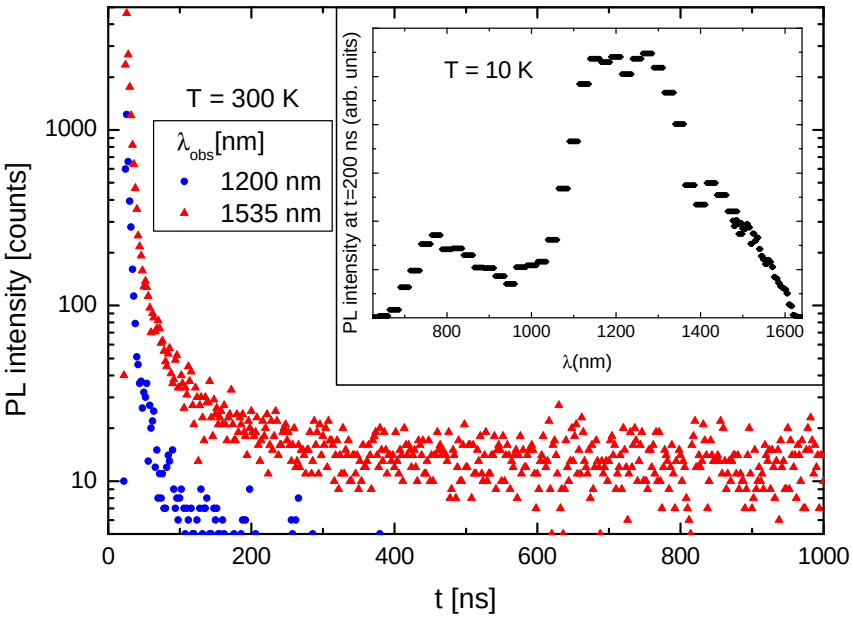

Figure 2.6: *Room temperature PL decay kinetics recorded at λ = 1200 nm (maximum of the PL broad band shown in Fig. 2.4) and λ = 1535 nm. In the inset, the spectrum recorded at t = 200 ns (with a time window of 2 ns) after the laser excitation pulse, at T = 10 K, is shown.*

pulse, at T = 10 K, shows the broad band centered at $\lambda \approx 1200$ nm. The lifetime of this PL band, as mentioned before, shortens at higher temperatures, becoming practically negligible at RT. This can be seen in the main panel, where the RT PL transient kinetics recorded at the maximum of the band (1200 nm) is compared to the Er-related PL at 1535 nm. The origin of the band centered at $\lambda \approx 1200$ nm is usually identified as recombination at defects, but its broadness and fast kinetics seem to contradict this identification; future investigations—outside of the scope of this thesis—may elucidate this point.

In Figure 2.7, the high-resolution kinetics of the excitonic luminescence from Si NCs can be followed in the panel **a**. An intense PL signal with a fast decay, also characterized in the sub-μs time domain, is observed after the excitation pulse. This is stretched until the final slower tail—in the order of 30 to 50 μs—is achieved, as shown in Figure 2.5. Panel **b** of the same figure shows the Er-related PL kinetics for the first microsecond after the excitation pulse, at T

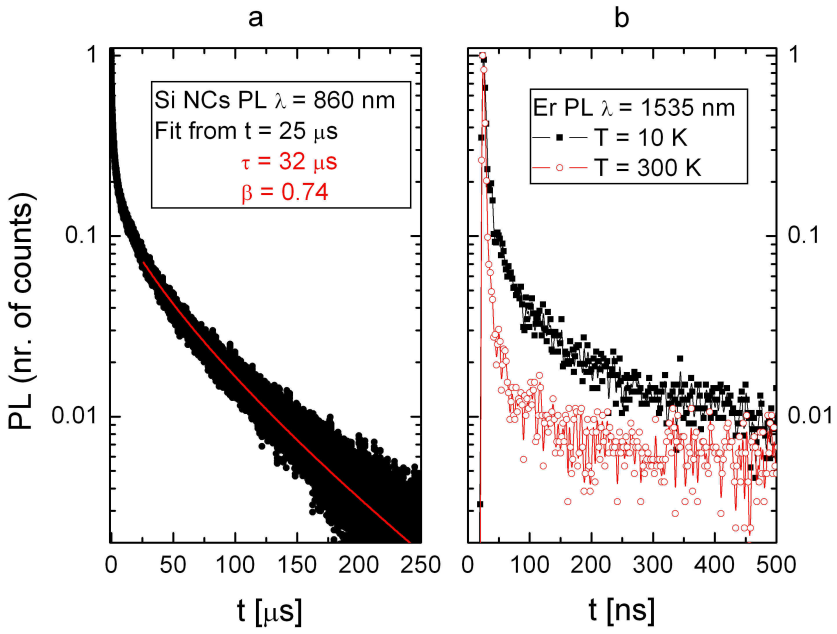

Figure 2.7: *In panel* **a***: Si NCs PL kinetics, recorded at λ = 860 nm, and room temperature; time resolution of the system was 2 ns. Excitation was provided with a 5 ns pulse, at λ_{exc} = 450 nm. Initial nanoseconds decay is stretched and followed by a final decay with characteristic lifetime of thick microseconds. In panel* **b***: Er-related 1.5 μm PL kinetics for the first microsecond after the excitation pulse is shown, at T = 10 K and RT.*

= 10 K and RT; this time regime corresponds to the region labelled as *Region I* in Fig. 1.2, discussed in the previous section 2.1.

As shown previously in section 2.1 and reference [73], the microsecond rise of the Er-related PL transient, $\tau_{Er}^{rise} \approx 3.5$ μs, is paralleled by the decay of Si NCs PL, characterized by a stretched exponential with a time constant of $\tau_{NC} \approx 1.2$ μs, on that time scale. We note that the indicated relatively fast decay of Si NCs luminescence slows down once Er emission attains its maximum. At this stage the nanocrystals-mediated excitation of Er is completed or saturated [61] and its further decay at the NC-related PL is decoupled from Er. Careful inspection of Fig. 2.2 reveals that this is not originating from zero: the rise of the Er-related PL characterized by $\tau_{Er}^{rise} \approx 3.5$ μs begins at about 50% of the maximum achieved intensity, as also observed in previous works [75].We conclude that the "residual concentration" of Er^{3+} ions involved in this process amounts to $\sim 0.2\%$ of the total Er content.

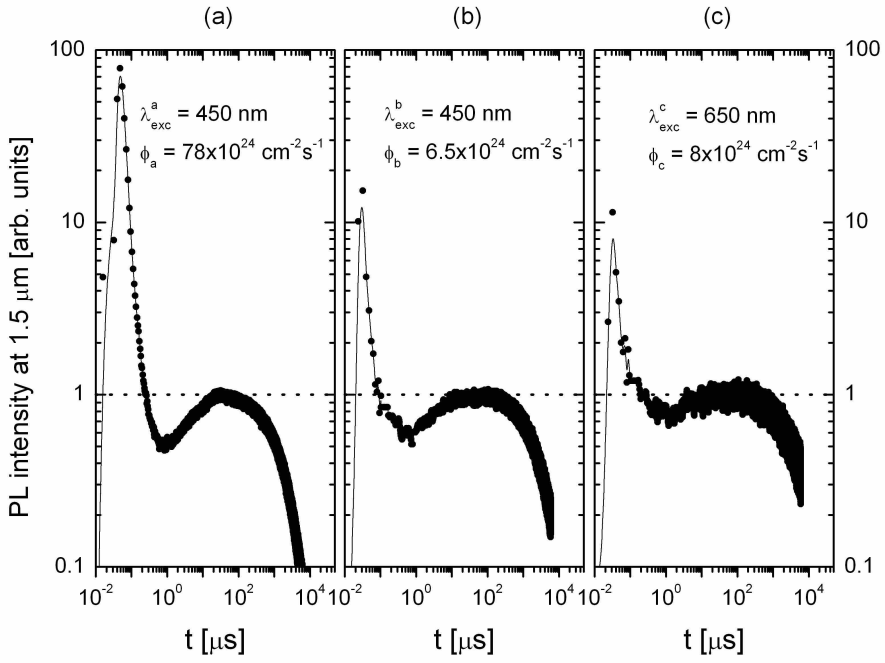

Figure 2.8: *Er-related PL kinetics, in double logarithmic scale for different excitation conditions, at RT. Intensity has been normalized to the maximum of the 'slow' component, in order to compare the fast-to-slow intensity ratio. In panels (***a***) and (***b***) the excitation wavelength (450 nm) has been kept constant, and flux has been decreased about one order of magnitude. In panels (***b***) and (***c***), flux has been kept in the same order of magnitude, and wavelength excitation has been increased to 650 nm.*

To validate the idea of hot carriers in the Si NCs being responsible of the submicrosecond Er-related luminescence—postulated in Sec. 2.1—, we investigate the intensity ratio between the fast and the slow components of Er PL for different excitation wavelengths and fluxes. Both, fast (nanoseconds) and slow (micro- and milliseconds) components of the Er-related transient PL must be governed by different excitation and de-excitation mechanisms. The intensity ratio of these components is thus likely to depend on the excitation conditions. Figure 2.8 shows full, high-resolution kinetics of Er^{3+} PL, under different excitation wavelengths and powers, normalized for the maximum intensity of the *slow* component. One can observe a higher *fast*-to-*slow* intensity ratio when higher power or larger photon energy quantum are used for excitation.

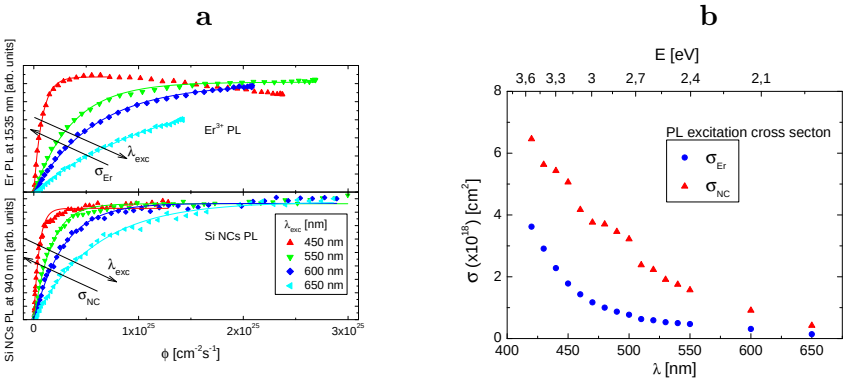

Figure 2.9: *In panel* **a**, *flux dependence of* Er^{3+} *and Si NCs PL for several excitation wavelengths is shown, recorded at RT. Equation 2.1 was used to fit the curves in the left side of the figure—***a**—*to obtain the PL excitation cross section of* Er^{3+} *and Si NCs PL, depicted as a function of excitation wavelength in the panel* **b** *of the figure.*

Excitation cross section measurements

The excitation cross section of Si NCs and Er PL, σ_{NC} and σ_{Er}, respectively, is of crucial importance to understand the excitation processes and energy transfer between Si NCs and Er^{3+} ions. In order to gain insight into this aspect, flux dependencies of Si NCs- and Er-related PL signals were recorded; a reference sample without Er doping was used for the NC-related PL measurements. In Figure 2.9, PL flux dependencies for different excitation wavelengths are shown, recorded at 1535 nm and 940 nm, for the Er-doped and Er-free samples, respectively. The curves have been fitted to the excitation dependence of PL intensity, derived from the rate equations for pulsed excitation—see equations B.8 and B.9 in Appendix B—,

$$I_{PL} \propto N^* = N(1 - e^{-\sigma\phi\Delta t}) \tag{2.1}$$

where I_{PL} is the time-integrated PL intensity, in arbitrary units; N^* is the number (concentration) of excited emitters (Er^{3+} ions or Si NCs, considering a limit of one radiative exciton per Si NC); N is the total number (concentration) of excitable Er^{3+} ions or NCs; σ is the effective excitation cross section; ϕ is the photon flux of excitation; and Δt the laser pulse duration. The effective excitation cross section, σ, is determined from the linear growth at low flux excitation. This is depicted for both, Si NCs and Er luminescence (σ_{NC} and σ_{Er}), as a function of the excitation wavelength in the panel **b** of the figure.

Directly related to the effective PL excitation cross section σ_{PL}, we studied the optical absorption coefficient α in our SiO_2:Si NCs reference sample. In the inset to Figure 2.10, the measured α_{NC} values are compared to those reported

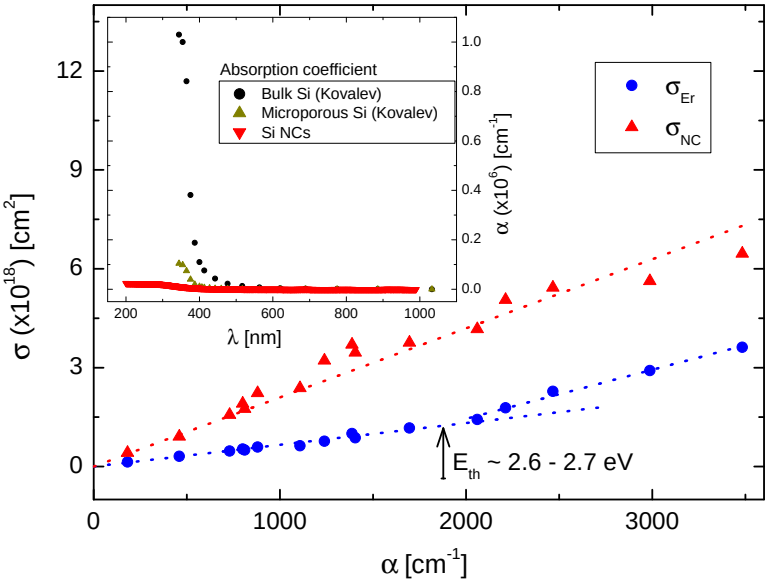

Figure 2.10: *Er- and Si NC-related effective excitation cross section σ_{PL} as a function of the optical absorption coefficient α measured for Si NCs, for each given excitation wavelength. In the inset, optical absorption coefficient is shown, measured in the investigated Si NCs, as a function of the wavelength, compared to values for bulk and microporous Si, previously published by Kovalev et. al [70].*

for microporous and bulk Si [70]. As can be seen, a considerable difference appears for shorter wavelengths.

The effective (Er- and NCs-related) PL excitation cross section values—Fig. 2.9—are plotted in the main panel of Fig. 2.10 as a function of the measured Si NCs' absorption coefficient α, as a function of excitation wavelength λ_{exc}. A linear relation between absorption and excitation can be observed in all the investigated range for Si NCs; in the case of Er-related luminescence, a change of the linear relation is observed at an energy threshold of $E_{th} \approx 2.6$ - 2.7 eV ($\approx$ 460 - 470 nm), energy above which the excitation cross section grows faster with the absorption.

2.2.3 Theory

In order to analyze the experimental results gathered in this section, we consider the possible processes of energy exchange between carriers confined in Si NCs and Er^{3+} ions in SiO_2 (outside NC).

Energy transfer between electrons and holes in NCs and f-electrons of Er^{3+} ion is implemented as an Auger process (*i.e.* via the Coulomb interaction). The energy can be transferred to an erbium ion either when a confined electron-hole pair recombines, or when an intra-band transition of confined carrier occurs. Both processes can be accompanied by multiphonon transitions to fulfill the energy conservation law, as the energy spectra of both electron systems are discrete. The momentum conservation law plays an important role in the Auger recombination processes as the large momentum should be transferred by the electron-hole recombination due to the indirect band structure of silicon.

Confined electrons and holes energy levels as well as their wave functions calculated in the multiband effective mass approximation [76] are used in this consideration. Details can be followed in the Appendix A.

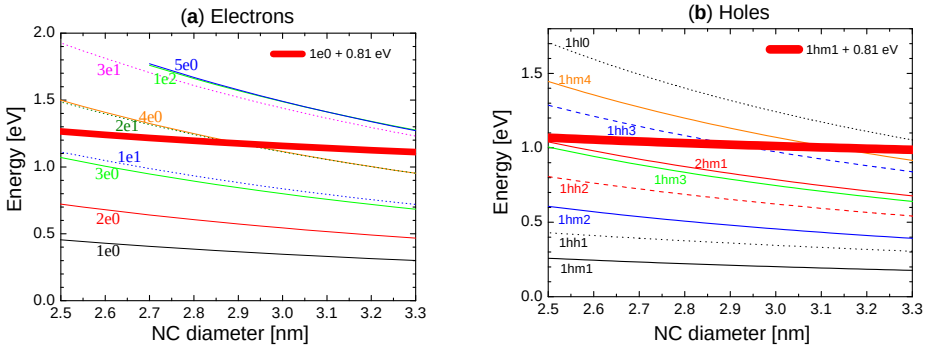

Figure 2.11: *Electrons* (**a**) *and holes* (**b**) *energy levels in Si NCs in* SiO_2*, as a function of NC diameter. The red stripe indicates the target energy range for transition from the ground level.*

The calculated lower energy levels of electrons and holes confined in Si NC of diameter in the range 2.5 nm – 3.3 nm are shown in Fig. 2.11. The energy range is limited to the one of optical pumping used in experiments (2.75 eV). Due to the large energy difference between neighboring space quantization levels energy relaxation of "hot" confined carriers is suppressed. Thus, the Auger excitation of erbium ions in silicon dioxide is possible, similar to impact ionization by hot carriers in bulk silicon, where it plays a significant role in electroluminescence, but just negligibly affects the excitation of erbium photoluminescence due to the fast energy relaxation of hot carriers in the bulk material.

Excitation due to intra-band transition

The transitions yielding the energy required to get the Er^{3+} ion into the first excited state $^4I_{15/2}$ (0.81 meV) with reasonable excess or shortage of energy, which can be covered by emission or absorption of phonons are summarized in Table 2.1.

Transition	$\boldsymbol{I_{i'i}(R)}$
$1hl_0 \rightarrow 1hm_2$	1.6×10^{-2}
$1hl_0 \rightarrow 1hm_1$	1.8×10^{-1}
$1hm_4 \rightarrow 1hm_1$	3.4×10^{-5}
$1hm_4 \rightarrow 1hh_1$	2.4×10^{-1}
$1hh_3 \rightarrow 1hm_1$	1.7×10^{-3}
$3e_1 \rightarrow 2e_0$	1.6×10^{-2}
$3e_1 \rightarrow 3e_0$	4.0×10^{-2}
$3e_1 \rightarrow 1e_1$	5.3×10^{-3}
$5e_0 \rightarrow 2e_0$	3.7×10^{-3}
$1e_2 \rightarrow 2e_0$	4.1×10^{-3}
$2e_1 \rightarrow 2e_0$	4.4×10^{-2}
$2e_1 \rightarrow 1e_0$	1.1×10^{-2}
$4e_0 \rightarrow 1e_0$	2.1×10^{-3}

Table 2.1: *Intra-band transitions suitable for 1.55 μm erbium luminescence excitation.*

The probability of Auger excitation of an erbium ion situated in SiO_2 at the distance a from the center of a Si NC as the result of the transition of a "hot" confined carrier from the state i into the state i' is given by the Fermi golden rule:

$$W_{i'i} = \frac{2\pi}{\hbar}\frac{1}{N_f}\sum_{ff'}\left|\langle f', i'|e\Phi|f, i\rangle\right|^2 J_T(N)\delta(E_i - E_{i'} - \Delta_{ff'} - N\hbar\omega_{\mathrm{ph}}), \quad (2.2)$$

where Φ is the potential created by the f-electron of the Er^{3+} ion; f, f' enumerate the states of f-electrons of the ion; and N_f is the degeneracy degree of the f state. The integration in the matrix elements of Eq. (2.2) is to be produced over the carriers confinement space.

Following the Appendix A.1, one finally gets for the probability of excitation:

$$W_{i'i} = \frac{\pi}{2\sqrt{\varepsilon_2}}\frac{1}{\tau_{\mathrm{rad}}}\frac{1}{R^4}\left(\frac{\hbar c}{\Delta_{ff'}}\right)^3\frac{e^2}{\varepsilon_2^2\Delta_E}I_{i'i}(a)J_T(N), \quad (2.3)$$

where ε_2 is the dielectric constant in SiO_2, $\tau_{\rm rad}$ the radiative lifetime of the erbium ion in the first excited state ($^4I_{13/2}$), R the radius of the NC, $\Delta_{ff'}$ the transition energy, Δ_E the value of the optical phonon in bulk Si, $I_{i'i}$ is a dimensionless factor defined in A.28, and $J_T(N)$ the phonon factor (A.5).

From (2.3) one gets using values $\tau_{\rm rad} = 2$ ms, and $R_{NC} = 1.55$ nm:

$$W_{i'i} = 8.3 \times 10^9 \left(\frac{1.55\text{nm}}{R}\right)^4 I_{i'i}(a) J_T(N) \text{ s}^{-1}. \tag{2.4}$$

The results of calculations of the factors $I_{i'i}(a)$ for electrons are shown in

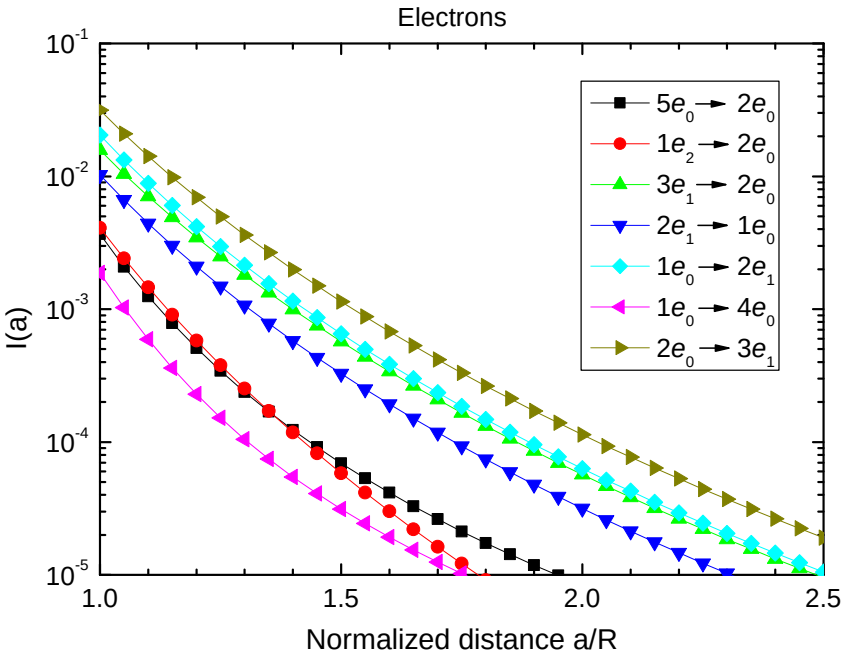

Figure 2.12: *Factors $I_{ii'}$ for erbium excitation/de-excitation by electron intra-band transitions.*

Fig. 2.12. Corresponding plots for holes can be found in [77]. It has been shown, that $I_{i'i}$ are actually functions of the relation a/R only, at least for NC sizes in the range 2.4–3.3 nm.

Producing the calculations analogous to the ones described in A.1 for the carriers being inside the NC, one can find that the contribution of confined carriers tunnelling to the excitation probability is given by an expression similar to Eq. 2.3 (A.20). Our calculations have shown that the input is negligible.

The parameters of the multiphonon transition accompanying the Auger processes are not well defined. There is no data on the electron-phonon interaction for Er^{3+} ions in the state $^4I_{13/2}$ in SiO_2. Thus, the interaction of confined carriers with optical phonons should be considered. The dispersion of optical phonons in bulk silicon can be neglected and the multimode model of the phonon transition becomes equivalent to the one-mode Huang-Rhys model [78]. Phonon factor $J_T(N)$ is presented in Table 2.2 calculated with a reasonable value of Huang-Rhys parameter $S = 0.1$ at room temperature. The interaction with optical phonons is forbidden for electrons in silicon, so one can suppose that the interaction of confined carriers with oxygen vibration is also responsible for multiphonon assisted Auger processes in the system under consideration. The values of phonon factor $J_T(N)$ at $\hbar\omega_{\rm ph} = 140$ meV corresponding to the oxygen vibrations are shown in Table 2.2 as well.

N	-2	-1	0	$+1$	$+2$	$+3$
$\hbar\omega_{\rm ph} =$ **60 meV**	5.2×10^{-5}	0.0096	0.87	0.098	0.0054	0.2×10^{-3}
$\hbar\omega_{\rm ph} =$ **140 meV**	9.0×10^{-8}	0.0004	0.9	0.091	0.0046	0.15×10^{-3}

Table 2.2: *Phonon factor $J_T(N)$ calculated with $S = 0.1$ for two different phonon energies $\hbar\omega_{\rm ph}$ and temperature $T = 300$ K.*

De-excitation of erbium by carriers confined in NCs

When considering erbium de-excitation due to intra-band transitions of confined carriers, one can use the same formulae from Sec. 2.2.3 (Appendix A.1), but interchanging initial and final states, as well as adjusting the phonon factor $J_T(N)$. If erbium excitation process takes place with carrier transition energy larger than $\Delta_{ff'} = 0.81$ eV and requires N phonons to be emitted, then the reverse process will be described by $J_T(-N)$ factor, which is much less than $J_T(N)$. That is why most of the processes appear either in excitation or in de-excitation section.

But not only the phonon factor is of importance here. One should also take into account that the transitions under consideration take place between degenerate states. So the total probability is achieved by summation over the final states and averaging over the initial ones. As the degeneracy degree can be different for initial and final states, the probability of excitation and de-excitation processes can be different even for those of them which do not need phonons. This difference might be considerable for confined carriers, especially for holes. Since most of upper levels are described by larger values of the total angular momentum F—see the description of the hole states in

Appendix A—, having greater degeneracy degree, the probability of erbium de-excitation should be higher for the processes which do not require any phonons to be emitted or absorbed.

The transitions of confined carriers which can assist erbium de-excitation are listed in Table 2.3 (only transitions from the first levels are considered). The plots of corresponding factors $I_{i'i}(a)$ have been published in Ref. [77].

Transition	$\boldsymbol{I_{i'i}(R)}$
$1hm_1 \rightarrow 1hh_3$	9.7×10^{-4}
$1hm_1 \rightarrow 2hm_1$	3.6×10^{-3}
$1hm_1 \rightarrow 1hm_3$	1.0×10^{-3}
$1hm_1 \rightarrow 1hm_4$	1.4×10^{-4}
$1hh_1 \rightarrow 1hh_3$	2.3×10^{-3}
$1hh_1 \rightarrow 1hm_4$	4.7×10^{-1}
$1e_0 \rightarrow 2e_1$	2.0×10^{-2}
$1e_0 \rightarrow 4e_0$	1.9×10^{-3}
$1e_0 \rightarrow 1e_1$	9.4×10^{-2}
$1e_0 \rightarrow 3e_0$	4.0×10^{-3}
$2e_0 \rightarrow 3e_1$	3.2×10^{-2}

Table 2.3: *Intra-band transitions suitable for erbium de-excitation from the first excited state due to confined carrier transition*

Red stripes in Fig. 2.11 mark the energy range of Δ_E width corresponding to the energies of possible transitions from the ground electron and hole levels, which are responsible for erbium luminescence quenching. One can see that such transitions are mostly suppressed for NC diameters in the range from 2.8 to 3.3 nm. The scheme in Fig. 2.13 shows electron and hole intra-band transitions, inducing erbium excitation and de-excitation most effectively for NC size in the range 2.55–2.85 nm, and 2.8–3.3 nm. (The calculations for the range 2.55 to 2.85 nm have been performed analogously to the described for the range 2.8 to 3.3 nm.) The corresponding probabilities are shown in Fig. 2.14, panels **a**—averaged over the range of NC diameter 2.55-2.85 nm—and **b**, respectively.

Erbium excitation by the recombination of confined carriers

Let us consider the excitation of Er^{3+} ions by recombination of confined electron and hole. For the NCs under consideration ($d \sim 3.1$ nm) the recombination energy is larger than 1.5 eV. Therefore the energy transfer to the Er^{3+}

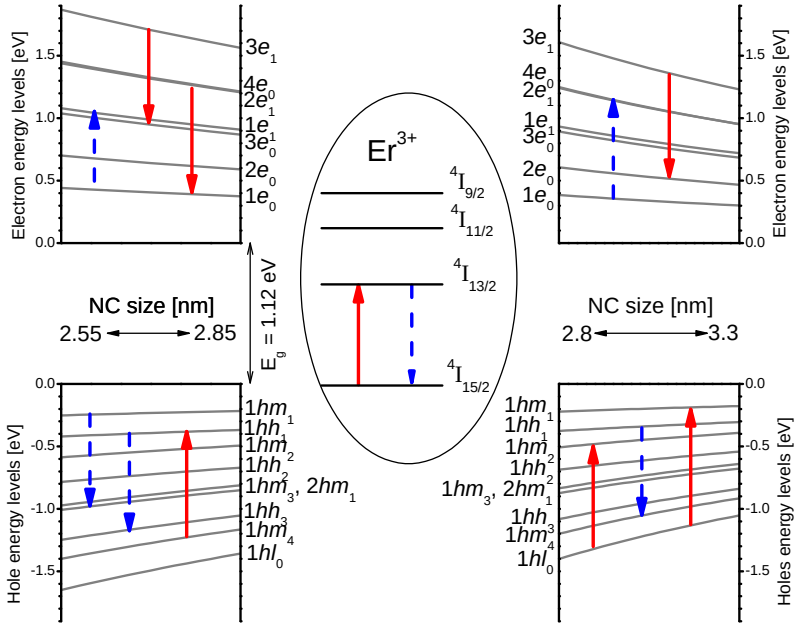

Figure 2.13: *Energy levels in Si nanocrystal of diameter $D = 2.7$ nm and $D = 3.1$ nm, with dispersion in size of 14% in SiO_2, and the most effective transitions leading to Er^{3+} excitation and de-excitation.*

ion by an Auger recombination of such an exciton can be effective only if it causes the direct transition of the ion into the third excited state $^4I_{9/2}$ (energy of transition from the ground state $^4I_{15/2}$ is $\Delta_{03} = 1.55$ eV), the fourth $^4F_{9/2}$ (transition energy $\Delta_{04} = 1.9$ eV) or higher excited states. One should notice that Er^{3+} ions can not be excited directly into the state $^4I_{13/2}$ via such a process. In order to calculate the transition probability we can use formula (A.8), just assuming that initial and final states of confined carriers now belong to different bands and dividing the probability by the degeneracy of the final state, since only one final state is empty if there is one electron-hole pair in the NC. One should also choose appropriate parameters of the phonon system. The calculations can be followed in the Appendix A.2.

From the data presented in Table A.2, one can see that the electron-hole recombination can effectively excite an Er^{3+} ion situated inside the NC or at a very short distance from its boundary on a nanosecond or even shorter time scale. However, this ultrafast excitation process does not lead to an immediate excitation of the first $^4I_{13/2}$ excited state of the Er^{3+} ion relevant for the 1.55 μm emission. Transition to this state can occur only via a subsequent

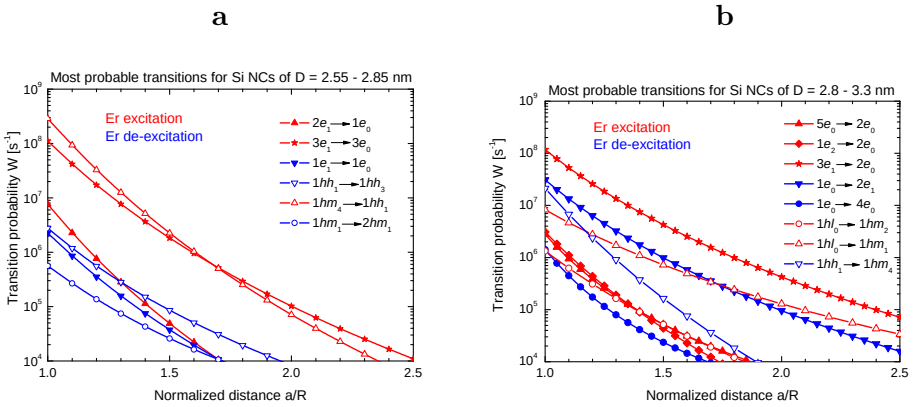

Figure 2.14: *The probability of Er^{3+} ion excitation and de-excitation by localized electrons and holes intra-band transitions for NC diameter being in range of 2.55–2.85 nm (panel* **a***) and 2.8–3.3 nm (panel* **b***).*

multiphonon relaxation process which takes place on a microsecond time scale.

Dipole-dipole contribution to the inter-band Auger process

When the erbium ion is situated at a distance $a \gg R$ one can expand the Coulomb interaction of the electron-hole pair in the NC with the erbium ion into the series over the coordinate of the confined carrier. In the leading order such an approximation results into the dipole-dipole interaction being the reason for the so-called Förster mechanism of excitation [79]. In this case the large excess momentum of the confined pair is transferred to the boundary of the NC in the process of recombination or the recombination is accompanied by emission of a phonon as in the radiative exciton recombination [76].

Calculations in A.3 show that the Förster mechanism does not work effectively for the considered system, especially at some distance from the NC, because the radiative recombination of confined carriers is a faster process.

2.2.4 Discussion

Before comparing our microscopic model of energy transfer processes in the SiO_2:(Er, Si NCs) system with experiments and drawing conclusions, we summarize briefly the experimental findings which need to be accounted for:

PL spectrum

i The center of the observed Si NC-related PL band is in good agreement with the expected emission energy from Si NCs under consideration (main diameter 3.1 nm). The band is, however, broader than expected from the nanocrystals' size dispersion ($\sim 14\%$).

ii The higher energy side of the Si NCs spectrum band suffers from temperature quenching.

iii Integrated Er-related PL intensity is temperature independent. By increasing the temperature, the band broadens and the maximum intensity decreases, but the total integrated intensity remains constant. The broadening at RT is produced at the higher energy side of the spectrum band, only.

iv At 10 K, emission peaks at 1.26 and 1.57 eV—assigned to higher excited states of the Er^{3+} ions—appear, superimposed on the Si NC-related band.

Er-related PL kinetics

i Immediate rise following the laser pulse, indicating a fast excitation, completed within ~ 20 ns.

ii Fast de-excitation: Er-PL decays initially with a time constant of 5-10 ns, followed by a slower decay with $\tau \approx 100$ ns.

iii A separate channel of microseconds excitation (paralleled by Si NC-related de-excitation), followed by the final milliseconds radiative decay.

iv The intensity ratio of the fast and slow decay components of Er^{3+} PL depends on the excitation conditions; a higher excitation flux or a higher excitation photon energy, results in an increase of the fast-to-slow PL intensity ratio.

v The microseconds rise of the Er-related PL dynamics does not originate from zero. There is a "residual concentration" of Er^{3+} ions that are excited in the sub-microseconds time window and decay radiatively.

Si NC-related PL kinetics

i Three decay regions: sub-μs decay, followed by a slower stretch exponential with a time constant of the order of a few μs, and final decay with τ in the 50 - 100 μs.

ii Time-resolved PL spectrum: The spectral maximum shifts toward lower energies for longer delays, *i.e.* the lifetime increases at lower emission energies. The spectrum measured for the sub-μs time region is blue-shifted in comparison to the spectrum measured at the "tail" of the PL decay.

Excitation cross-section and absorption measurements

i Absorption coefficient for Si NCs diverges from those of bulk-Si and microporous Si at shorter wavelengths.

ii Effective excitation cross-section of Er^{3+} PL does not scale with the absorption coefficient for shorter wavelengths than $\lambda \lesssim 500$ nm, for which the excitation cross section increases faster than the absorption. In contrast, the excitation cross section of Si NCs PL follows a linear relationship with the absorption coefficient, for the investigated range $\lambda \geq 420$ nm.

In what follows, we are going to use the outcome of our theoretical calculations, in order to describe and explain our experimental results. We have shown that the quickest excitation processes of the first excited state of the Er^{3+} ion proceed via the intra-band cooling of carriers confined in the NC. Further, we have also established that Er^{3+} ions in contact with the Si NC can also acquire excitation due to the recombination of carriers in the NC. The Auger process with the carriers recombination induced by the dipole-dipole interaction has been ruled out from the relevant excitation processes—see Sec. 2.2.3. The excitation and de-excitation rates of the Er^{3+} ion —shown in Fig. 2.14 as a function of the distance to the NCs, for the most probable transitions—are the inverse of the characteristic excitation and de-excitation times, which have been recorded experimentally.

We begin by quantifying the percentage of Er^{3+} ions subjected to a particular excitation/de-excitation processes summarized in Fig. 2.13. We have generated a simulation of the Er^{3+} distribution as a function of the distance from the nearest Si NC—see Fig. 2.15. This is based on the concentration of Er and NCs, 2.8×10^{19} cm^{-3} and 4.13×10^{18} cm^{-3}, respectively, and mean volume of Si NCs ($V_{NC} = 1.56\times10^{-20}$ cm^3), assuming a random distribution of both, Si NCs and Er^{3+} ions in the SiO_2 matrix. As can be seen, the majority of the Er^{3+} content, more than 90%, is positioned outside the NCs, only 6.6% of the Er^{3+} content would be placed inside the NCs volume. In addition to this statistical prediction, we note that considering the sample preparation method [64], during the annealing process a considerable part of the Er^{3+}

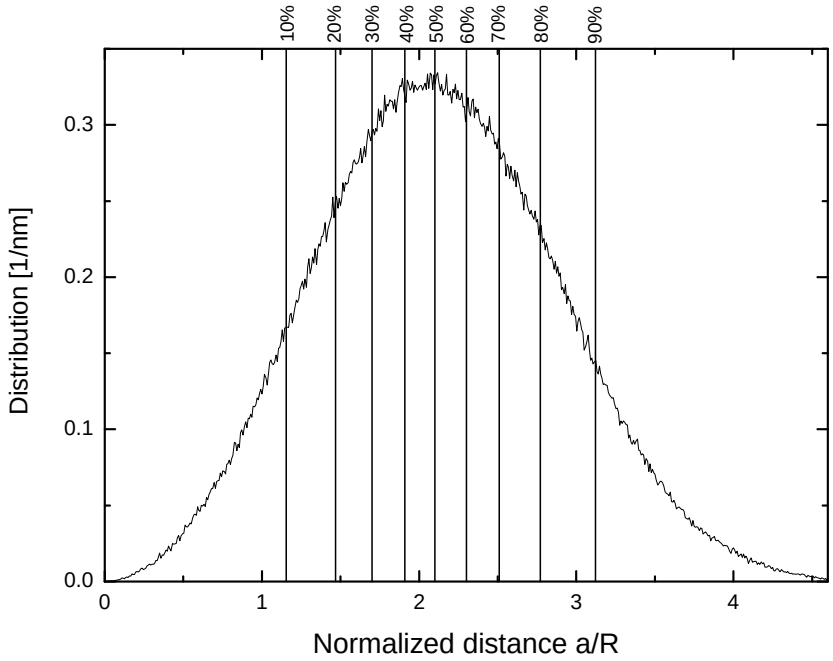

Figure 2.15: *Simulation of the distance distribution of Er^{3+} ions to the center of their nearest neighboring NC assuming a random distribution of both: 6.6% of the Er^{3+} ions are contained inside NCs.*

ions inside the NCs will be forced to the outside of a crystalizing NC and will diffuse to this surface layer. Consequently, it will become trapped at the Si NC/SiO_2 boundary. These Er^{3+} ions are susceptible of virtually instantaneous excitation directly into the first excited state, via direct absorption of photons. We also note that the Er^{3+} ions remaining in the NC will induce a donor center, as a result of which they will de-excite non-radiatively very fast. This fast-excitation-fast-de-excitation process is independent of temperature.

The observed fast (sub-microsecond) Er-related PL is only possible when Er^{3+} is excited directly into the first excited state $^4I_{13/2}$. When the excitation proceeds via higher excited states, the intrinsic relaxation time down to the first excited state, in the order of 1 to 2 μs, prevents appearance of the sub-microsecond PL. For the Er^{3+} ions outside the NCs, the 'fast' transfer between Si NCs and Er^{3+} into the first excited state is governed by an Auger-process accompanied by an intra-band transition of a confined carrier. In Fig. 2.14, we have presented the calculated probabilities of the Er^{3+} excitation, directly

into the first excited state, as a function of a/R (a is the distance to the NC, and R is the radius of the NC) for the most effective processes. These processes are illustrated schematically in Fig. 2.13. In the figure, the probabilities of de-excitation processes are presented too.

Under our excitation conditions, we estimate an average creation of about 5 electron-hole pairs per Si NC. As can be seen, the most effective process of excitation is given by the transition $3e_1 \rightarrow 2e_0$. We note that to create electrons in the $3e_1$ state under optical pumping, the photon energy must be $h\nu \geq 2.65$ eV. Alternatively, under conditions where more than one e-h pair are created in the Si NC, one carrier can be promoted to the mentioned $3e_1$ state by an Auger process involving a non-radiative recombination of another e-h pair (multiple exciton generation).

As we can see from Fig. 2.7, in panel **b**, the fast excitation of Er^{3+} ions is completed 20 ns after the excitation pulse, and we have estimated in the previous section and in [73] that $\sim 50\%$ of the Er^{3+} content is involved in this fast process. From Figs. 2.14 and 2.15, one concludes that, according to our calculations, after 20 ns ($W = (20\ ns)^{-1} = 5{\times}10^7\ s^{-1}$), about 10% of all the Er content in the sample could be excited by the process labelled as $3e_1 \rightarrow 2e_0$ (or $1hm_4 \rightarrow 1hh_1$ in the case of the calculations centered at a NC diameter of D = 2.7 nm). However, the calculation of probabilities has been produced for strictly spherical Si quantum dots; in this case, strong selection rules appear and only matrix elements of some higher multipoles of the electric field potential lead to considerable non-vanishing contributions, causing a strong decrease of the probability with increasing distance from Er^{3+} to Si NCs. *E.g.*, the Auger process accompanied by the $3e_1 \rightarrow 2e_0$ transition is dominated by the quadrupole-dipole interaction (the dipole is related to Er^{3+}). Therefore one expects that the real probabilities might be higher than the calculated ones, and will decrease less abruptly with distance, due to non-sphericity of Si NCs. This will improve the agreement with our experimental results.

In the previous section 2.1 we have estimated that $\sim 0.5\%$ of the total Er^{3+} ions decay radiatively ($\tau \sim 3$ ms) after excitation. From these 0.5% of ions, $\sim$ 50% have been excited due to the fast process, but have not been de-excited by the inverse mechanism: the "residual concentration". The other $\sim 50\%$ ($\sim$ 0.25% of the total Er^{3+} content in the sample) have been excited due to inter-band recombination of the carriers in the NC. In our theoretical considerations we have shown that the excitation via an Auger process, accompanied by the recombination of an exciton in the Si NC can only take place via contact—see Sec. 2.2.3. This excitation of Er^{3+} takes place into the second or higher excited state of the 4f shell of Er^{3+}. The characteristic excitation of the 1.5

μm Er^{3+} PL is, in this case, a two-step process with time constant $\tau = \tau_1 + \tau_2$, where τ_1 is the characteristic Er excitation into one of the higher excited states by the band-to-band recombination of confined carriers, on the nanosecond or even shorter time scale (see Table A.2), and $\tau_2 \approx 1.2$ μs is the relaxation time of the excited Er^{3+} from the higher into the first excited state $^4I_{13/2}$. This process is responsible for the μs rise of the Er-related PL signal.

Following the described model, one expects a dependence of the *fast*-to-*slow* Er^{3+} PL ratio on the number of "hot carriers" confined in the Si NCs: a high number of "hot" carriers will favor the fast intra-band excitation process and thus increase the relative importance of the "fast" Er^{3+} PL. This is indeed confirmed in Fig. 2.8, where we can see that under excitation conditions when creation of "hot" carriers is more likely, *i.e.* excitation with higher energy photons or high flux pumping and subsequent multiple carrier generation in the NCs, the fast-to-slow PL intensity ratio of Er PL increases. In the case of formation of several electron-hole pairs per Si NC, these can undergo a quick Auger recombination process, and in that way the excess pairs escape from participating in the "slow" excitation transfer process.

The sequence of excitation and de-excitation processes is therefore as follows:

i After the laser pulse, an Auger-like process of fast excitation takes place, by intra-band relaxation of "hot" carriers transferring their excess energy directly into the first excited state of Er^{3+} ion. Up to $\sim 50\%$ of all the Er^{3+} content is in the effective range of this interaction, before the de-excitation processes start to decrease the number of excited ions.

ii Fast de-excitation of Er^{3+} takes place by a reverse process, transferring energy to carriers confined in the NCs. This process must be phonon assisted when the involved transitions do not match the energy conservation requirements; which will manifest in a slower PL decay and temperature dependence of the characteristic decay constant. The "hot" carriers in the NCs undergo a quick intra-band relaxation, which reduces the number of carriers available for the "quick" excitation process.

   A small percentage of the excited Er^{3+} ions described in (i) will overcome the fast de-excitation, giving rise to the "residual concentration" of Er^{3+} which is excited in the nanoseconds time window, and de-excites radiatively. This is revealed in the Er^{3+} PL kinetics as the non-zero origin of the microsecond rise and subsequent radiative decay of Er^{3+} PL.

iii Once the confined carriers have cooled down to the bottom (top) of the conduction (valence) band, there is a probability of Er^{3+} excitation by

recombination, to the upper Er excited states, as described above. This probability exists also on shorter time scales, but the number of Er^{3+} ions which can be accessed is low, and therefore this inter-band process is covered by the intra-band excitation process.

Therefore, based on the presented experimental data and theoretical modelling, we conclude that three types of optically active Er^{3+} ions coexist in the investigated material:

- Type 1: Er^{3+} ions that can only be excited resonantly, under direct excitation. These ions have predominantly radiative decay—like Er^{3+} in SiO_2—and are at large enough distance from the Si NCs to prevent their interaction.

- Type 2: Er^{3+} ions that are excited by energy transfer from inter-band recombination of excitons in Si NCs, at the microseconds time regime and which decay predominantly radiatively ($\tau \sim$ 2-3 ms), independent of temperature. This type of Er^{3+} ions are those accounted for in the usual estimations of optical activity measurements and constitute about 0.25% to 0.5% of the total Er^{3+} content.

- Type 3: Er^{3+} ions excited via the intra-band transition of carriers in the NCs and with very strong non-radiative quenching, responsible for the sub-μs PL described above, whose properties mirror those of Er^{3+} in crystalline-Si ($\sim$ 50% of Er^{3+}). A small percentage of these ions, will overcome the fast non-radiative de-excitation, and will be also accounted for in optical activity measurements.

Finally, for the sake of completeness we note that in addition to these, there could also be Er dopants which are not optically active due to, *e.g.* precipitation.

An independent confirmation of the proposed excitation model of Er^{3+} ions by intra-band transitions of confined carriers in the Si NC is indeed given by Fig. 2.10. There, for excitation energy higher than $E_{th} \approx$ 2.6 - 2.7 eV, a new excitation mechanism appears, increasing the ratio between absorption and effective excitation cross section of Er PL. This threshold marks the energy which is sufficient to create a "hot" carrier that can excite Er^{3+} directly into the first excited state by cooling into the bottom of the conduction band (or the top of the valence band). The consequences of this are further discussed in the following section of this chapter, Sec. 2.3.

2.2.5 Conclusions

With the results of this study, an important puzzle concerning the mechanism of excitation of Er^{3+} by Si NCs has been solved. We have shown that the "missing" dopants that were apparently losing optical activity upon doping with Si NCs, and which did not contribute to PL, are actually very efficiently excited by the Si NCs, via an intra-band Auger transfer process, but undergo also a very effective excitation back-transfer process. The back-transferred carriers can again excite the Er^{3+} ion or escape from being available for the intra-band excitation process due to a thermalization and Auger recombination processes inside a NC. Such a kinetics leads to the effective recombination rate of Er^{3+} in the environment of Si NCs exceeding by two orders of magnitude the fastest quenching rate (due to the Auger process involving free carriers) reported, to our knowledge, for Er in crystalline Si. Future research will tell whether the SiO_2:(Er, Si NCs) material can be engineered in such a way that the sensitization of Er emission is realized without the detrimental effect of reduction of the concentration of Er^{3+} ions, and with the temperature-stable, predominantly radiative recombination. On the other hand, the very efficient PL quenching observed here for Er dopants inside Si NCs might be explored for GHz modulation of the 1.5μm emission from Er-doped structures.

2.3 Space-separated quantum cutting

For optimal energy conversion in photovoltaic devices (electricity to and from light) one important requirement is that the full energy of the photons is used. However, in solar cells a single electron-hole pair of specific energy is generated, regardless of the incoming photon energy once it is above a certain threshold, with the excess energy being lost to heat. In the so-called quantum cutting process, a high-energy photon can be divided into two, or more, photons of lower energy. Such manipulation of photon quantum size can then very effectively increase the overall efficiency of a device. In the current work, we demonstrate (space-separated) photon cutting by Si nanocrystals; nearby Er^{3+} ions and neighboring nanocrystals are used to detect this effect.

2.3.1 Introduction

One of the major problems in photovoltaic devices is the large range of wavelengths in which the energy conversion has to take place. As an example, a solar cell must work well in the visible range, where most energy is available, but should also be able to convert the ultra-violet (UV) and infrared (IR) parts of the spectrum, which still contain a substantial fraction of the solar energy. Effective harvesting of energy from UV and IR photons is a necessary condition for improving efficiency of solar cells and to reduce the cost-per-watt. On the smaller energy side, conversion is limited by the band gap E_g below which photon absorption is not possible. On the other side of the spectrum, for high-energy photons, a substantial part of the incoming photon energy $h\nu$ is often wasted in the conversion, as the energy excess $h\nu$-E_g is transformed into kinetic energy of the electron-hole pair, and subsequently lost to heat. Thus, a band gap-optimized *pn*-junction ("first generation") solar cell is a one-electron-hole-pair-for-one-photon device, whose (external) efficiency is limited to about 30%—the Shockley-Queisser limit [63]—, for a band gap of 1.1 eV, close to that of silicon. Even modern (organic) materials [80, 81] and device designs, such as thin-film devices [82] ("second generation"), or Grätzel cells of blended hole-transporting and electron-transporting materials [83] ("third generation"), do not escape from this theoretical limit. Stacked layers (tandem devices, "fourth generation") with the band gap of each layer optimized for a specific wavelength can increase the efficiency, at the expense of a higher complexity and cost of the device.

A similar situation takes place in light-emitting devices. Ideally, these should generate photons only in the visible range, whereas the existing devices often emit in a much wider spectrum, for instance fluorescent lamps. By using fluorescence, the energy of the emitted UV photons can be reduced

to the visible range, but also in this case, in the one-photon-for-one-photon down-conversion, a large part of the photon energy is lost.

For photovoltaic applications it is therefore very relevant to develop a scheme that allows using the excess energy otherwise lost in conversion. An elegant solution is to use quantum cutting. This process entails transformation of a high-energy photon into two (or more) photons of smaller energy, hence "cutting" the energy quantum. Ideally, the down-converted photons are in the suitable range of the spectrum and can be further used without loss of energy. Such a quantum cutting has been demonstrated in rare-earth systems [84] and found its usage in fluorescent tubes. A similar idea involves generation of multiple electron-hole pairs by a single high-energy photon absorbed in a nanocrystal . This process, termed MEG (multiple exciton generation) or CM (carrier multiplication), has indeed been observed in NCs made from different semiconductor materials [85–90], including a remarkable seven excitons for a single incoming photon [91]. Recently, it has also been demonstrated in colloidal silicon NCs [92]. Lifetimes of multi-excitons in a nanocrystal were found to be very short (50 -100 ps and shorter, depending on material and NC size [93]) due to the enhanced Auger recombination and subsequent fast carrier cooling [94]. Therefore, harvesting of this energy—via carrier extraction or light generation—is difficult, as only the "last" exciton has relatively long lifetime and is "useable".

In the present work we report on the observation of quantum cutting in NCs of silicon, still the most popular material for electronic and photovoltaic applications, embedded in a SiO_2 matrix. In this case we show that in the quantum cutting process, energy can be transmitted to outside the photo-excited system. In the piloting experiment, we employ Er^{3+} ions outside the nanocrystals as receptors of the down-converted energy and use their characteristic photoluminescence (PL) for detection of the phenomenon. Subsequently, we demonstrate that a similar space-separated quantum cutting (SSQC) process takes place between Si NCs themselves.

2.3.2 Results

In the PL experiments, the signal integration has been performed over the entire PL decay time window (typically from 1 to a few ms for NC- and Er-related PL, respectively), and the recorded PL intensity value therefore reflects predominantly contributions of relatively slow radiative processes. In particular, for the Er-related emission, only the ms component due to Er^{3+} ions in SiO_2 is accounted for, with contribution from fast decaying dopants [73]—see Sec. 2.2—being negligible. A Varian Cary-50 UV-VIS spectrophotometer was used for absorption measurements in the visible and the UV. All the measurements

described in this section were performed at room temperature.

In the first experiment the Er-related PL was monitored as a function of excitation wavelength and compared to the absorption of the sample at that wavelength. At the start of a cycle, a nanocrystal absorbs a photon and an electron-hole pair is created. Upon its recombination, one relaxation path will transfer the energy to a neighboring Er^{3+} ion, placing it in an excited state. Subsequently, the Er^{3+} ion relaxes back to the ground state by emitting a long-wavelength (IR) photon which can be detected as PL at 1535 nm. From this scenario it follows that the Er-related PL should be correlated to photon absorption by Si NCs. (It should be mentioned that under conditions of the experiment no direct absorption by Er takes place, and therefore any Er-related emission must originate by photon absorption in Si NCs.) From this it follows that the total number of photons emitted (by Er) should be correlated to the total number of photons absorbed (by Si NCs). In order to describe that we introduce the PL quantum efficiency, which we define as the ratio of number of photons coming out of the sample to the number of photons absorbed: $\eta = \mathrm{N}_{PL}/\mathrm{N}_{abs}$. Because, in our setup, the luminescence intensity is not calibrated and its absolute value cannot be measured, we cannot determine the absolute values of this efficiency. Nevertheless, the relative efficiency allows for direct comparison of different mechanisms leading to emission in the same system investigated in the same set-up, as reported here. Figure 2.16 shows the experimentally measured quantum efficiency of Er PL. Each data point in this figure represents the ratio of the PL excitation cross-section to the fraction of absorbed photons for a particular wavelength of the incoming light—see the Appendix B for a detailed derivation of the relative quantum efficiency. In each case, the PL excitation cross-section was determined from the slope of the plot of PL intensity vs. laser photon flux in the linear region. In this way, the effective excitation cross-section of Er emission at different wavelengths can be compared, and that is what is most relevant for the experiment. The wavelength dependence of the fraction of the incident light that is absorbed by the sample is measured in a separate experiment.

For a single-photon generation process, the correlation between the number of absorbed and emitted photons is linear and the ratio constant: with certain efficiency a long wavelength photon is emitted by the Er^{3+} ion for every short-wavelength photon absorbed by the Si NC. From Fig. 2.16 it is evident that this scenario is indeed followed for the lower range of excitation energies. However, in the figure a clear enhancement is seen for energies above a certain threshold, around 2.6 eV (480 nm). This shows that, at this energy, the quantum efficiency of the energy transfer to Er increases as here double-photon generation sets in. The relevant process is schematically illustrated

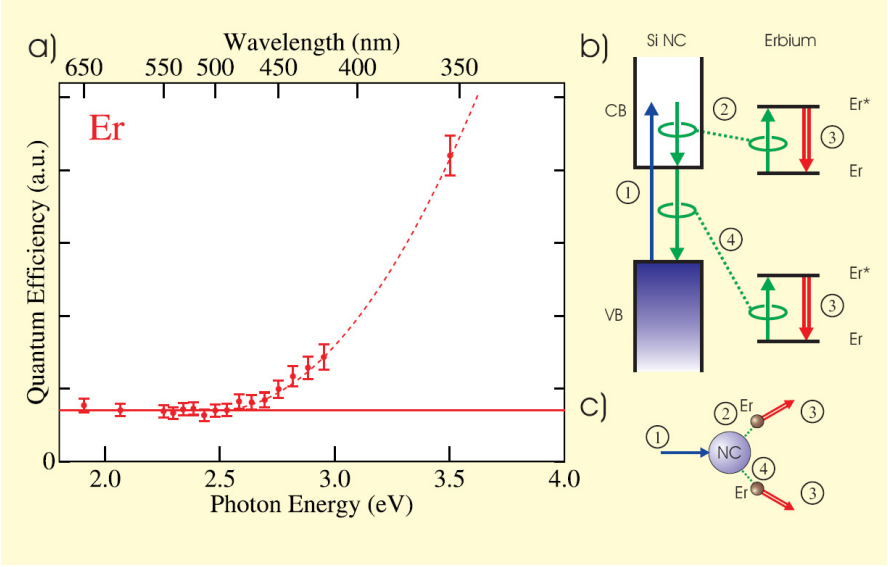

Figure 2.16: *Space-separated quantum cutting in Er - Si NCs system. (a) Relative quantum efficiency of Er-related photoluminescence (detected at 1535 nm) as a function of excitation energy. The quantum efficiency (number of emitted photons per number photons absorbed in the sample) is determined here as the ratio of the (effective) excitation cross-section of Er PL and absorbed fraction of incident photons, at a particular wavelength. For each data point the absorbed photon fraction was measured and the excitation cross-section was determined from the plot of photoluminescence intensity vs. excitation photon flux. As can be seen, the quantum efficiency is constant up to certain photon energy. This indicates a single photon process: one-photon-in, one-photon-out. The relation deviates from constant for the excitation energy at which the quantum cutting process sets in, and a possibility of emission of two photons per one absorbed photon appears. In this case, the energy of the incoming photon is divided by the nanocrystal over two nearby Er^{3+} ions. The solid line represents a fit to the data points that are (assumed to be) on a line, whereas the dashed line at higher energies is a mere guide-to-the-eye. The error bar reflects the uncertainty in the value of the power of the laser, 10% for OPO and 15% for UV lasers, expressed as the standard deviation determined in a separate series of measurements. On the right side (b), a schematic diagram of the space-separated quantum cutting (SSQC) process is shown: (1) Excitation of the silicon nanocrystal (Si NC) with high energy (UV) light exciting an electron from the valence band (VB) to the conduction band (CB) creating a "hot" electron-hole pair with excess energy. (2) Intra-band Auger process exciting an Er^{3+} ion and removing the excess energy. (3) Er-related PL. (4) Excitation of a second Er^{3+} ion by conventional inter-band Auger process. At the bottom right (c), a cartoon illustrating the photon cutting process with excitation of two nearby Er^{3+} ions is shown.*

in the right hand part (b) of Fig. 2.16; the excess energy ΔE of the "hot" carrier (ΔE = hν - E_{NC}, where hν and E_{NC} are photon and exciton energies, respectively) is large enough to allow for an Auger process of intra-band relaxation with simultaneous Er excitation [73]. As a result, two Er^{3+} ions can be excited per single photon absorbed by a NC, with the second one due to a conventional band-to-band Auger process, as indicated in the schematic. Analyzing the energy diagram in Figure 2.16, indeed, such a process is expected for photon energies exceeding the sum of the Si NC band gap (1.5 eV) and the Er excitation (0.8 eV), thus above 2.3 eV. (We point out that the decay time and also the saturation level of Er-related PL are identical for below- and above-threshold pumping.)

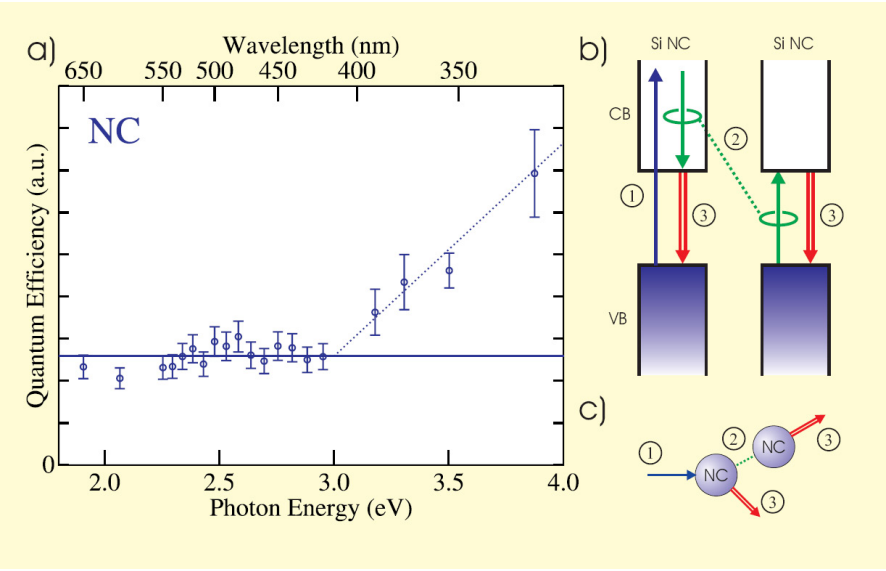

Figure 2.17: *Space-separated quantum cutting between Si NCs, as observed in Er-free solid state dispersion of Si NCs in a SiO_2 matrix. (a) Quantum efficiency of the NC-related photoluminescence (detected at 914 nm) as a function of excitation energy, illustrating that (neighboring) nanocrystals can themselves also be the energy-receiving systems. Quantum cutting appears now at a larger energy of the incoming photon because the band gap of Si NCs is larger than the Er excitation energy, and a larger UV photon excess energy (hν - E_{NC}) is thus needed. On the right side (b), a diagram for the involved processes is shown: (1) Excitation of the Si NC with high energy (UV) light creating "hot" electron-hole pair with excess energy. (2) Intra-band Auger process exciting a neighboring NC removing the excess energy. (3) NC exciton luminescence. At the bottom right (c), a schematic illustration of the process is given: one photon is absorbed by one NC, two photons are emitted by distinct NCs.*

While the above-described experiment concerns Er excitation by Si NCs, it illustrates the SSQC process, with an Er^{3+} ion serving as a receptor [95] of the down-sized energy quanta. In a similar way, part of the energy can be transferred to create an exciton in a neighboring nanocrystal, by converting a high-energy (UV) photon absorbed in one of them, with the only condition that these NCs are located within the energy transfer range [73]. In order to demonstrate this process, we performed a similar experiment for a sample without Er doping, correlating the Si NC-related exciton PL, monitored at 914 nm, to the absorbed photon fraction. The results are illustrated in Figure 2.17. Again, a constant ratio is concluded which, in this case, extends to a larger energy range. This was anticipated, as the double-photon generation is expected only for photons with quantum energy at least twice that of the NC band gap, $h\nu > 2E_{NC} \approx 3$ eV. In full agreement with this expectation, we see that the data obtained in the UV range fall clearly outside the dependence determined for low-energy excitation. This result demonstrates that the nanocrystals themselves can also be the receiving elements in the space-separated quantum cutting process, albeit at higher energies; a second Si NC can be excited by a neighboring Si NC containing a "hot" electron-hole pair. The partly de-excited first Si NC will still produce photoluminescence due to the "cold" electron-hole pair (exciton). Thus, when the energy of the incident photon exceeds a certain threshold, relaxation back to the ground state can occur through emission of two photons in the Si NC exciton PL wavelength range.

2.3.3 Discussion

We will now comment on a possible physical mechanism behind the SSQC phenomenon. As pointed out before, the SSQC bears close resemblance to the multiple exciton generation (MEG) process in which two, or more, electron-hole pairs are induced in one NC upon absorption of a single photon. The microscopic origin of MEG is under debate and several possibilities have been put forward. These include:

i Impact ionization by a hot carrier created as the result of the photon absorption [87, 88],

ii Coherent superposition of single and multiexciton states [96] due to the strong Coulomb interaction of carriers confined in NCs, which should take place when the energy relaxation rate of a single electron-hole pair is lower than both the two-exciton state thermalization rate and the rate of Coulomb coupling between single and two-exciton states, and

iii Multiexciton formation via a virtual state [97, 98]. This process can be described by second order perturbation theory and here two possible scenarios, with comparable rates, have been proposed. The first one proceeds via a virtual single exciton state. In this case, the direct optical transition from vacuum to a single exciton state is followed by the transition into the final two-exciton state due to Coulomb interaction [97]. In the second channel, the first step is the transition initiated by the Coulomb interaction from vacuum to a bi-exciton state, and the second step is optical intra-band transition [98].

The processes (ii) and (iii) can be responsible for MEG without any delay, *i.e.* in the moment of the photon absorption, and can be effective for production of multiple excitons in a single NC. However, extra excitons occurring in the same NC are recombining on a picosecond time scale [93].

The impact ionization process (i) starts with some delay after the absorption. It proceeds via a real state, when the hot electron-hole pair is created by the absorbed photon with energy exceeding the energy gap. This process is well known for bulk semiconductors, where it increases the number of photo-excited excitons by less than $\sim 1\%$. One may expect that the impact ionization rate should rise dramatically in the case of NCs due to strong Coulomb interaction of confined carriers and the decreasing rate of the phonon emission due to discrete spectrum [87, 88]. Indeed, pseudopotential calculations predict a higher rate of impact ionization in CdSe dots than in bulk material for electrons with excess energies just above the bottom of conduction band [99].

Our preliminary theoretical considerations indicate that the impact ionization is the most suitable process to account for the SSQC phenomenon reported here. The effective dielectric constant governing the Coulomb interaction between carriers in different NCs embedded in SiO_2 matrix is considerably smaller than the dielectric constant of Si. Using the Auger recombination rate (the reverse process to the impact ionization) inside the silicon NC calculated before [100], we have got the value of the order of 10^{10} - 10^{11} s^{-1} for the rate of the process under consideration for two NCs at a distance of less than 1 nm. This rate is comparable to the energy relaxation rate determined by the Auger process between carriers confined in one silicon NC of 3 nm diameter when there is one exciton per NC [65]. From the NC-NC distance distribution depicted in Fig. 2.18 we conclude that more than 50% of all NCs have their closest neighbor at a distance of less than 1 nm from the surface, *i.e.* sufficiently close to facilitate the proposed energy transfer.

We point out that the observed linear increase of quantum efficiency of SSQC for photon energy higher than the threshold value, experimentally observed in this study for Si NCs—see Fig. 2.17—is in agreement with the

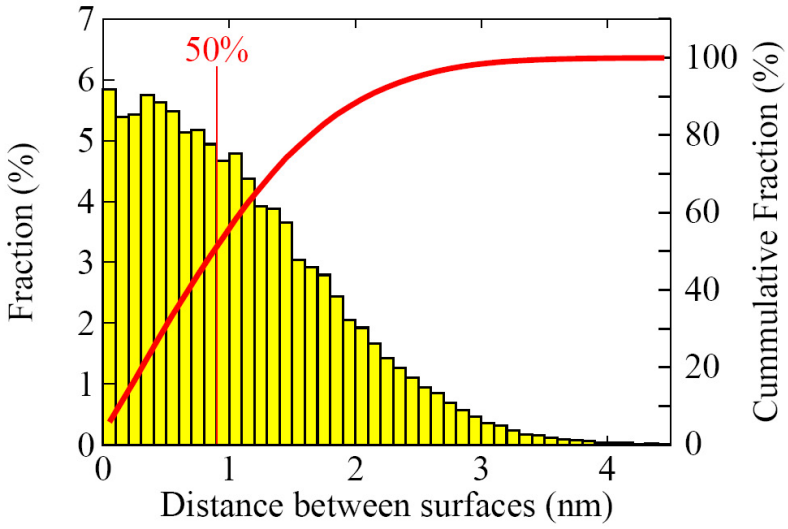

Figure 2.18: *A simulation of the nearest-neighbor distance distribution for the solid-sate dispersion of Si NCs in a SiO_2 matrix (Er-free) investigated in this study. As can be seen, more than 50% of all NCs have a nearest neighbor closer than 1 nm from their surface.*

calculated linear increase of the number of final states [101] and therefore supports the microscopic mechanism based on impact ionization. Yet additional support comes from measurements performed in a sample with similar Er concentration and NC size, but with a smaller NC concentration, *i.e.* with a larger Er - NC separation. In this case the observed SSQC process shows the similar onset energy but lower quantum efficiency, providing an independent verification of the proposed mechanism.

For completeness' sake, we recall that the Förster resonant energy transfer (FRET) which was shown to be responsible for long-range energy transfer in a closely packed CdSe quantum solid [102], has low probability for Si NCs due to indirect band gap. It is nevertheless fair to mention that the final identification of the microscopic mechanism of the SSQC process (as well as that of MEG) will require further investigation. In particular, kinetics of the process should be investigated by PL and induced absorption.

2.3.4 Conclusions

Summarizing, we have shown here how quantum cutting (one photon in, two photons out) can take place in systems based on Si NCs. In contrast to the earlier work on multi-exciton generation in semiconductor nanocrystals, the energy quanta down-converted in the SSQC process are transferred to external objects—Er^{3+} ions and neighboring nanocrystals—from where they can be emitted in the form of photons, or differently harvested. In this way, true space-separated photon cutting takes place. The demonstration of the SSQC process for Si is technologically interesting in view of the prominent role of Si and Si-derived materials in electronic, optoelectronic and especially in photovoltaic applications. Moreover, the use of nanocrystals provides the additionally appealing aspect that the energy levels can be tuned to suit the application by changing the size of the particles [103, 104]. On the other side, efficiency of the SSQC process discussed here can be adjusted by changing the separation between individual NCs. The ideas and results presented here may lead the way to a substantial improvement of photovoltaic devices, both solar cells and light-emitting elements. For solar cells it has been shown theoretically that multiple exciton generation [105] and photon down-conversion [106] can increase the efficiency beyond the Shockley-Queisser limit. Interestingly, the indirect nature of the band gap of Si, which is preserved in Si NCs, and which is detrimental for photonic applications, turns out to be beneficial here, as the relatively long exciton lifetime (in comparison to direct band gap NCs) simplifies energy extraction for photovoltaic applications.

3 Er-doped large band gap hosts

They sentenced me to twenty years of boredom
For trying to change the system from within
I'm coming now, I'm coming to reward them
...

Leonard Cohen, "First we take Manhattan"

3.1 Photoluminescence and excitation spectroscopy of Er^{3+} in GaN

The infrared photoluminescence at 1.5 μm due to the $^4I_{13/2} \rightarrow {}^4I_{15/2}$ transition of Er^{3+} ions has been investigated for GaN:Er^{3+} layers grown by MBE. Low temperature high resolution measurements performed under continuous illumination at the wavelength $\lambda_{exc} = 532\ nm$, quasi resonant to one of the intra 4f-shell transitions, revealed that the 1.5 μm band consists of up to eight individual spectral components. In excitation spectroscopy, a temperature dependent splitting of resonant bands was observed. Based on these experimental results, a possible multiplicity of optically active centers formed by Er doping in GaN layers is discussed.

3.1.1 Results

For over a decade, rare earth (RE) doped III-V semiconductors are widely investigated for their photonic properties and applications in optoelectronics [107, 108]. GaN as a host for RE ions is of interest due to its wide band gap, that guarantees luminescence at room temperature [109]. Er doping of GaN has been successfully used for fabrication of green light emitting devices [110].

Such a material is also interesting for luminescence at 1.5 μm, coincident with the minimum absorption losses in optical fibers. The 1.5 μm emission from GaN:Er^{3+} is the focus of this section. The GaN:Er^{3+} samples used for these experiments were kindly provided by Dr. A.J. Steckl, from the University of Cincinnati; these were grown on a p-type (111) Si substrate, using the Solid Source Molecular Beam Epitaxy (SSMBE) method, after deposition of an AlN buffer layer. Details of preparation procedure can be found in Ref. [111]. The experiments described in this section were carried on a particular sample grown at an Er cell temperature of 860^0C, Ga cell temperature of 935^0C and substrate temperature of 650^0C. The concentration of Er was [Er] $\approx$ 1 at.%.

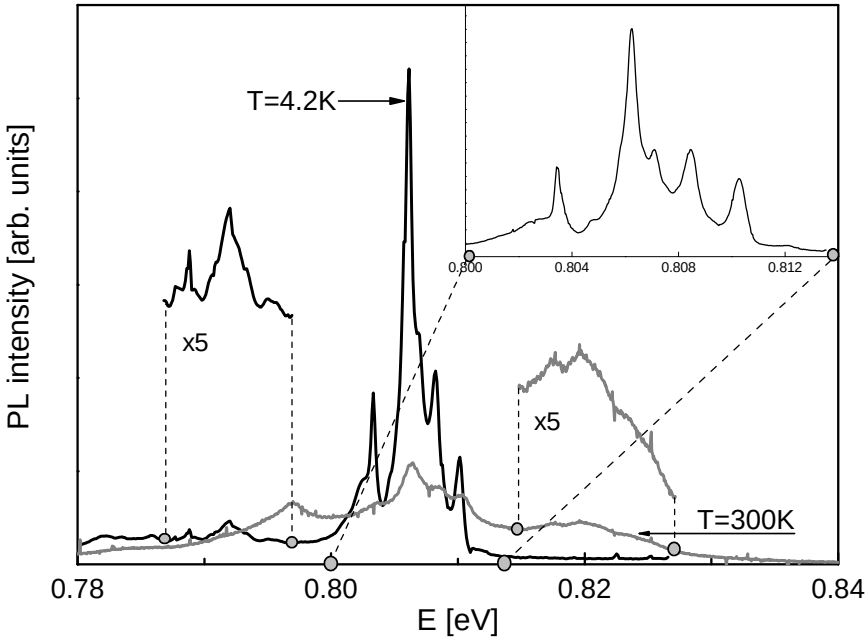

Figure 3.1: $^4I_{13/2}\rightarrow{}^4I_{15/2}$ *emission spectrum from GaN:*Er^{3+} *under excitation to the* $^2H_{11/2}$ *multiplet (*λ_{exc}*=532 nm), recorded at 4.2 K (black line) and room temperature (grey line); phonon replica and anti-Stokes luminescence are shown five-fold amplified. Inset: high resolution spectrum for the main band at 4.2 K (range 0.800-0.814 eV).*

Figure 3.1 shows the integrated intensity of the 1.5 μm PL band originating from the $^4I_{13/2}\rightarrow{}^4I_{15/2}$ Er^{3+} intra-4f shell transition. The sample was excited resonantly with a Nd:YVO_4 based laser operating in a continuous mode at λ_{exc} = 532 nm, on-off modulated with a mechanical chopper. The sample was placed in a He gas flow cryostat and the measurements were taken at 4.2

K-to-room temperature range. PL signal was dispersed with a high resolution 1 m spectrometer and detected with a Ge detector. A photo multiplier tube was used to record decay kinetics of the PL signal.

The black line in Fig. 3.1 presents the PL spectrum of the sample in the 1.5 μm range taken at 4.2 K. A phonon replica of the band can be seen at energy lower by 14 meV. Such a separation does not coincide with the optical phonon in GaN, so a local phonon is probably involved. The grey line in the figure shows the PL spectrum at room temperature. A similar band is repeated at 14 meV above the main spectrum, representing anti-Stokes luminescence. The inset to the figure depicts a high resolution scan of the main PL band at 4.2 K: up to eight well resolved peaks can be distinguished.

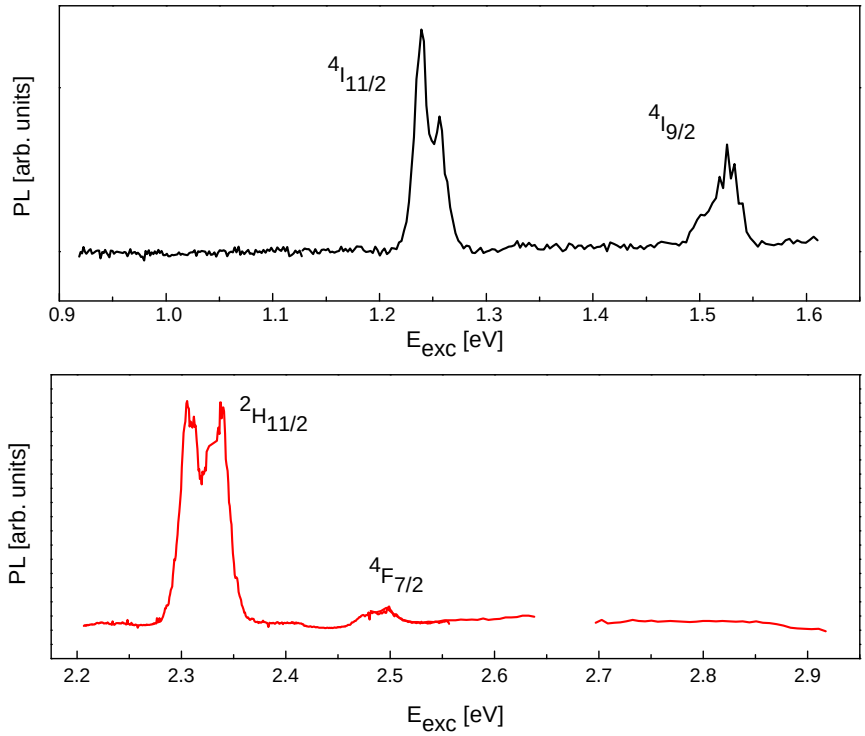

Figure 3.2: *PLE spectrum at 1537 nm (0.807 eV) taken at room temperature. Excitation is provided by a pulsed OPO. Individual bands are identified with the corresponding intra-4f transitions.*

Figure 3.2 shows the integrated room temperature PL intensity of the 1.5 μm band as a function of excitation energy (PLE). The tunable sub-band

excitation was provided by a Nd:YAG pumped optical parametric oscillator. The 350.4 nm line of an Ar^+ ion laser was used for over-band gap excitation. As can be seen, in the regime of below band gap excitation only energies resonant with one of the 4f shell transitions lead to the 1.5 μm emission. The individual PLE bands can be identified with transitions from the ground state ($^4I_{15/2}$) to the $^4I_{11/2}$, $^4I_{9/2}$, $^2H_{11/2}$ and $^4F_{7/2}$ excited states, respectively. In addition, we note that three of the PLE bands split in two components; their separation differs per band.

3.1.2 Discussion

The observed splitting of the PLE bands (Fig. 3.2), together with the multiple structure reported in the high resolution spectrum (Fig. 3.1), can indicate existence of more than one type of Er-related optically active center in the studied sample. We investigated this possibility further by monitoring the 1.5 μm band under selective excitation tuned to individual components of the PLE bands. Identical spectra have been obtained with E_{exc}= 1.23, 1.25, 1.48, 1.51, 2.31, 2.35 and 2.50 eV. Also for over band gap excitation (3.54 eV) no difference has been seen in the structure of the 1.5 μm PL band. We also investigated the decay characteristics of individual components of the 1.5 μm band under selective excitation and found no differences as nearly identical decay times were measured independently of the excitation energy. Finally, the PLE spectra taken at a range of temperatures from 10 K to room temperature are depicted in Fig. 3.3. We observe that the relative intensity of the two components for each PLE band changes with temperature. While the higher energy component of the band enhances at lower temperatures, the lower energy component quenches and disappears.

Er^{3+} level	E position (eV)	E splitting (meV)
$^4I_{15/2}$	0	12
$^4I_{11/2}$	1.25	3.8
$^4I_{9/2}$	1.5	11
$^2H_{11/2}$	2.3	23.6

Table 3.1: *Splitting of Er^{3+} states as deduced from the temperature dependence of the PLE bands.*

Taking into account the Er^{3+} levels splitting due to the crystal field, we will try to interpret the double structure of the PLE bands and its temperature dependence considering thermalization within the ground state. At low temperatures, only the lowest level at the ground energy state is populated. At a

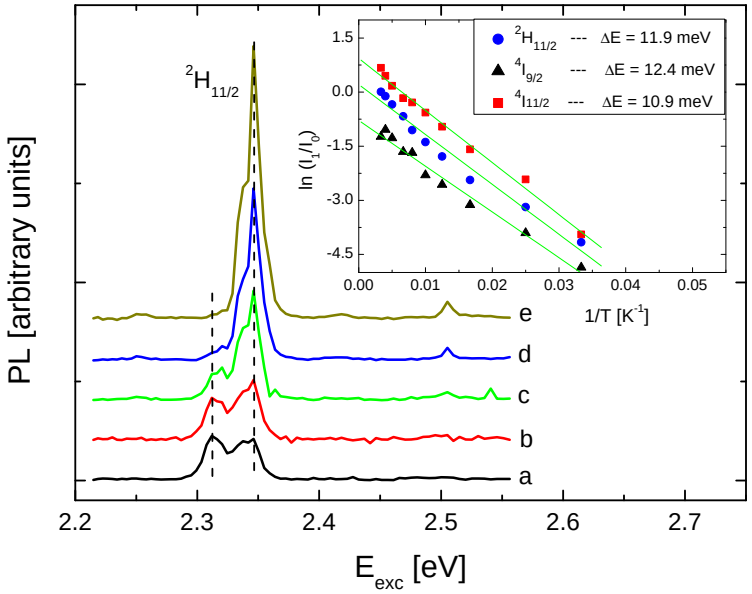

Figure 3.3: *Temperature dependence of the $^2H_{11/2}$ excitation band, monitored with the spectrometer set at 1537 nm. T = 300, 200, 100, 50 and 10 K from (a) to (d), respectively. In the inset to the figure, Arrhenius plots of intensity ratio of 2 components of individual PLE bands are given.*

higher temperature, Er^{3+} ions thermalize and populate upper levels leading to appearance of new components in the PLE band. Since not only the ground state, but also the excited states of Er^{3+} ions will be split, the energy distance between the components can be different for specific PLE bands and also not coincident with the ground state splitting.

In this simple model, for each excitation wavelength, the luminescence intensity is proportional to population of the ground state level. If we consider splitting of the ground state into 2 levels, the upper one being populated by thermalization from the lower one, the intensity ratio of the PLE band components I_1/I_0 will be given as:

$$I_1/I_0 \propto N_1/N_0 = A \ \exp(-\Delta E/k_B T), \tag{3.1}$$

where N_1, N_0, ΔE and k_B are populations in the upper and the lower ground state levels, the ground state splitting and the Boltzmann constant, respectively. In the inset of Fig. 3.3, the intensity ratio of the two components of the three investigated PLE bands is plotted versus the inverse of temperature. A

similar activation energy of $\Delta E \approx 12$ meV is obtained for all of them. Following the assumed model, this value corresponds to the energy separation within the ground state. Based on this, we can estimate the excited states splitting—see Table 3.1. We can conclude that the experimental data obtained thus far can be satisfactory interpreted involving only one type of optically active Er^{3+} center in the investigated GaN layers.

3.2 On 2.7 μm emission from Er-doped large band gap hosts

The potential of Er-doped Cs_2NaYF_6 and GaN for mid-infrared emission at $\lambda \approx 2.7$ μm is investigated using time-resolved optical spectroscopy. This emission results from electronic transitions between the second ($^4I_{11/2}$) and first ($^4I_{13/2}$) excited states of the Er^{3+} ion. By recording the photoluminescence transients for the $^4I_{11/2} \rightarrow {}^4I_{15/2}$ and $^4I_{13/2} \rightarrow {}^4I_{15/2}$ transitions after pulsed excitation, we determine the lifetime of the $^4I_{11/2}$ level and demonstrate that the $^4I_{13/2}$ state is populated from this level. Our results indicate that both hosts should enable 2.7 μm emission, whose intensity is temperature-stable but subject to concentration quenching.

3.2.1 Introduction

Mid-infrared laser radiation in the 2 - 3 μm range has applications in the fields of remote sensing, trace gas monitoring, and laser surgery [112]. Currently, optically (flashlamp or diode) pumped rare-earth RE-doped insulating inorganic crystals or glasses are used as laser sources in this range [113]. Especially for laser surgery applications, research towards tunable and more compact, electrically pumped sources is still ongoing. In the past few years, ZnSe:Cr^{2+} has emerged as widely tunable laser medium, covering the complete 2 - 3 μm range, but electrical pumping of such crystals is yet to be demonstrated [112, 114]. The design of more compact MIR lasers has focused towards diode-pumped fiber lasers [115]. However, electrically pumped media, preferably compatible with Si technology, would result in possible development of even cheaper and more compact sources. Visible electroluminescence from RE doped hexagonal GaN, epitaxially grown on Si substrates, has already been demonstrated several years ago [110]. Recently, a CMOS-compatible spin coating technique for GaN powders on Si has been developed and green luminescence has been obtained from Er-doped powders [116]. As the intra-4f transition between the second ($^4I_{11/2}$) and first ($^4I_{13/2}$) excited states of the Er^{3+} ion is in the range of interest (2.7 - 3.0 μm, depending on the host), it is interesting to explore the potential of Er-doped GaN as active MIR lasing medium.

In the present work, we address temporal aspects of the $^4I_{11/2} \rightarrow {}^4I_{13/2}$ transition of Er^{3+} in GaN, as well as possible luminescence quenching mechanisms. To this end, the kinetics of photoluminescence for the $^4I_{11/2} \rightarrow {}^4I_{15/2}$ transition at $\lambda \approx 1.0$ μm and the $^4I_{13/2} \rightarrow {}^4I_{15/2}$ transition at $\lambda \approx 1.5$ μm are studied. We hereby take advantage of the highly sensitive and fast detectors, developed for this wavelength range. Meanwhile, special precautions, to be taken when directly detecting radiation with $\lambda > 2.5$ μm in order to prevent

absorption by air (water) and commonly used silica lenses, are avoided. In a similar way, we have also studied Er^{3+}-doped Cs_2NaYF_6. In this crystal Er^{3+} can only be incorporated on Y^{3+} positions, which have O_h point group symmetry and are widely spaced (nearest neighbor distance 0.64 nm [117]). As these crystals accept Er concentrations up to 100% (all Y^{3+} ions substituted), they present a good model system for investigating the influence of Er-concentration on the 2.7 μm emission.

3.2.2 Experimental details

The $Cs_2NaY_{1-x}Er_xF_6$ crystals (x = 0.001, 0.01, 0.1, and 1) were hydrothermally grown, using Er_2O_3 as dopant [118]. The hexagonal GaN:Er^{3+} samples were epitaxially grown on a p-type (111) Si substrate, after deposition of an AlN buffer layer, using the solid source molecular beam epitaxy method [111]. The Er-concentration in these samples is estimated at 1 at.%.

Time-resolved PL measurements were performed using a Nd:YAG-pumped optical parametric oscillator as tunable pulsed laser excitation source, generating 5 ns pulses, with a maximum energy of 1 mJ, at a repetition rate of 10 Hz in the λ = 410 - 2200 nm range. For measurements at low temperature, the GaN samples, which exhibit good thermal conductivity, were placed in a closed-cycle cryostat, with a minimum operation temperature of $\sim$ 20 K, whereas for the poorly conducting Cs_2NaYF_6 crystals a He flow cryostat was used. The luminescence light was dispersed with a 1 m monochromator and detected with a liquid N_2-cooled InGaAs photomultiplier (300 - 1700 nm). For the slow kinetics in Cs_2NaYF_6 the excitation repetition rate was lowered by blocking laser pulses with a shutter. The detector was operated in photon counting mode for detecting the much faster kinetics of Er^{3+} in GaN.

3.2.3 Results and discussion

In Fig. 3.4 the TR PL for the $^4I_{11/2} \rightarrow {}^4I_{15/2}$ and $^4I_{13/2} \rightarrow {}^4I_{15/2}$ transitions in a 1% Er^{3+}-doped $Cs_2NaY_{(1-x)}F_6$ crystal (x = 0.01), measured at 4.2 K, is shown. In view of the large average dopant ion spacing at this concentration, only limited effects of Er-Er interactions and energy migration between Er^{3+} ions are expected. The PL transients are analyzed assuming first order decay kinetics in an atomic three levels system (see excitation schemes in Fig. 3.4), leading to

$$I_{PL}(t) = A(e^{-t/\tau_d} - e^{-t/\tau_r}), \tag{3.2}$$

where τ_r and τ_d represent the rise and decay times of the signal, respectively, which correspond to the population time and lifetime of the upper level involved in the detected luminescence transition. Traces (a) and (b) are recorded

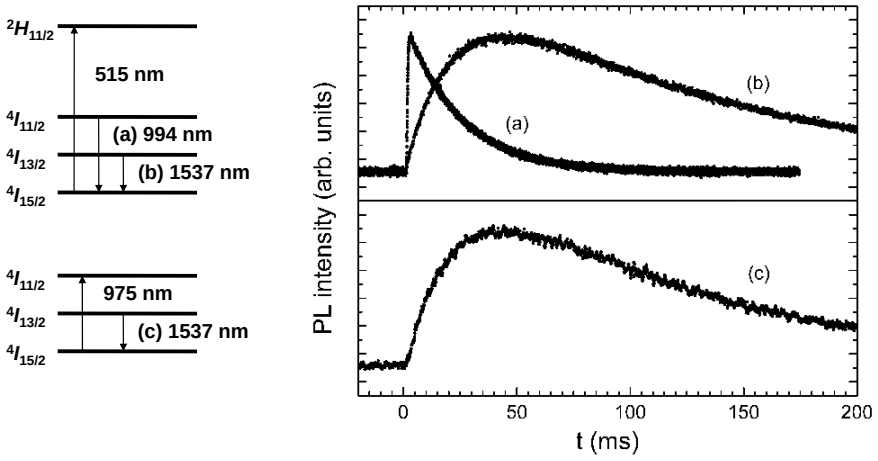

Figure 3.4: *Time resolved PL of the transitions from the second and first excited states of* Er^{3+} *in* $Cs_2NaY_{1-x}Er_xF_6$ *(x = 0.01) at 4.2 K. PL excitation schemes are shown at the left.*

after exciting the Er^{3+} ions to the $^2H_{11/2}$ level, which presents the highest excitation efficiency for 1.54 μm emission. The TR PL from the second excited state is perfectly reproduced assuming a rise time of 0.5 ms and a decay time of 21 ms. Although in principle several relaxation paths from the $^2H_{11/2}$ to the $^4I_{13/2}$ are possible, the kinetics of luminescence from the first excited state show a single rise time of 21 ms and a decay time of 100 ms. These results indicate that the lifetimes of the second and first excited states of Er^{3+} in Cs_2NaYF_6 are 21 and 100 ms, respectively, and that the $^4I_{13/2}$ state is (nearly) exclusively populated from the $^4I_{11/2}$ level. In order to check the lifetime assignations, the TR PL from the $^4I_{13/2}$ level has also been recorded after excitation to the second excited state (trace (c)). Essentially the same kinetics as for excitation to the $^2H_{11/2}$ level are observed. In this way we rule out the possibility that the measured decay time of the $^4I_{11/2} \rightarrow {}^4I_{15/2}$ transition would correspond to the lifetime of some intermediate long living state in the decay path from the $^2H_{11/2}$ level. Thus, it is demonstrated that transitions between the second and first excited states of Er^{3+} take place in these crystals and the long lifetimes of the levels involved indicate that they occur to large extent by radiative decay.

In order to examine possible quenching mechanisms for this luminescence, the lifetime of the $^4I_{11/2}$ level has also been measured at room temperature and for other Er^{3+} concentrations. The results, summarized in Table 3.2,

x	4.2 K	300 K
0.001	21_3	9_2
0.01	21_3	12_2
0.1	1.4_2	1.1_2
1	1.1_2	0.7_2

Table 3.2: *Lifetime (in ms) of the Er^{3+} $^4I_{11/2}$ level in $Cs_2NaY_{1-x}Er_xF_6$ at 4.2 K and room temperature. The error in the last digit is indicated as a subscript.*

show that temperature only has a minor effect on the 2.7 μm luminescence. In contrast, at high Er-concentrations an important quenching of the $^4I_{11/2}$ lifetime is observed, most probably as a result of interactions (cross-relaxation, upconversion) between Er^{3+} ions.

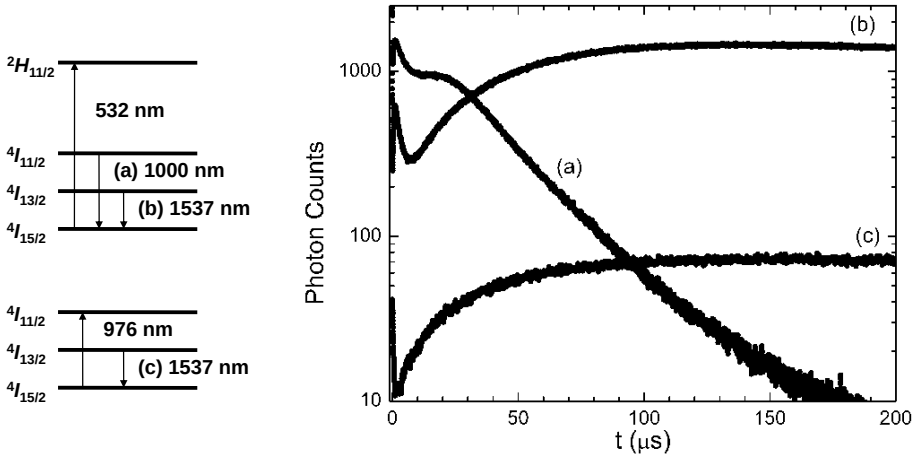

Figure 3.5: *Time resolved PL of the transitions from the second and first excited states of Er^{3+} in GaN (1 at.% doping concentration) at 20 K. PL excitation schemes are shown at the left.*

Figure 3.5 presents PL transients for a 1% Er^{3+}-doped GaN sample at 20 K. These signals have a more complicated time-dependence than those for the insulating material. A fast component, observed in the traces after excitation to the $^2H_{11/2}$ level ((a) and (b)) with a decay time of ~ 3 μs, is most probably related to visible green emission ($^4S_{3/2} \rightarrow {}^4I_{15/2}$). The slow components hereafter do not exhibit single first order decay kinetics, as described by Eq. 3.2. This is most probably a result of the formation of multiple Er^{3+} centers

in these samples, as earlier reported for similarly grown structures [119]. The TR PL corresponding to the $^4I_{11/2} \rightarrow {}^4I_{15/2}$ transition (trace (a)) has a rise time of 7 - 10 μs and a decay time of 20 - 40 μs. The sum of these time constants roughly corresponds to the rise time of the $^4I_{13/2} \rightarrow {}^4I_{15/2}$ transition (30 - 50 μs, trace(b)). After direct excitation to the $^4I_{11/2}$ level, the latter transition has a rise time in the 30 - 40 μs range (trace(c)). These results thus show that the lifetime of the second excited state of Er^{3+} in this sample is 20 - 40 μs and the cumulative lifetime of the intermediate levels ($^2H_{11/2} \rightarrow {}^4I_{11/2}$) amounts to 7 - 10 μs. The lifetime of the first excited state is found in the 1 - 1.5 ms range. In addition, it is demonstrated that the population of the $^4I_{13/2}$ level is dominated by transitions from the second excited state. At room temperature, the lifetime of the $^4I_{11/2}$ level is found to be $\sim$ 18 μs. Again, no dramatic temperature quenching is observed for this transition.

As 2.7 μm emission from GaN:Er^{3+} is envisaged, it still has to be demonstrated that radiative transitions between the $^4I_{11/2}$ and the $^4I_{13/2}$ levels take place. Comparing the results for GaN with those for Cs_2NaYF_6 at low Er concentration, we find that the rise time of the $^4I_{11/2} \rightarrow {}^4I_{15/2}$ transition and the lifetime of the $^4I_{13/2}$ level are $\sim$ 70 times shorter. The lifetime of the second excited state of Er^{3+}, however, appears to be shortened by an additional factor of $\sim$ 8, pointing to some non-radiative decay mechanism. One might consider multi-phonon relaxation between the $^4I_{11/2}$ and the $^4I_{13/2}$ level, which would imply that practically no radiative transitions between these levels occur. As only 5 longitudinal optical (LO) lattice phonons ($\hbar\Omega \sim 90$ meV [120]) are required to bridge the gap between the second and first excited state, multi-phonon relaxation may indeed be important [121]. This would, however, further imply that the lifetimes of the $^4S_{3/2}$ and $^4F_{9/2}$ levels experience an even stronger non-radiative quenching, as for these levels multi-phonon relaxation to the next state only requires 4 LO phonons. The rise time observed for the $^4I_{11/2} \rightarrow {}^4I_{15/2}$ transition and the occurrence of visible luminescence from these higher excited states (see *e.g.* [119]) do not support such a quenching mechanism. In fact, observations of phonon replicas in the PL of GaN:Er^{3+} rather suggest coupling to the transverse optical (TO) phonon mode ($\hbar\Omega \sim 68$ meV) with a very small coupling strength (S = 0.02) [119] or to a local vibrational mode (14 meV) [122]—see previous section. In either case, multi-phonon relaxation is not expected to dominate the $^4I_{11/2} \rightarrow {}^4I_{13/2}$ transition. On the other hand, the doping level of the GaN sample is comparable to that of the $Cs_2NaY_{0.9}Er_{0.1}F_6$ crystal, for which an important concentration quenching of the $^4I_{11/2}$ lifetime is seen. We therefore believe that the 2.7 μm emission from the GaN sample is also strongly quenched by interactions between Er^{3+} ions, which are possibly related with the appear-

ance of visible (green, red) luminescence as well. Further experiments on GaN crystals with lower Er-concentrations are being undertaken in order to verify these hypotheses.

3.2.4 Conclusions

From time-resolved photoluminescence measurements in the near IR for a $Cs_2NaY_{1-x}Er_xF_6$ concentration series and for a 1 at.% Er^{3+}-doped GaN sample, we have determined the lifetime of the second excited state of the Er^{3+} ion and shown that the first excited state is predominantly populated through $^4I_{11/2} \rightarrow {}^4I_{13/2}$ transitions. It is argued that the latter transitions are not governed by multi-phonon relaxation. Hence, it is demonstrated that these materials should exhibit 2.7 μm emission, which is almost independent of temperature, but most likely shows an important concentration quenching. Realization of electrically driven MIR emission from Er-doped GaN, compatible with Si technology, thus seems feasible.

A Calculations of energy exchange between Si NCs and Er^{3+} ions

Confined electrons and holes energy levels as well as their wave functions calculated in multiband effective mass approximation [76] are used in this consideration. Luttinger Hamiltonian in the spherical approximation has been used for holes and the strong anisotropy of the electron effective mass in silicon has been taken into account. The wave function and flux continuities were the boundary conditions used. When calculating wave functions outside the NC, isotropic effective masses being equal to m_0 and $5m_0$ were used for electron and hole states correspondingly. Spin-orbit splitting was neglected in both Si and SiO_2.

The conduction band of Si has six equivalent minima in the first Brillouin zone, situated in the neighborhoods of the six X-points. The wave function of electron can be presented in the form:

$$\psi_\nu^e = \xi^e(\mathbf{r}) u_{c\nu} \exp(i\mathbf{k}_{0\nu}\mathbf{r}), \tag{A.1}$$

where $u_{c\nu}$ and $\mathbf{k}_{0\nu} = 0.85 \times (2\pi/a_{\text{lat}})$ are the Bloch amplitude and wave vector corresponding to the bottom of valley ν ($a_{\text{lat}} = 0.54$ nm is the lattice constant of silicon). Envelope functions $\xi^e(\mathbf{r})$ are found as a result of a numerical solution to the Schrödinger equation after separating the angular part $\exp(im\phi)$ as there is a strong anisotropy of the electron effective mass: $m_\parallel = 0.916m_0$, $m_\perp = 0.19m_0$. There are series of electron states for each value of $M = |m|$ (m can be any integer number): 6 times degenerate in energy for $M = 0$, and 12 times degenerate for $M \geq 1$. (This degeneracy is given without taking an addition spin degeneracy into account.) So the states are marked with the letter e with an index, indicating the value of M, and the number in a series in front of it. For example, the ground state is marked as $1e_0$, which means that this is the first state with $M = 0$.

There are three types of hole states in spherical quantum dots: i) mixed states (hm) formed by the combination of heavy and light ones, ii) heavy hole

(hh) states, and iii) light hole (hl) states. Each state is also characterized by the full angular momentum F (0 for the light hole states and positive integer for the other ones) and it is $2F + 1$ times degenerate as the projection M of momentum F onto the quantization axis (arbitrary selected) can be any integer number having absolute value not larger than F. The space quantization forms a series of each type of the states with fixed F. So they are marked with the letters showing the type of the states with index indicating the value of F, and the number in a series in front of it all. For example, the hole state with the lowest energy is of mixed type—$1hm_1$.

The calculated lower energy levels of electrons and holes confined in Si NC of diameter in the range 2.9 nm ÷ 3.3 nm are shown in Fig. 2.12. The energy range is limited to the one of optical pumping used in experiments (2.85 eV). Due to the large energy difference between neighboring space quantization levels energy relaxation of "hot" confined carriers is suppressed. Thus, an Auger excitation of erbium ions in silicon dioxide is possible, similar to the impact ionization by hot carriers in bulk silicon, where it plays a significant role in electroluminescence, but just negligibly affects the excitation of the erbium photoluminescence due to the fast energy relaxation of hot carriers in the bulk material.

A.1 Excitation due to intra-band transition

When dealing with the Coulomb interaction between an f-electron of an Er^{3+} ion situated in SiO_2 and a carrier confined in Si NC, one should take into account the difference in dielectric constant values of Si ($\varepsilon_1 = 12$) and SiO_2 ($\varepsilon_2 = 2$). Note that the Auger process is determined by the high frequency dielectric constant, as the transition energy $\Delta_{ff'}$ is much larger than the lattice vibration energy [78].

The potential created by a point charge q at the distance $\mathbf{a}$ from the center of the sphere of radius R ($R < a$) with dielectric constant ε_1 in the media with dielectric constant ε_2 is obtained as a solution to the Poisson equation and is given by the equations:

$$\Phi_1(\mathbf{r}, \mathbf{a}) = \frac{q}{\varepsilon_2 a}\left[1 + \sum_{l=1}^{\infty}\left(\frac{r}{a}\right)^l \frac{(2l+1)\varepsilon_2}{l\varepsilon_1 + (l+1)\varepsilon_2} P_l(cos\vartheta)\right], \tag{A.2}$$

inside the sphere ($r < R$), and

$$\Phi_2(\mathbf{r}, \mathbf{a}) = \frac{q}{\varepsilon_2|\mathbf{r} - \mathbf{a}|} - \frac{q(\varepsilon_1 - \varepsilon_2)}{\varepsilon_2 r}\sum_{l=1}^{\infty}\left(\frac{R}{a}\right)^{l+1} \frac{l}{l\varepsilon_1 + (l+1)\varepsilon_2}\left(\frac{R}{r}\right)^l P_l(cos\vartheta), \tag{A.3}$$

outside the sphere ($r > R$), where ϑ is the angle between $\mathbf{r}$ and $\mathbf{a}$: $\cos(\vartheta) = (\mathbf{r}, \mathbf{a})/ra$. Note that the Coulomb potential in the case of interaction of two charges is given by $\frac{1}{2}\left[\Phi(\mathbf{r}, \mathbf{a}) + \Phi(\mathbf{a}, \mathbf{r})\right]$, but it is easy to show that in our case $\Phi(\mathbf{r}, \mathbf{a}) = \Phi(\mathbf{a}, \mathbf{r})$.

The probability of Auger excitation of an erbium ion situated in SiO_2 at the distance a from the center of a Si NC as the result of the transition of a "hot" confined carrier from the state i into the state i' is given by the Fermi golden rule:

$$W_{i'i} = \frac{2\pi}{\hbar}\frac{1}{N_f}\sum_{ff'}\left|\langle f', i'|e\Phi|f, i\rangle\right|^2 J_T(N)\delta(E_i - E_{i'} - \Delta_{ff'} - N\hbar\omega_{\text{ph}}), \quad \text{(A.4)}$$

where Φ is the potential created by the f-electron of the Er^{3+} ion; f, f' enumerate the states of f-electrons of the ion; and N_f is the degeneracy degree of the f state. The integration in the matrix elements of Eq. (A.4) is to be produced over the carriers confinement space and the f-electron coordinate. Due to the energy conservation law, confined carrier transition is accompanied by the emission of N phonons with energy $\hbar\omega_{\text{ph}}$.

In the Huang-Rhys model (the model of two displaced oscillators with the same frequency), the phonon factor $J_T(N)$ is given by [123]:

$$J_T(N) = \exp\left[-2S\left(N_T + \frac{1}{2}\right)\right]\exp\left[\frac{N}{2}\frac{\hbar\omega_{\text{ph}}}{kT}\right] I_N\left[2S\sqrt{N_T\left(N_T+1\right)}\right] \quad \text{(A.5)}$$

where S is the Huang-Rhys factor which in the one mode approximation is given by

$$S = \frac{\varepsilon_{\text{opt}} - \varepsilon_{\text{th}}}{\hbar\omega_{\text{ph}}} \quad \text{(A.6)}$$

with ε_{opt} and ε_{th} corresponding to the optical and thermal ionization energy, respectively; N_T is the Bose-Einstein factor:

$$N_T = \frac{1}{\exp\left(\frac{\hbar\omega_{\text{ph}}}{kT}\right) - 1}\ , \quad \text{(A.7)}$$

and $I_N(x)$ is the modified Bessel function of order N.

As the energy levels are highly degenerate, one should produce averaging over all the initial states with the energy E_i and sum over all the final states corresponding to the energy E_i' in Eq. (A.4). All these states are actually split due to nonsphericity of NCs and other factors. This fact is taken into account by assuming the broadening of levels and adding the value δE to the argument of δ-function in Eq. (A.4) and averaging over this value in the energy range

$\Delta_E = 60$ meV, which is equal to the energy of optical phonon in bulk Si. Eq. (A.4) transforms into

$$W_{i'i} = \frac{2\pi}{\hbar}\frac{1}{\Delta_E}\frac{1}{N_i}\sum_{M,M'}\frac{1}{N_f}\sum_{ff'}\left|\langle f';i',M'|e\Phi|f;i,M\rangle\right|^2 J_T(N) \tag{A.8}$$

where N_i is the degeneracy degree of the initial state i. M and M' enumerate the degenerate states of levels i and i', and final and initial energies are related through

$$E'_i \simeq E_i - \Delta_{f,f'} - N\hbar\omega_{\rm ph} \tag{A.9}$$

.

Let us consider the potential Φ in Eqs. (A.4, A.8). Introducing the coordinate $\mathbf{r}'$ related to the center of the ion ($r' \lesssim r_f$, where r_f is the size of the f-shell) and using the fact that $r_f \ll a$, the potential can be expanded into a series by $\mathbf{r}'$ taking into account the linear term only:

$$\Phi(\mathbf{r},\mathbf{a}+\mathbf{r}') \approx \Phi(\mathbf{r},\mathbf{a}) + \frac{\partial\Phi(\mathbf{r},\mathbf{a})}{\partial\mathbf{a}}\mathbf{r}'. \tag{A.10}$$

In order to use formulae (A.2) and (A.3) the integration in matrix elements in Eq. (A.8) should be produced over $\mathbf{r}'$ for $0 < r' < r_f$. Relatively high energy barriers at the boundary of NC (3.2 and 4.3 eV for electrons and holes, respectively) allow only a small portion of the confined carriers charge density to penetrate outside. The charge density of confined carriers occurring in SiO_2 due to tunnelling accounts just a few percents [76]. Therefore the largest contribution is given by the Coulomb interaction induced by the carrier density inside the NC. To that end, it is enough to use potential Φ_1 (see Eq. A.2) only. We can write for it

$$\frac{\partial\Phi_1(\mathbf{r},\mathbf{a})}{\partial\mathbf{a}} = \frac{q}{a^2\varepsilon_2}\mathbf{J}, \tag{A.11}$$

where

$$\mathbf{J} = -\frac{\mathbf{a}}{a}J_1 + \frac{\mathbf{r}}{r}J_2, \tag{A.12}$$

and

$$J_1 = 1 + \sum_{l=1}^{\infty}\frac{(2l+1)\varepsilon_2}{l\varepsilon_1+(l+1)\varepsilon_2}\left(\frac{r}{a}\right)^l\left[(l+1)P_l(\cos\vartheta) + \cos\vartheta\frac{\partial P_l(\cos\vartheta)}{\partial\cos\vartheta}\right], \tag{A.13}$$

$$J_2 = \sum_{l=1}^{\infty}\frac{(2l+1)\varepsilon_2}{l\varepsilon_1+(l+1)\varepsilon_2}\left(\frac{r}{a}\right)^l\frac{\partial P_l(\cos\vartheta)}{\partial\cos\vartheta}. \tag{A.14}$$

So, Eq. (A.8) transforms into

$$W_{i'i} = \frac{2\pi e^2}{\hbar \Delta_E \varepsilon_2^2 a^4} \frac{1}{N_i} \sum_{M,M'} \frac{1}{N_f} \sum_{ff'} \left| \mathbf{d}_{ff'} \langle i', M' | \mathbf{J} | i, M \rangle \right|^2 J_T(N), \tag{A.15}$$

where the ion dipole momentum is given by

$$\mathbf{d}_{ff'} = \int \psi^*_{f'}(\mathbf{r}) \mathbf{r} \psi_f(\mathbf{r}) \mathrm{d}^3\mathbf{r}. \tag{A.16}$$

Averaging Eq. (A.15) over the directions of $\mathbf{d}_{ff'}$ one gets

$$W_{i'i} = \frac{2\pi e^2}{3\varepsilon_2^2 \hbar \Delta_E R^4} \frac{1}{N_f} \sum_{ff'} |\mathbf{d}_{ff'}|^2 I_{i'i}(a) J_T(N), \tag{A.17}$$

where the dimensionless factor $I_{i'i}(a)$ is defined by

$$I_{i'i}(a) = \frac{1}{N_i} \left(\frac{R}{a} \right)^4 \sum_{M,M'} |\langle i', M' | \mathbf{J} | i, M \rangle|^2, \tag{A.18}$$

where the square of the matrix element absolute value is assumed to be averaged over the directions of vector a.

Introducing the radiative lifetime τ_{rad} of the erbium ion in the first excited state ($^4I_{13/2}$) [124]

$$\frac{1}{\tau_{\mathrm{rad}}} = \frac{1}{N_{f'}} \sum_{ff'} \frac{4}{3} e^2 d_{ff'}^2 \frac{\sqrt{\varepsilon_2} (\Delta_{ff'})^3}{\hbar^4 c^3}, \tag{A.19}$$

one gets finally

$$W_{i'i} = \frac{\pi}{2\sqrt{\varepsilon_2}} \frac{1}{\tau_{\mathrm{rad}}} \frac{1}{R^4} \left(\frac{\hbar c}{\Delta_{ff'}} \right)^3 \frac{e^2}{\varepsilon_2^2 \Delta_E} I_{i'i}(a) J_T(N). \tag{A.20}$$

Evaluation of Eq. (A.20) using values $\tau_{\mathrm{rad}} = 2$ ms, and $R_{NC} = 1.55$ nm leads to

$$W_{i'i} = 8.3 \times 10^9 \left(\frac{1.55\mathrm{nm}}{R} \right)^4 I_{i'i}(a) J_T(N)\ \mathrm{s}^{-1}. \tag{A.21}$$

The results of calculations of the factors $I_{i'i}(a)$ for electrons are shown in Fig. 2.12. Corresponding plots for holes can be found in [77]. It has been shown that $I_{i'i}$ are actually the functions of the relation a/R only, at least for NC sizes in the range 2.4–3.3 nm.

For completeness, we consider the contribution of carrier density outside the dot to the probability of Er^{3+} excitation. The potential Φ_2 given by Eq. (A.3) should be used outside the NC. We get

$$\frac{\partial \Phi_2(\mathbf{r},\mathbf{a})}{\partial \mathbf{a}} = \frac{q}{R^2\varepsilon_2}\mathbf{J}', \tag{A.22}$$

where

$$\mathbf{J}' = \frac{\mathbf{a}R}{a^2}J_1' - \frac{\mathbf{r}R}{ar}J_2' + \frac{(\mathbf{r}-\mathbf{a})R^2}{|\mathbf{r}-\mathbf{a}|^3}, \tag{A.23}$$

$$J_1' = \sum_{l=1}^{\infty} \frac{\varepsilon_1-\varepsilon_2}{l\varepsilon_1+(l+1)\varepsilon_2}\left(\frac{R}{a}\right)^{(l+1)}\left(\frac{R}{r}\right)^{(l+1)}\left[(l+1)P_l(\cos\vartheta)+\cos\vartheta\frac{\partial P_l(\cos\vartheta)}{\partial\cos\vartheta}\right], \tag{A.24}$$

$$J_2' = \sum_{l=1}^{\infty} \frac{\varepsilon_1-\varepsilon_2}{l\varepsilon_1+(l+1)\varepsilon_2}\left(\frac{r}{a}\right)^{l}\frac{\partial P_l(\cos\vartheta)}{\partial\cos\vartheta}\,. \tag{A.25}$$

Producing the calculations analogous to the ones described above for the carriers being inside the NC, one can find that the contribution of the confined carriers tunnelling to the excitation probability is given by an expression similar to Eq. (A.20). Our calculations have shown that the input is negligible.

The parameters of the multiphonon transition accompanying the Auger processes are not well defined. There is no data on the electron-phonon interaction for Er^{3+} ions in the state $^4I_{13/2}$ in SiO_2 either. Thus the interaction of confined carriers with optical phonons should be considered. The dispersion of optical phonons in bulk silicon can be neglected and the multimode model of phonon transition becomes equivalent to the one-mode Huang-Rhys model [78]. Phonon factor $J_T(N)$ is presented in Table A.1 (and 2.2) calculated with a reasonable value of Huang-Rhys parameter $S = 0.1$ at room temperature. The interaction with optical phonons is forbidden for electrons in silicon, so one can suppose that the interaction of confined carriers with oxygen vibration is also responsible for multiphonon assisted Auger processes in the system under consideration. The values of phonon factor $J_T(N)$ at $\hbar\omega_{\rm ph} = 140$ meV corresponding to the oxygen vibrations are shown in Table A.1 as well.

N	-2	-1	0	$+1$	$+2$	$+3$
$\hbar\omega_{\rm ph} =$ **60 meV**	5.2×10^{-5}	0.0096	0.87	0.098	0.0054	0.2×10^{-3}
$\hbar\omega_{\rm ph} =$ **140 meV**	9.0×10^{-8}	0.0004	0.9	0.091	0.0046	0.15×10^{-3}

Table A.1: *Phonon factor $J_T(N)$ calculated with $S = 0.1$ for two different phonon energies $\hbar\omega_{\rm ph}$ and temperature $T = 300$ K.*

A.2 Erbium excitation by the recombination of confined carriers

Let us consider the excitation of Er^{3+} ions by recombination of confined electron and hole. For the NCs under consideration ($d \sim 3.1$ nm) the recombination energy is larger than 1.5 eV. Therefore the energy transfer to the Er^{3+} ion by an Auger recombination of such an exciton can be effective only if it causes the direct transition of the ion into the third excited state $^4I_{9/2}$ (energy of transition from the ground state $^4I_{15/2}$ is $\Delta_{03} = 1.55$ eV), the fourth $^4F_{9/2}$ (transition energy $\Delta_{04} = 1.9$ eV) or higher excited states. One should notice that the Er^{3+} ion can not be excited directly into the state $^4I_{13/2}$ via such a process. In order to calculate the transition probability we can use formula (A.8), just assuming that initial and final states of confined carriers now belong to different bands and dividing the probability by the degeneracy of the final state as far as only one final state is empty if there is one electron-hole pair in the NC. One should also choose appropriate parameters of the phonon system.

Crucial for the matrix element evaluation is keeping in mind that the value $\hbar\Delta k$ of momentum transmitted during recombination process is large. The minima of the conduction band in k-space is shifted from the Γ point by the wave vector $k_0 = 0.85k_X$ (k_X is the Brillouin zone edge). And it was shown in Ref. [125] that the momentum to transmit is even larger than $\hbar k_0$: $\hbar\Delta k = 1.15\hbar k_X$. Such a great momentum can only be transferred to the f-shell of the erbium ion by the Coulomb interaction at a distance less than the lattice constant of silicon. So the interaction has a contact character and is determined by the electron and hole wave function values at the position $\mathbf{a}$ of the erbium.

Once carriers are strongly confined in the NC, and the tunnelling is weak, the interaction is possible either inside the NC or in its vicinity. When dealing with the Coulomb interaction at distances smaller than the lattice constant, no screening should be taken into account any more, and the effective dielectric constant value can be assumed to be $\varepsilon_{\text{eff}} = 1$. In this case the absolute value square of the matrix element in Eq. (A.8) averaged over the degenerate electron and hole states can be calculated in analogy to bulk Auger processes [126, 127] as

$$\overline{|\langle f', i'|e\Phi|f, i\rangle|^2} = \frac{(2\pi)^2 e^4}{\varepsilon_{\text{eff}}^2} |\langle f|z^2|f'\rangle|^2 \, |\langle u_0|u_{cz}\rangle|^2 \left|\xi^{e,i}(\mathbf{a})\right|^2 \frac{1}{N_{i'}} \sum_{M'} \left|\xi^{h,i'}_{M'0}(\mathbf{a})\right|^2, \tag{A.26}$$

where $\xi^{e,i}(\mathbf{r})$ is the electron envelope function in the initial state and for shortness of notations the total hole wave function in the final state is written as

$\psi^{h,i'}_{FM}(\mathbf{r}) = \sum_m \xi^{h,i'}_{Mm}(\mathbf{r}) u_m$ with u_m ($m = -1, 0, +1$) being the hole Bloch functions; $N_{i'} = 2F' + 1$ is the degeneracy of the hole state; $|\langle u_0 | u_{cz}\rangle| \approx 0.25$ is the overlap integral between the bottom of the valence band $\Gamma^l_{25'}$ and the second conduction band $\Delta^c_{2'}$ with k at the position in the first Brillouin zone where the first conduction band has its minimum [128]. Using expression (A.26) for the right hand side of Eq. (A.8) divided by $N_{i'}$ we get the expression for the transfer probability for given position of Er^{3+} and radius of the NC

$$W_{\mathrm{tr}}(\mathbf{a}; R) = \frac{3\pi}{2} \frac{1}{\hbar^2 \omega_{\mathrm{ph}}} \left(\frac{e^2}{\varepsilon_{\mathrm{eff}} R} \right)^2 Q(\mathbf{a}; R) \, |\langle u_0 | u_{cz}\rangle|^2 \, \frac{\gamma_f r_f^4}{R^4} \, J_T(N). \tag{A.27}$$

Here the factor $\gamma_f r_f^4$ comes from the summation over f and averaging over f' of the absolute value square of the matrix element $\langle f | z^2 | f' \rangle$, where $r_f \approx 0.43$ Å is the radius of the $4f$-shell of the Er^{3+} ion and the unknown factor γ_f is of the order of 1. We have introduced a dimensionless factor $Q(\mathbf{a}; R)$ defined by

$$Q(\mathbf{a}; R) = \left(\frac{4\pi}{3} R^3 \right)^2 \left| \xi^{e,i}(\mathbf{a}) \right|^2 \frac{3}{N_{i'}} \sum_{M'} \left| \xi^{h,i'}_{M'0}(\mathbf{a}) \right|^2 . \tag{A.28}$$

If we assume the homogeneous probability distribution for the Er^{3+} ion inside the NC then the probability of excitation transfer averaged over the position of the Er^{3+} ion inside the NC is given by Eq. (A.27) where in place of $Q(\mathbf{a}; R)$ we have

$$Q_{\mathrm{in}}(R) = \frac{1}{\frac{4\pi}{3} R^3} \int_{a<R} \mathrm{d}^3\mathbf{a} \, Q(\mathbf{a}; R). \tag{A.29}$$

In order to calculate the average transfer probability at some distance D from the NC boundary we introduce

$$Q_{\mathrm{surf}}(R) = \frac{1}{4\pi} \int \mathrm{d}\Omega \, Q(\mathbf{R}; R), \tag{A.30}$$

where the integral is taken over the full solid angle Ω. Then the abovementioned probability is given by Eq. (A.27) where in place of $Q(\mathbf{a}; R)$ we have

$$Q_{\mathrm{surf}}(R) \exp[-2(\tilde{\kappa}_e + \tilde{\kappa}_h) D/R]. \tag{A.31}$$

Here the dimensionless factors

$$\tilde{\kappa}_{e(h)} = \sqrt{\frac{2 m^{\mathrm{o}}_{e(h)} [U_{e(h)} - E_{e(h)}] R^2}{\hbar^2}} \tag{A.32}$$

determine the decay of the electron and hole wave functions outside the NC, E_e and E_h are the electron and hole quantization energies, $m_e^{\rm o}$ and $m_h^{\rm o}$ are the electron and hole masses outside the NC and $U_e = 3.2$ eV and $U_h = 4.3$ eV are the corresponding energy barriers at the NC boundary. For the considered NCs $2(\tilde{\kappa}_e + \tilde{\kappa}_h)$ is on the order of 10^2 (see Table A.2). Therefore the probability of the excitation transfer by the electron-hole recombination decays rapidly with increase of the distance between the erbium and NC. It becomes negligible at the distance of only several angstroms.

For local vibrations of erbium ions in fluorozirconate glass by optical transitions from the higher excited states into the ground state the values around $\hbar\omega_{\rm ph} = 60$ meV and $S = 0.1$ were reported in Ref. [129]. Notice that bulk optical phonons in Si also have approximately the same energy. These values we have used for the calculation of the phonon factor $J_T(N)$ in the transfer probability (see Table A.1). For the estimation of the transfer probability we have also used $\gamma_f = 1$. Then Eq. (A.27) can be written as

$$W_{\rm tr} = 0.8\times 10^{11}\, Q J_T(N)\ {\rm s}^{-1}. \tag{A.33}$$

We have analyzed transitions induced by electron and holes being in one of the two lowest states. The numerical factors $Q_{\rm in}$ and $Q_{\rm surf}$ are given in Table A.2 for $R = 1.55$ nm together with the corresponding energies which should be compensated by phonons and the decay factor $2(\tilde{\kappa}_e + \tilde{\kappa}_h)$.

Transition	$\boldsymbol{E_{i'i} - \Delta_{03}}$	$\boldsymbol{E_{i'i} - \Delta_{04}}$	$\boldsymbol{Q_{\rm in}}$	$\boldsymbol{Q_{\rm surf}}$	$\boldsymbol{2(\tilde{\kappa}_e + \tilde{\kappa}_h)}$
$\boldsymbol{1e_0 \to 1hm_1}$	-41 meV	-391 meV	1.34	0.043	98.9
$\boldsymbol{2e_0 \to 1hm_1}$	186 meV	-164 meV	1.24	0.98	98.0
$\boldsymbol{1e_0 \to 1hh_1}$	128 meV	-222 meV	1.06	0.19	97.7
$\boldsymbol{2e_0 \to 1hh_1}$	327 meV	-23 meV	0.77	0.20	96.8

Table A.2: *Calculated parameters of several interband transitions for NC diameter of 3.1 nm.*

A.3 Dipole-dipole contribution

The probability of the excitation governed by the dipole-dipole interaction can be presented as

$$W_{\rm dd} = \frac{8\pi}{3}\frac{1}{\hbar^2\omega_{\rm ph}}\frac{e^4}{\varepsilon_{\rm eff}^2 a^6} d_{\rm ex}^2 \sum_{j\geq 3} d_{0j}^2 J_T(N_j), \tag{A.34}$$

where $J_T(N_j)$ is the phonon factor and $d_{\rm ex}$ is the dipole momentum of the confined exciton, which can be estimated by using the its relation to the confined exciton radiative lifetime

$$\frac{1}{\tau_{\rm ex}^{\rm rad}} = \frac{4e^2 E_{\rm ex}^3 d_{\rm ex}^2 n_{\rm eff}}{3\hbar^4 c^3}. \tag{A.35}$$

Here $E_{\rm ex}$ is the exciton energy and the effective refraction index $n_{\rm eff}$ is determined by the formula [130]

$$n_{\rm eff} = \left(\frac{\varepsilon_{\rm m}}{\varepsilon_{\rm eff}}\right)^2 {\varepsilon_{\rm m}}^{1/2}, \tag{A.36}$$

where $\varepsilon_{\rm Si}$ and $\varepsilon_{\rm m}$ are the dielectric constants of silicon and medium, respectively, and $\varepsilon_{\rm eff} = (\varepsilon_{\rm Si} + 2\varepsilon_{\rm m})/3$.

Matrix elements d_{0j} in (A.34) correspond to the transitions in the f-shell of Er^{+3}, and can be expressed via the corresponding oscillator strengths P_{0j}:

$$d_{0j}^2 = \frac{3\hbar^2}{2m_0 \Delta_{0j} n_{\rm m}} P_{0j}, \tag{A.37}$$

where, in the simplest approximation, $n_{\rm m}$ is the refraction index of the medium [131]. To our knowledge, there are no data in the literature concerning the oscillator strengths of transitions between the levels of the Er^{3+} ion in the considered inhomogeneous media. However, we can estimate them via the oscillator strengths found for several glasses and solutions [131,132]: $P_{03} = 1 - 3\times10^{-7}$ for transition ${}^4I_{9/2} \rightarrow {}^4I_{15/2}$, $P_{04} \approx 2\times10^{-6}$ for transition ${}^4I_{9/2} \rightarrow {}^4I_{15/2}$. Based on these data we estimate $d_{03}^2 = 1 \times 10^{-22}$ cm^2, $d_{04}^2 = 7 \times 10^{-22}$ cm^2.

The calculation leads to the estimation

$$W_{\rm dd} \lesssim 10^{-1} \left(\frac{R}{a}\right)^6 \frac{1}{\tau_{\rm ex}^{\rm rad}}. \tag{A.38}$$

Thus, one can see that the Förster mechanism does not work effectively for the considered system, especially at some distance from the NC, because the radiative recombination of confined carriers is a quicker process. Again the excitation of the first excited state of the Er^{3+} is additionally delayed by the multiphonon relaxation from the higher excited states.

B The relative quantum efficiency

In absorption measurements, the intensity of light transmitted through a sample is given by

$$I_1 = I_0 \exp(-\alpha L), \tag{B.1}$$

with I_0 the incident intensity, L the sample thickness, and α the absorption coefficient. (For this analysis, the reflection is neglected; in any case, wavelength-independent reflection will not influence the conclusion.) The fraction of photons that are absorbed from the beam, the absorbance signal S_{abs}, is thus:

$$S_{abs} = \frac{I_0 - I_1}{I_0} = 1 - \exp(-\alpha L), \tag{B.2}$$

and ranges from 0 (full transmission) to 1 (full absorption). The number of photons absorbed per pulse is then equal to the number of photons incident on the sample (given by the product of the beam area A, the photon flux ϕ, and the laser pulse length Δt), and the fraction given above:

$$N_{abs} = \phi \Delta t A S_{abs}. \tag{B.3}$$

(Measurements of absorption are performed at low intensity to avoid non-linear effects such as double-photon absorption). If PL occurs with an efficiency η, the number of photons emitted after each pulse is

$$N_{PL} = \eta N_{abs} = \eta \phi \Delta t A S_{abs}. \tag{B.4}$$

The luminescence signal S_{PL} is proportional to the number of photons emitted:

$$S_{PL} = \chi N_{PL} = \chi \eta \phi \Delta t A S_{abs}, \tag{B.5}$$

where the factor χ is a function of the geometry of the setup, the efficiency of the photodetector, etc. We define the PL yield Y_{PL} as the derivative of the PL intensity vs. flux:

$$Y_{PL} \equiv \frac{dS_{PL}}{d\phi} = \chi \eta \Delta t A S_{abs}, \tag{B.6}$$

and the ratio of luminescence yield and the absorbance signal is given by

$$\frac{Y_{PL}}{S_{abs}} = \chi\eta\Delta t A. \tag{B.7}$$

The above formula B.7 contains only constants, except for η, which can depend on the wavelength.

When changing to another setup, χ, Δt, and A can change. However, in order to be able to compare data from different setups, the measurements can be auto-calibrated on the saturation behavior. The saturation of photoluminescence intensity on increase of flux can be described as follows:
The number of emitters (Si NCs or Er^{3+}) in the excited state that contribute to PL under illumination during the laser pulse, N^*, is governed by simple kinetics:

$$\frac{dN^*}{dt} = \sigma_{PL}\phi(N - N^*) - \frac{N^*}{\tau}, \tag{B.8}$$

with t time, N the number of excitable units (for instance proportional to the number of NCs or Er^{3+} in the area under illumination), τ the relaxation time, and σ_{PL} the PL excitation cross-section. When the laser pulse length Δt is short compared to τ, as is the case in the current study, the second term, describing de-excitation, can be ignored. The solution, when allowing only for single PL excitation (one photon can produce only one excitation in the emitting center) is then given by:

$$N^* = N[1 - \exp(-\sigma_{PL}\phi\Delta t)]. \tag{B.9}$$

By definition, the number of photons emitted is equal to N^*, when only radiative recombination is considered, and proportional to N^* when also non-radiative recombination is allowed. We assume here that maximum one exciton per nanocrystal can contribute to photon generation. It is well established that a strong Auger quenching takes place between excitons located within the same Si NC. Consequently, in case that multiple excitons per NC are generated during the laser pulse, only one of them will survive the non radiative recombination, and contribute a photon to the PL signal, either by emitting a photon (NC-related PL) or by transferring its energy to dopant (Er-related PL). This assumption is directly confirmed by the fact that the PL intensity saturation level is independent of the excitation wavelength—see Fig. 2.9 for the photon flux dependence of Er-related PL intensity. The time-integrated PL signal after excitation is then proportional to N^*, which thus saturates upon increase of photon flux ϕ:

$$S_{PL} = \chi N_{PL} = \chi N^* = \chi N[1 - \exp(-\sigma_{PL}\phi\Delta t)]. \tag{B.10}$$

The PL excitation cross-section σ_{PL} (and the product χN) can be determined by fitting the measured PL intensity dependence on photon flux, also shown in Fig. 2.9. In particular, we note that at infinite flux and small flux the above equation gives, respectively:

$$S_{PL,max} = \chi N, \tag{B.11}$$

$$Y_{PL} \equiv \left| \frac{dS_{PL}}{d\phi} \right|_{\phi \to 0} = \chi N \sigma_{PL} \delta t. \tag{B.12}$$

Comparison of Eq. B.6 with the last equation tells us that $N\sigma_{PL} = \eta S_{abs}$. In other words, the quantum efficiency is linked to the experimentally measured parameters as:

$$\eta = \frac{N\sigma_{PL}}{S_{abs}}. \tag{B.13}$$

Because knowledge of N cannot be obtained (only the product χN can be determined by fitting), only the relative quantum efficiency can be determined and is proportional to the ratio of the fitting parameter σ_{PL} and the measured absorbance signal S_{abs}.

Since the PL saturation level is independent of excitation wavelength, *i.e.* $S_{PL,max}$ is independent of λ_{ex}, this implies that N is a constant not depending on λ_{ex}. Thus, plotting the ratio of PL cross-section and absorbance signal will directly give us information about the relative quantum efficiency η. This method has been used for preparation of Figures 2.16 and 2.17 in section 2.3.

Bibliography

[1] C. Kittel, *Introduction to solid state physics* (John Wiley and Sons, 1996).

[2] P. Y. Yu and M. Cardona, *Fundamentals of semiconductors* (Springer, 1996).

[3] G. Davies, Physics Reports (Review section of Physics Letters) **176**, 83 (1989).

[4] M. Forcales, *Two-color spectroscopy of energy transfers in Si:Er* (Universiteit van Amsterdam, 2004).

[5] M. Klik, *Energy transfer processes in optically doped matrices: a spectroscopical approach* (Universiteit van Amsterdam, 2005).

[6] N. Q. Vinh, H. Przybylińska, Z. F. Krasil'nik, and T. Gregorkiewicz, Phys. Rev. Lett. **90**, 066401 (2003).

[7] M. Forcales, T. Gregorkiewicz, and J. M. Zavada, Solid-State Electronics **47**, 165 (2003).

[8] M. Forcales, T. Gregorkiewicz, I. V. Bradley, and J-P. R. Wells, Phys. Rev. B **65**, 195208 (2002).

[9] S. Coffa, G. Franzò, F. Priolo, A. Polman, and R. Serna, Phys. Rev. B **49**, 16313 (1994).

[10] F. Priolo, G. Franzò, S. Coffa, A. Polman, S. Libertino, R. Barklie, and D. Carey, J. Appl. Phys. **78**, 3874 (1995).

[11] F. P. Widdershoven and J. P. M. Naus, Mater. Sci. and Eng. B **4**, 71 (1989).

[12] C. Delerue and M. Lannoo, Phys. Rev. Lett. **67**, 3006 (1991).

[13] P. Wagner and J. Hage, Appl. Phys. A **49**, 123 (1989).

[14] D. T. X. Thao, C. A. J. Ammerlaan, and T. Gregorkiewicz, J. Appl. Phys. **88**, 1443 (2000).

[15] M. Forcales, M. A. J. Klik, N. Q. Vinh, J. Phillips, J-P. R. Wells, and T. Gregorkiewicz, J. of Lumin. **102**, 85 (2003).

[16] I. Tsimperidis, T. Gregorkiewicz, H. H. P. Th. Bekman, and C. J. G. M. Langerak, Phys. Rev. Lett. **81**, 4748 (1998).

[17] M. A. J. Klik, T. Gregorkiewicz, I. V. Bradley, and J-P. R. Wells, Phys. Rev. Lett. **89**, 227401 (2002).

[18] B. N. Murdin, K. Litvinenko, D. G. Clarke, C. R. Pidgeon, P. Murzyn, P. J. Phillips, D. Carder, G. Berden, B. Redlich, A. F. G. van der Meer, S. Clowes, J. J. Harris, L. F. Cohen, T. Ashley, and L. Buckle, Phys. Rev. Lett. **96**, 096603 (2006).

[19] G. von Helden, I. Holleman, A. J. A. van Roij, G. M. H. Knippels, A. F. G. van der Meer, and G. Meijer, Phys. Rev. Lett. **81**, 1825 (1998).

[20] M. Forcales, T. Gregorkiewicz, M. S. Bresler, O. B. Gusev, I. V. Bradley, and

J-P. R. Wells, Phys. Rev. B **67**, 085303 (2003).
[21] M. Forcales, T. Gregorkiewicz, and M. S. Bresler, Phys. Rev. B **68**, 035213 (2003).
[22] F. Priolo, G. Franzò, S. Coffa, and A. Carnera, Phys. Rev. B **57**, 4443 (1998).
[23] F. Priolo, S. Coffa, G. Franzò, C. Spinella, A. Carnera, and V. Bellani, J. Appl. Phys. **74**, 4936 (1993).
[24] J. M. Langer, T. Langer, G. L. Pearson, B. Krukowska-Fulde, and U. Piekara, Phys. Stat. Sol. (b) **66**, 537 (1974).
[25] M. L. W. Thewalt, D. Labrie, and T. Timusk, Sol. St. Comm. **53**, 1049 (1985).
[26] L. C. Kimerling, K. D. Kolenbrander, J. Michel, and J. Palm, Solid State Physics **50**, 333 (1997).
[27] R. A. Soref, Proc. IEEE **81**, 1993 (1993).
[28] J. Michel, L. V. C. Assali, M. T. Morse, and L. C. Kimerling, Semiconductors and Semimetals **7**, 111 (1998).
[29] S. Coffa, G. Franzò, and F. Priolo, MRS Bulletin **XX**, 25 (1998).
[30] P. M. Fauchet, Materials Today **8**, 26 (2005).
[31] Wai Lek Ng, M. A. Lourenco, R. M. Gwilliam, S. Ledain, G. Shao, and K. P. Homewood, Nature **410**, 192 (2001).
[32] M. A. Green, J. Zhao, A. Wang, P. J. Reece, and M. Gal, Nature **412**, 805 (2001).
[33] L. Pavesi, L. Dal Negro, C. Mazzoleni, G. Franzò, and F. Priolo, Nature **408**, 440 (2000).
[34] S. Tiwari, F. Rana, H. Hanafi, A. Hartstein, E. F. Crabbé, and K. Chan, Appl. Phys. Lett. **68**, 1377 (1995).
[35] R. J. Walters, G. I. Bourianoff, and H. A. Atwater, Nature Materials **4**, 143 (2005).
[36] B. Andreev, V. Chalkov, O. Gusev, A. Emel'yanov, Z. Krasil'nik, V. Kuznetsov, P. Pak, V. Shabanov, V. Shengurov, V. Shmagin, amd M. Stepikhova N. Sobolev, and S. Svetlov, Nanotechnology **13**, 97 (2002).
[37] H. Rong, A. Liu, R. Jones, O. Cohen, D. Hak, R. Nicolaescu, A. Fang, and M. Paniccia, Nature **433**, 292 (2005).
[38] O. Boyraz and B. Jalali, Optics Express **12**, 5269 (2004).
[39] H. Rong, R. Jones, A. Liu, O. Cohen, D. Hak, A. Fang, and M. Paniccia, Nature **433**, 725 (2005).
[40] A. Liu, R. Jones, L. Liao, D. Samara-Rubio, D. Rubin, O. Cohen, R. Nicolaescu, and M. Paniccia, Nature **427**, 615 (2004).
[41] V. R. Almeida, C. A. Barrios, R. R. Panepucci, and M. Lipson, Nature **431**, 1081 (2004).
[42] V. A. Joshkin, J. C. Roberts, F. G. McIntosh, S. M. Bedair, E. L. Piner, and M. K. Behbehani, Appl. Phys. Lett. **71**, 234 (1997).
[43] Y. S. Bai and R. Kachru, Phys. Rev. Lett. **78**, 2944 (1997).
[44] J. Ashley, M-P. Bernal, G. W. Burr, H. Coufal, H. Guenther, J. A. Hoffnagle, C. M. Jefferson, B. Marcus, R. M. Macfarlane, R. M. Shelby, and G. T. Sincerbox, IBM J. R. & D. **44**, 341 (2000).
[45] S. Lanzerstorfer, L. Palmetshofer, W. Jantsch, and J. Stimmer, Appl. Phys. Lett. **72**, 809 (1998).

[46] M. Markman, E. Neufeld, A. Sticht, K. Brunner, and G. Abstreiter, Appl. Phys. Lett. **78**, 210 (2001).
[47] G. E. Moore, Electronics **38**, (1965).
[48] S. Coffa, G. Franzò, and F. Priolo, Appl. Phys. Lett. **69**, 2077 (1996).
[49] C. E. Chryssou, A. J. Kenyon, T. S. Iwayama, C. W. Pitt, and D. E. Hole, Appl. Phys. Lett. **75**, 2011 (1999).
[50] D. Pacifici, G. Franzò, F. Priolo, F. Iacona, and L. Dal Negro, Phys. Rev. B **67**, 245301 (2003).
[51] P. G. Kik, M. L. Brongersma, and A. Polman, Appl. Phys. Lett. **76**, 2325 (2000).
[52] D. Kovalev, H. Heckler, M. Ben-Chorin, G. Polisski, M. Schwartzkopff, and F. Koch, Phys. Rev. Lett. **81**, 2803 (1995).
[53] M. E. Castagna, S. Coffa, M. Monaco, L. Caristia, A. Messina, R. Mangano, and C. Bongiorno, Physica E **16**, 547 (2003).
[54] A. Nazarov, J. M. Sun, W. Skorupa, R. A. Yankov, I. N. Osiyuk, I. P. Tjagulskii, V. S. Lysenko, and T. Gebel, Appl. Phys. Lett. **86**, 151914 (2005).
[55] M. J. A. de Dood, J. Knoester, A. Tip, and A. Polman, Phys. Rev. B **71**, 115102 (2005).
[56] V. M. Agranovich and M. D. Galanin, *Electronic Excitation Energy Transfer in Condensed Matter* (Elsevier, 1982).
[57] X. L. Wu, Y. F. Mei, G. G. Siu, K. L. Wong, K. Moulding, M. J. Stokes, C. L. Fu, and X. M. Bao, Phys. Rev. Lett. **86**, 3000 (2001).
[58] R. A. Senter, C. Pantea, Y. Wang, H. Liu, T. W. Zerda, and J. L. Coffer, Phys. Rev. Lett. **93**, 175502 (2004).
[59] K. Imakita, M. Fujii, and S. Hayashi, Phys. Rev. B **71**, 193301 (2005).
[60] J. Lee, J. H. Shin, and N. Park, J. Lightwave Technol. **23**, 19 (2005).
[61] M. Wojdak, M. Klik, M. Forcales, O. B. Gusev, T. Gregorkiewicz, D. Pacifici, G. Franzò, F. Priolo, and F. Iacona, Phys. Rev. B **69**, 233315 (2004).
[62] P. G. Kik and A. Polman, J. Appl. Phys. **88**, 1992 (2000).
[63] W. Shockley and H. J. Queisser, J. Appl. Phys. **32**, 510 (1961).
[64] M Fujii, M. Yoshida, Y. Kanzawa, S. Hayashi, and K. Yamamoto, Appl. Phys. Lett. **71**, 1198 (1997).
[65] F. Trojánek, K. Neudert, M. Bittner, and P. Malý, Phys. Rev. B **72**, 075365 (2005).
[66] J. P. Wilcoxon, G. A. Samara, and P. N. Provencio, Phys. Rev. B **60**, 2704 (1999).
[67] Y. M. Niquet, C. Delerue, G. Allan, and M. Lannoo, Phys. Rev. B **62**, 5109 (2000).
[68] I. N. Yassievich, A. S. Moskalenko, and A. A. Prokofiev, Opt. Mat. **28**, 810 (2006).
[69] C. Delerue, M. Lannoo, G. Allan, E. Martin, I. Mihalcescu, J. C. Vial, R. Romestain, F. Muller, and A. Bsiesy, Phys. Rev. Lett. **75**, 2228 (1995).
[70] D. Kovalev, H. Heckler, G. Polisski, and F. Koch, Phys. Stat. Sol. B **215**, 871 (1999).
[71] N. Q. Vinh M. S. Bresler I. Izeddin, M. A. J. Klik and T. Gregorkiewicz, Phys. Rev. Lett. **99**, 077401 (2007).

[72] F. Priolo, C. D. Presti, G. Franzò, A. Irrera, I. Crupi, F. Iacona, G. Di Stefano, A. Piana, D. Sanfilippo, and P. G. Fallica, Phys. Rev. B **73**, 113302 (2006).
[73] I. Izeddin, A. S. Moskalenko, I. N. Yassievich, M. Fujii, and T. Gregorkiewicz, Phys. Rev. Lett. **97**, 207401 (2006).
[74] A. S. Moskalenko, J. Berakdar, A. A. Prokofiev, and I.N. Yassievich, Phys. Rev. B **76**, 085427 (2005).
[75] M. Fujii, K. Imakita, K. Watanabe, and S. Hayashi, J. Appl. Phys. **95**, 272 (2004).
[76] A. S. Moskalenko, J. Berakdar, A. A. Prokofiev, and I. N. Yassievich, Phys. Rev. B **76**, 085427 (2007).
[77] A. A. Prokofiev, A. S. Moskalenko, and I. N. Yassievich, Mat. Science and Eng. B in press (2008).
[78] V. N. Abakumov, V. I. Perel, and I. N. Yassievich, *Nonradiative Recombination in Semiconductors*, Vol. 33 of *Modern Problems in Condensed Matter Sciences* (Elsevier, 1991).
[79] T. Förster, Ann. Physik **2**, 55 (1948).
[80] W. U. Huynh, J. J. Dittmer, and A. P. Alivisatos, Science **195**, 2425 (2002).
[81] P. Peumans, S. Uchida, and S. R. Forrest, Nature **425**, 158 (2003).
[82] B. O'Regan and M. A. Grätzel, Nature **353**, 737 (1991).
[83] A. Shah, P. Torres, R. Tscharner, N. Wyrsch, and H. Keppner, Science **285**, 692 (1999).
[84] R. T. Wegh, H. Donker, K. D. Oskam, and A. Meijerink, Science **283**, 663 (1999).
[85] A. Luque, A. Martí, and A. J. Nozik, MRS Bull. **32**, 236 (2007).
[86] A. J. Nozik, Physica E **14**, 115 (2002).
[87] R. D. Schaller and V. I. Klimov, Phys. Rev. Lett. **92**, 186601 (2004).
[88] R. J. Ellingson, M. C. Beard, J. C. Johnson, P. Yu, O. I. Mićić, A. J. Nozik, A. Shabaev, and A. L. Efros, Nano. Lett. **5**, 865 (2005).
[89] R. D. Schaller, M. A. Petruska, and V. I. Klimov, Appl. Phys. Lett. **87**, 253102 (2005).
[90] J. E. Murphy, M. C. Beard, A. G. Norman, S. P. Ahrenkiel, J. C. Johnson, P. Yu, O. I. Mićić, R. J. Ellingson, and Arthur J. Nozik, J. Am. Chem. Soc. **128**, 3241 (2006).
[91] R. D. Schaller, M. Sykora, J. M. Pietryga, and V. I. Klimov, Nano Lett. **6**, 424 (2006).
[92] M. C. Beard, K. P. Knutsen, P. Yu, J. M. Luther, Q. Song, W. K. Metzger, R. J. Ellingson, and A. J. Nozik, Nano Lett. **7**, 2506 (2007).
[93] V. I. Klimov, A. A. Mikhailovsky, D. W. McBranch, C. A. Leatherdale, and M. G. Bawendi, Science **287**, 1011 (2000).
[94] E. Hendry, M. Koeberg, F. Wang, H. Zhang, C. de Mello Donegá, D. Vanmaekelbergh, and M. Bonn, Phys. Rev. Lett. **96**, 057408 (2006).
[95] A. Polman, Physica B **300**, 78 (2001).
[96] A. Shabaev, A. L. Efros, and A. J. Nozik, Nano Lett. **6**, 2856 (2006).
[97] R. D. Schaller, V. M. Agranovich, and V. I. Klimov, Nature Phys. **1**, 189 (2005).
[98] V. I. Rupasov and V. I. Klimov, Phys. Rev. B **76**, 125321 (2007).
[99] M. Califano, A. Zunger, and A. Franceschetti, Appl. Phys. Lett. **84**, 2409 (2004).

[100] I. Mihalcescu, J. C. Vial, A. Bsiesy, F. Muller, R. Romestain, E. Martin, C. Delerue, M. Lannoo, and G. Allan, Phys. Rev. B **51**, 17605 (1995).
[101] G. Allan and C. Delerue, Phys. Rev. B **73**, 205423 (2006).
[102] C. R. Kagan, C. B. Murray, and M. G. Bawendi, Phys. Rev. B **54**, 8633 (1996).
[103] K. K. Nanda, F. E. Kruis, and H. Fissan, Nano Lett. **1**, 605 (2001).
[104] C. B. Murray, D. J. Norris, and M. G. Bawendi, J. Am. Chem. Soc. **115**, 8706 (1993).
[105] M. C. Hanna and A. J. Nozik, J. Appl. Phys. **100**, 074510 (2006).
[106] T. Trupke, M. A. Green, and P. Würfel, J. Appl. Phys. **92**, 1668 (2002).
[107] R. G. Wilson, R. N. Schwartz, C. R. Abernathy, S. J. Pearton, N. Newman, M. Rubin, T. Fu, and J. M. Zavada, Appl. Phys. Lett. **65**, 22 (1994).
[108] J. M. Zavada and D. Zhang, Solid State Electron. **38**, 1285 (1995).
[109] P. N. Favennec, H. L'Haridon, M. Salvi, D. Moutennet, and Y. Le Guillou, Electron. Lett. **25**, 718 (1989).
[110] A. J. Steckl, J. C. Heikenfeld, D. S. Lee, M. J. Garter, C. C. Baker, Y. Q. Wang, and R. Jones, IEEE J. Selec. Top. Quant. Electron. **8**, 749 (2002).
[111] D. S. Lee, J. Heikenfeld, A. J. Steckl, U. Hommerich, J. T. Seo, A. Braud, and J. M. Zavada, Appl. Phys. Lett. **79**, 719 (2001).
[112] E. Sorokin and I. T. Sorokina, Appl. Phys. Lett. **80**, 3289 (2002).
[113] S. D. Jackson and A. Lauto, Laser Surg. Med. **30**, 184 (2002).
[114] V. Y. Ivanov, M. Godlewski, A. Szczerbakow, A. Omel'Chuk, A. Davydov, N. Zhavoronkov, and G. Raciukaitis, Acta Phys. Pol. A **105**, 553 (2004).
[115] M. Pollnau and S. D. Jackson, Top. Appl. Phys. **89**, 219 (2003).
[116] H. Q. Wu, C. B. Poitras, M. Lipson, J. Hunting, and F. J. DiSalvo, Appl. Phys. Lett. **86**, 191918 (2005).
[117] P. A. Tanner, Y. L. Liu, N. M. Edelstein, K. M. Murdoch, and N. M. Khaidukov, J. Phys. Condens. Matter **9**, 7817 (1997).
[118] J. R. G. Thorne, M. Jones, C. S. McCaw, K. M. Murdoch, R. G. Denning, and N. M. Khaidukov, J. Phys. Condens. Matter **11**, 7851 (1999).
[119] V. Dierolf, C. Sandmann, J. M. Zavada, P. Chow, and B. Hertog, J. Appl. Phys. **95**, 5464 (2004).
[120] H. Siegle, G. Kaczmarczyk, L. Filippidis, A. P. Litvinchuk, A. Hoffmann, and C. Thomsen, Phys. Rev. B **55**, 7000 (1997).
[121] M. D. Shinn, W. A. Sibley, M. G. Drexhage, and R. N. Brown, Phys. Rev. B **27**, 6635 (1983).
[122] I. Izeddin, T. Gregorkiewicz, D. S. Lee, and A. J. Steckl, Superlat. Microstr. **36**, 701 (2004).
[123] B. K. Ridley, *Quantum Processes in Semiconductors* (Oxford Science Publications).
[124] A. Suchocki and J. M. Langer, Phys. Rev. B **39**, 7905 (1989).
[125] A. A. Prokofiev, I. N. Yassievich, H. Vrielinck, and T. Gregorkiewicz, Phys. Rev. B **72**, 045214 (2005).
[126] I. N. Yassievich and L. C. Kimerling, Semicond. Sci. Technol. **8**, 718 (1993).
[127] A. S. Moskalenko, I. N. Yassievich, M. Forcales, M.Klik, and T. Gregorkiewicz, Phys. Rev. B **70**, 155201 (2004).
[128] M. Cardona and F.H. Pollak, Phys. Rev. **142**, 530 (1966).

[129] M. D. Shinn, W. A. Sibley, M. G. Drexhage, and R. N. Brown, Phys. Rev. B **27**, 6635 (1983).
[130] A. Thraendhardt, C. Ell, G. Khitrova, and H. M. Gibbs, Phys. Rev. B **65**, 035327 (2002).
[131] B. R. Judd, Phys. Rev. **127**, 750 (1962).
[132] W. J. Miniscalco, J. Lightwave Techn. **9**, 234 (1991).

Summary

This thesis presents PhD promotion research on spectroscopy of optoelectronic media carried out at the Van der Waals-Zeeman Institute for Experimental Physics of the University of Amsterdam, during the years 2003 to 2007. Using a range of electro- and photoluminescence techniques, the investigations deal with various aspects of energy transfer processes in the material. These are studied from a fundamental point of view, and the conclusions are considered in view of prospective practical applications. The relevant theoretical modeling is developed in order to interpret the data and to propose microscopic models.

The Introduction starts by reflecting on the motivation of this research. After pointing out the importance of electronics—and therefore the element silicon—in modern society: the *silicon age*, its fundamental physical limits are presented. It is concluded that suitable alternatives need to be studied, and developed. In this context it is argued that *photonics – i.e.* the use of photons, instead of electrons, as information carriers – is an attractive field which could respond to the societal demand for ever smaller and faster devices. Doping of semiconductors with rare earth ions—and especially with erbium in view of its technologically important 1.5 μm emission—, and the use of nanostructured silicon are two prominent realizations of Si photonics. Both are considered in this thesis and several aspects are studied in detail.

After exposing the motivation for the research, the Introduction presents some basic concepts of condensed matter physics, necessary for the investigations: the definition of semiconductor materials and some considerations on their optical properties, a brief characteristics of the element silicon, and the concept of optical doping of a semiconductor describing the use of rare earth ions and silicon nanocrystals.

In Chapter 1, an in-depth study of optical properties of silicon doped with erbium ions is presented. The Section 1.1of the chapter deals with fundamental aspects of energy transfer between the host, silicon, and the optically active element, the rare earth ion erbium. Making use of a nanostructured sample consisting of a series of nanolayers of undoped and Er-doped silicon, and applying a Free Electron Laser for two-color spectroscopy, provides evidence that

proves the role of the erbium-related donor in the host-mediated optical excitation of erbium. Based on these results, a new excitation mechanism in this system is proposed and then confirmed by excitation spectroscopy.

While the first section of Chapter 1 is related to fundamental aspects of the optical excitation of erbium-doped crystalline silicon, Section 1.2 proves the potential of the multinanolayer system for applications. There, a fully CMOS compatible electro-optical converter with memory function is presented. Its electrically driven optical *write-read-erase* functionality is demonstrated outside cryogenic temperatures. A cross point memory array based erbium-doped silicon is proposed as a photonic memory device.

Chapter 2 focuses on the problem of sensitization of erbium in a silicon dioxide matrix with silicon nanocrystals. This system combines positive features of erbium-doped crystalline silicon with those of erbium-doped silicon dioxide. The key points are the high excitation cross section of the optical excitation of erbium via the silicon nanocrystals (similar to that of erbium excitation via the crystalline silicon host) and the thermal stability of the photoluminescence of erbium dispersed in a silicon dioxide matrix. Full understanding of the sensitization mechanism is of crucial importance for exploration of the potential of this material in the field of silicon photonics. In order to achieve that, a series of samples exhibiting simultaneous photoluminescence from both, erbium and silicon nanocrystals, were investigated by time-resolved spectroscopy with a high resolution obtained by implementation of a photon counting detection technique.

In the first Section 2.1 of Chapter 2, a fast erbium-related photoluminescence component, sensitized by silicon nanocrystals, is reported. Its a characteristic time decay is in the nanoseconds range – between five and six orders of magnitude faster than the usually reported radiative decay of erbium. Excitation and de-excitation, responsible for this fast component take place within the first microsecond after the laser excitation pulse, i.e., before the previously reported, microseconds excitation of erbium by the silicon nanocrystals takes place. An Auger process related to cooling and re-heating of confined carriers by transitions between the space-quantized levels of the silicon nanocrystals is proposed as the mechanism responsible for this fast photoluminescence band. With the new evidence at hand, a long-standing problem of apparent loss of optical activity of erbium dopants upon sensitization with silicon nanocrystals is cleared up, and it is shown that up to 50% of the total erbium content in the sample is excited via the newly proposed fast mechanism (while the excitation is immediately quenched by the reverse process).

The following Section 2.2 develops fully the model proposed in the previous Section 2.1 and exhaustively investigates the energy transfer processes between

silicon nanocrystals and erbium. All photoluminescence bands are identified and their kinetics investigated in detail. Accordingly, a comprehensive model of energy transfer mechanism for light generation and quenching in the system is proposed. The necessary theoretical framework is developed, yielding the microscopic understanding of the underlying physical mechanisms. The observed photoluminescence spectra, high-resolution dynamics, and excitation cross section measurements are combined with theoretical modeling and simulations rendering a consistent microscopic description of the sensitization effect and its limitations.

One of the consequences of the model proposed in Section 2.1 and developed in Section2.2 is the appearance of a second excitation mechanism when a photon with sufficient quantum energy is absorbed by a silicon nanocrystal. In this case, there exists a probability for this photon to "divide" its energy inducing two excitation processes of two erbium ions. In the so-called *quantum cutting* process, a high energy photon can be divided into two or more quanta of lower energy. The object of investigation of Section 2.3 is the photon cutting by silicon nanocrystals; nearby erbium ions and neighboring nanocrystals are used to enable this effect. The experiments demonstrate that above a certain energy threshold for the quantum energy of the incoming photons (defined by the sum of the silicon nanocrystal band gap and the energy necessary for excitation of the neighboring probe – either an erbium ion or another nanocrystal) the relative quantum efficiency of the excitation mechanism increases. This is explained in terms of two subsequent excitation processes: the primary one due to the intra-band cooling of the "hot" carrier within the quantized states of the nanocrystal, followed by a secondary excitation due to the inter-band recombination of the electron-hole pair.

The excitation increase by photon cutting process taking place between silicon nanocrystals is of paramount importance for photovoltaic applications. In solar cells, a substantial part of the incoming photon energy in the high-energy range of the solar spectrum is wasted to heat, as the excess energy of the absorbed photon is converted into kinetic energy of the electron-hole pair. This is one of the limiting factors for the maximum efficiency of solar cells. Therefore, as argued in Section 2.3, the space-separated quantum cutting process may lead the way to a substantial improvement of photovoltaic devices.

Finally, in Chapter 3, the optical properties of erbium-doped large band gap hosts are investigated. In Section 3.1, photoluminescence and photoluminescence excitation spectroscopies are applied to erbium-doped gallium nitride samples. Based on these results, the possible multiplicity of the erbium sites in this host is discussed. In Section 3.2, the potential of erbium doping for realization of mid-infrared emission at the wavelength of 2.7 μm, due to the

transition between the second and the first excited states, is studied. For that purpose, a large band gap fluoride crystal is used. In this material erbium occupies a well-defined substitutional site only, is used.. The results obtained for the fluoride serve to facilitate the understanding of the erbium-doped gallium nitride system. By recording the photoluminescence transients for several transition, lifetimes of the individual excited states are determined. The results indicate that erbium doping of both hosts should enable the mid-infrared emission.

Samenvatting

Deze thesis beschrijft PhD promotieonderzoek betreffende spectroscopie in optoelektronische media, voltrokken op het Van der Waals-Zeeman Instituut voor Experimentele Fysica op de Universiteit van Amsterdam gedurende de jaren 2003 tot en met 2007. Vanuit een experimentele benadering worden in het onderzoek verscheidene aspecten behandeld aangaande energieoverdracht in het bovengenoemde materiaal, waarbij gebruik gemaakt wordt van een range aan elektro- en fotoluminescentie spectroscopie technieken. Deze worden bestuurd vanuit een fundamentele invalshoek en conclusies worden getrokken met het oog op toekomstige praktische toepassingen. Theoretische beschouwingen zijn uitgevoerd om de data te interpreteren en microscopische modellen voor te stellen.

De Introductie beschrijft de motivatie voor het verrichte onderzoek. Nadat er wordt geattendeerd op het belang van het gebruik van elektronica—en zodoende het element silicium—in de huidige maatschappij: de *silicon age*, worden de fundamentele fysische limieten te berde gebracht. Hiervoor dienen adequate oplossingen worden bestudeerd en ontwikkeld. Wegens de vele nadelige effecten is *photonics*—*i.e.* het gebruik van fotonen in plaats van elektronen als informatiedragers—een aantrekkelijke aanpak voor het oplossen en vermijden van complicaties die zich voordoen. Het doteren van halfgeleiders met zeldzame aardmetalen—met name erbium met een emissiegolflengte die optimaal is voor telecommunicatieve doeleinden—en het gebruik van nanogestruktureerd silicium zijn twee prominente voorbeelden voor silicium *photonics*. Van beide zijn verscheidene aspecten bestudeerd en uiteengezet in deze thesis.

Na het beschrijven van de motivatie van het onderzoek zullen er in de Introductie tevens basisconcepten van de gecondenseerde materie worden besproken die noodzakelijk zijn om een fundamenteel begrip te krijgen voor de uitgevoerde experimenten: de definitie van een halfgeleider materiaal, waarbij wordt ingegaan op de optische eigenschappen, een korte beschrijving van het element silicium en het concept van optisch doteren van een halfgeleider met zeldzame aardmetalen en silicium nanokristallen.

In Hoofdstuk 1 wordt een diepgaand onderzoek gepresenteerd aangaande

de optische eigenschappen van silicium gedoteerd met erbium-ionen. In de eerste Paragraaf 1.1 worden de fundamentele aspecten behandeld betreffende energieoverdracht tussen het *host* materiaal silicium en het optisch actieve materiaal (het zeldzame aardion erbium). Op het sample, erbium-gedoteerd silicium in een nanolagen-configuratie, worden met behulp van het gebruik van een Vrije Elektronen Laser *two-color* spectroscopie experimenten verricht om bewijs te vergaren over de rol van een erbium-gerelateerd donor niveau wat een belangrijke rol speelt in de optische excitatie van erbium via het *host* materiaal. Met de verkregen resultaten in ogenschouw genomen wordt er innovatief excitatiemechanisme in dit systeem voorgesteld en gedemonstreerd.

Waar het eerste gedeelte van Hoofdstuk 1 meer gericht is op de fundamentele aspecten van de optische excitatie van erbium-gedoteerd bulk silicium, wordt er in Paragraaf 1.2 besproken welke mogelijkheden er zijn omtrent toepassingen met het systeem met multi-nanolagen configuratie. Er wordt een CMOS compatibel elektro-optische schakelaar met geheugen-functie gedemonstreerd, die boven cryogene temperaturen functioneert en elektrisch aangestuurde optische *write-read-erase* functionaliteit vertoont; ook wordt er een op erbium-gedoteerd silicium gebaseerd *cross point memory array* geopperd als geheugen fotonisch apparaat.

Hoofdstuk 2 focust op de sensibilisering van erbium met silicium nanokristallen in een siliciumdioxide matrix. Dit systeem combineert de positieve eigenschappen van erbium-gedoteerd bulk silicium met die van erbium-gedoteerd siliciumdioxide. Een belangrijk aspect van dit systeem is de hoge excitatie crosssectie van de optische excitatie van erbium via silicium nanokristallen (vergelijkbaar met die van erbiumexcitatie via bulk silicium). Naast dit aspect is de thermische stabiliteit van de fotoluminescentie van erbium geïmplementeerd in een siliciumdioxide matrix eveneens van groot belang. Mitsdien is het begrip van de sensibilisering van erbium met behulp van silicium nanokristallen van cruciaal belang om een optimale ontwikkeling van de mogelijkheden met dit materiaal te verkrijgen. Om dit te bereiken zijn er hoog-resolutie tijdgerelateerde spectroscopie metingen verricht (uitgevoerd met het gebruik van een *photon counter*) op een serie samples, die geselecteerd zijn wegens het vertonen van zowel erbium als silicium nanokristal fotoluminescentie.

In de eerste Paragraaf 2.1 van het hoofdstuk wordt een snelle erbium-gerelateerde fotoluminescentie component, gesensibiliseerd door silicium nanokristallen, met een karakteristieke vervaltijd in de orde van nanoseconden gerapporteerd; deze is tussen de vijf en zes ordes van grootte kleiner dan de gebruikelijk gerapporteerde vervaltijden van erbium fotoluminescentie. De excitatie en de-excitatie van deze snelle component, die plaatsvindt in de eerste microseconde na de excitatiepuls van de laser, verschijnt voor de normaal ge-

rapporteerde microseconde excitatie van erbium door silicium nanokristallen. Een Auger proces gerelateerd aan overgangen van ladingsdragers tussen gekwantiseerde niveaus van silicium nanokristallen wordt voorgesteld als mechanisme achter deze snelle fotoluminescentie band. Aan de hand van dit nieuwe bewijs kan een al lang bestaand probleem van verlies van optische activiteit van erbium na sensibilisering door silicium nanokristallen worden verklaard en wordt er aangetoond dat tot 50

De volgende Paragraaf 2.2 beschrijft tot in details het model voorgesteld in 2.1 en er wordt besproken hoe de energieoverdracht tussen silicium nanokristallen en erbium tot stand komt. Verschillende fotoluminescentie emissiebanden worden geïdentificeerd en hun kinetica wordt in detail onderzocht. Een uitgebreid model van het mechanisme van energieoverdracht voor lichtgeneratie in het systeem wordt voorgesteld. In het bijzonder worden de fotoluminescentiespectra, hoge-resolutie fotoluminescentie kinetica en de metingen van de excitatie cross-secties gecombineerd met berekeningen van de verschillende mogelijke excitatie en de-excitatie mechanismen in het systeem, om een consistente microscopische beschrijving van het sensibiliseringseffect en de beperkingen daarvan te kunnen geven.

Eén van de gevolgen van het model dat in Paragraaf 2.1 wordt voorgesteld en dat in Paragraaf 2.2 verder wordt ontwikkeld, is het verschijnen van een tweede excitatie-mechanisme wanneer een foton met voldoende kwantumenergie door een silicium nanokristal wordt geabsorbeerd. In dit geval bestaat er een mogelijkheid dat dit foton zijn energie "verdeelt"wat leidt tot twee excitatieprocessen. In het zogenaamde *kwantumsplitsingproces*, kan één hoog energetisch foton in twee of meerdere energiequanta worden verdeeld. Het onderwerp van onderzoek van Paragraaf 2.3 is het splitsen van fotonen met silicium nanokristallen, waarbij nabijgelegen erbiumionen en naburige nanokristallen worden gebruikt om dit effect mogelijk te maken. De experimenten tonen aan hoe de relatieve kwantumefficiëntie van het excitatiemechanisme toeneemt boven een bepaalde energiedrempelwaarde van een geabsorbeerd foton; deze is gedefinieerd als de som van de bandkloofenergie van het silicium nanokristal en de noodzakelijke excitatie-energie van de naburige *probe* (een erbiumion dan wel een andere nanokristal). Dit wordt verklaard door een eerste excitatie toe te schrijven aan het intraband koelen van een "hete" ladingsdrager - gecreëerd door de absorptie van een inkomend foton - binnen de gekwantiseerde niveaus van nanokristal. Vervolgens vindt er een secundaire excitatie plaats door middel van de interband recombinatie van het elektron-gat paar.

De gemeten toename van de kwantumefficiëntie in het geval van kwantumsplitsing door silicium nanokristallen is van groot belang voor fotovoltaïsche

toepassingen. In zonnecellen wordt een wezenlijk deel van de inkomende fotonenergie in de hoge-energierange van het zonnespectrum omgezet in warmte, aangezien het teveel aan energie van het geabsorbeerde foton in kinetische energie van het elektron-gat paar wordt omgezet; dit is één van de beperkende factoren voor de efficiëntie van zonnecellen. Zoals besproken in Paragraaf2.3, kan het *space-separated quantum cutting* proces tussen silicium nanokristallen uitermate geschikt zijn voor een aanzienlijke verbetering van fotovoltaïsche apparaten.

Tot slot in Hoofdstuk 3, worden de optische eigenschappen van de erbium-gedoteerde grote-bandkloof-materialen onderzocht. In Paragraaf 3.1 worden fotoluminescentie en excitatie fotoluminescentie spectroscopie toegepast op erbium-gedoteerd galliumnitride. Met de verkregen resultaten wordt de multipliciteit van de erbiumposities in het host rooster besproken. In Paragraaf 3.2 wordt de potentie van het gebruik van erbium voor middel-infrarode emissie bij de golflengte van 2.7 μm (de overgang van het tweede naar het eerste geëxciteerde niveau) bestudeerd. Om dit te doen wordt een groot-bandkloof fluoridekristal gebruikt, waarin de introductie van erbium in alleen substitutionele posities resulteert, om begrip van het erbium-gedoteerde galliumnitride systeem te versimpelen. Door de tijdafhankelijkheid van de fotoluminescentie voor verscheidene overgangen van het erbiumion te registreren, wordt de levensduur van de hogere energieniveaus bepaald en de resultaten wijzen erop dat in beide host materialen de middel-infrarode emissie plaats zou kunnen vinden.

Acknowledgements

Needless to say, this thesis would not be in your hands without the invaluable help and support of so many people along the years I have spent in Amsterdam. First of all, Tom, thank you for welcoming me in your group five years ago, when you knew very little about me. In this time, I have never seen your office door closed for me—or for any other member of the group, for that matter—either for a scientific discussion or a simple rant. I have always appreciated your openness to discuss any subject and, even when we would defend confronted points of view, your will to provide a fair playground and your honesty in your arguments—which, in my opinion, is not incompatible with a mild cynicism. During our morning coffee time, our weekly group meetings, Friday beers, endless discussions, Christmas dinners, eventual desperation and hopes... I have learnt a lot from you and always appreciated the way you run the group. My arrival to Amsterdam would not have ever happened if Manu F. had not placed that little ad in Barcelona; I am grateful to him for that. And again, I can only thank him fir his warm welcome and guidance when I started working next to him; his advices and friendship meant and mean a lot to me and he has been the mirror where I could look at. Besides Tom and Manu, the group was composed by Mark Klik, Vinh, Maciej, and Bert, when I joined in. Every single line written in this thesis is supported by their work; I learnt from them all—it is a long and bizarre list—, and they left the best heritage I could find: I have exploited it with pleasure. Besides, the environment they managed to create in the office and the lab was always a motivation.

During my years in the group, new members have arrived and others have gone—that's life—, but its essence has suffered little changes. Partly, this has been achieved by the human quality and the hard work of the people involved. Henk, the quiet man, a pleasure to work with and whose unalterable nerves I wanted for myself in more than one occasion. The actual members of the group: Salvo, Ha, Dolf, and Wieteke; I must let you know that leaving the lab at this moment has been almost painful. You form a great team, and working with you was smooth and fun; I sometimes laugh all alone in the

middle of the street when some situations I got involved with you, guys, cross my mind. Peter Stallinga, who arrived to stir up the group, thank you for your provocations. One of my duties as a PhD student was the guidance of Bachelor and Master student projects. Mark S., Chris V., and, again, Dolf; I am afraid I have learnt more from you and these experiences, than you have possibly done from me. I also want to have a word for the people in the mechanical and electronic workshops who have been somehow related to my research; some of them maybe without knowing it, by their daily work, and others more directly involved into it, like Gerrit, who helped me to control the ever growing beast in the lab.

During my research, I have collaborated with other scientists outside my home Institute. Samples, theories, data, new labs, new experiments, new visions, discussions, flames... From this magma that defines Science itself, I have had the opportunity of working with some fabulous—in the strictly literal sense of the term: *of an incredible, astonishing, or exaggerated nature*—people. In a prominent place, I want to acknowledge Irina Yassievich, for whom I declare a genuine admiration. Both, as a scientist and in the personal side; for her brilliant ideas, her impetus and her strength, I can only be proud of co-authoring some of my papers with her. And by her side, a wild bunch of scientist from the IOFFE Institute in St. Petersburg. I have a mixed sensation of sadness and honor for co-authoring the last paper of Mischa Bresler, rest in peace, a brilliant scientist with a bitting intelligence. Oleg Gusev, an experimentalist among so many theorist. And the young generation: Andrey Moskalenko and Alexei Prokofiev. I am so indebted to all of them.

Still in Russia, but now from Nizhny Novgorod, I also had the pleasure of working with Boris Andreev, and use some of his samples to carry out the research performed in Chapter 1; my acknowledgments extend to Professor Krasil'nik. A separate chapter would be needed to describe one single working day with Vitalii Ivanov. I will only say here that this has been my closest experience to riding a wild horse... And I am glad that, not only I survived, but together we made a nice work while having some good laughs, chats, and shots.

My acknowledgements to Minoru Fujii, from Kobe University, for kindly providing me with the state-of-the-art nanocrystals samples used in Chapter 2, and for fruitful discussions in the lobbies of scientific meetings around the world. I also want to thank Professor Kimura for the interest he expressed for my work and Spanish classical music.

Those who have experience in beam-time experiments will understand the type of bounds that are developed among the people involved in the measurements. First, I would like to thank the FELIX staff, in Rijnhuizen, and

especially Vinh, for their skillful assistance during my days and nights there. I keep in my mind every person with whom I have spent hours in the FELIX experiments, going through stress, tensions, and sleepless nights.

Back to Amsterdam, I want to express my admiration and gratitude to the group leaders and staff members of the WZI. They have made the Lab a place with an outstanding scientific quality and a enviable atmosphere: somewhere where anyone would be willing to work in. Part of this success is also due to all the administrative and technical staff, for whom my gratitude is extended.

The real trouble comes now. Expressing, in printed words, my gratitude and feelings towards so many people, so many friends who were not directly related to my research and who are now part of my soul is "like dancing about architecture". I am going to do something unusual, which is sparing any name from now on. To all my friends, I know you are now reading this with a smile in your face. My justification—not my excuse—is the fear of forgetting someone important; besides, you know who you are.

I want to start with the wonderful people I have met working next to me, mainly, but not only, in the WZI and the ITF buildings. After hours in the darkness of the lab, and a labyrinth of data and equations, it has been very important to me looking up and finding always someone I could vent on, talk to, listen... someone with whom I could have a break, or a beer, or a laugh... The life of a young scientist implies movement, and master and PhD students, and post-docs have come in and out of Amsterdam during my own temporary period there, from all places around the Globe. I have met some really warm people, kind, funny, some of the smartest people I could ever think of. I will never forget some of them, and I want to thank them for their friendship and their personality—in so many cases, out of what is socially expected. I have shared many hours with many of you; in the building, sharing a coffee, so many evenings in the Kriterion, discussions, parties... This text is becoming unintelligible, as it is the nature of my acknowledgements to so many colleagues who became friends. Thank you again for insisting in going to a bar, for smoking in the corner of the courtyard, for becoming my confidants, for keeping me sane and for going insane together.

Outside the working environment, I have met so many interesting people with whom I have shared a part of my life in Amsterdam. Some for being my flatmates or neighbors in one or another of my multiple locations. The first person I met when I arrived to Amsterdam and with whom I shared a flat for several months; my crazy neighbors in Funen, that I discovered gradually, and whose *bonjour voisin!* I will always keep with me; my last flatmate with whom I shared so many conversations and the best apartment I will ever live in. Thank you all for being there. I have also shared great moments with some

collectives of people: the ESA people, the astronomers, the biologists from the VU, the Italians, the Italian astronomers, the Spaniards... without them life would have been so boring!

And, finally, among my friends, to those with whom I have shared my sorrows and joys; to those with whom I have laughed through the tears, with whom I have walk through all these years. As I said before: you know who you are. Thanks a lot.

Last but not least, I want to acknowledge all my family, for their support and for keeping me with my feet on the ground. To my parents, for the education they gave me and granted me; to my brother and sister, for keeping me awake; to Patricia, my aunts, uncles and cousins. Thank you all for your support, visits, and for being there.

Notes